Stable Colloidal Dispersions of Highly Concentrated Thermo-efficient Nanomaterials

by

Mohammad Sharif Hossain

A dissertation submitted to the Graduate Faculty of
Auburn University
in partial fulfillment of the
requirements for the Degree of
Doctor of Philosophy

Auburn, Alabama
May 06, 2017

Keywords: Colloid, nanoparticles, photochemistry, nanorods,
Phase change materials, clusters

Approved by

German Mills, Chair, Professor of Chemistry
Rik Blumenthal, Associate Professor of Chemistry
Vincenzo Cammarata, Associate Professor of Chemistry
Wei Zhan, Associate Professor of Chemistry
Jayhoon Khodadadi, Professor of Mechanical Enginerring

Abstract

Phase change materials (PCM) were utilized as solvents to synthesize small particles and stabilize them in those media in order to determine time independent thermal properties of nanostructure-enhanced phase change materials (NePCM). Spherical Ag particles in poly (ethylene glycol), PEG, and CuO rods in dodecane were achieved at high concentrations, these concentrated colloids exhibited a significant stability against precipitation at room temperature. The resulting nanoparticles and nanorods were characterized using UV-Visible spectrophotometry; transmission electron microscopy (TEM); Cytoviva optical microscopy; X-ray diffraction (XRD) and Fourier transform infrared spectroscopy, FTIR. Thermal conductivity enhancements were determined at different concentrations of particles as well as at different temperatures by using thermal analyzers (TPS 500 and KD2 Pro). Moreover, metallic Ag clusters were formed during illumination of organometallic Ag precursors in alkanes containing oleoyl sarcosine. Clusters were detected by UV-Vis and fluoresence spectroscopies and their concentrations were estimated from titration experiments. A novel feature of the clusters was their long lifetime even under air in non-polar solvents.

Acknowledgments

I would like to thank Dr. German Mills for his continuous support and motivation throughout my PhD research. Additional appreciation is given to the advisory committee, which consists of Dr. Rik Blumenthal, Dr. Vince Cammarata, Dr. Wei Zhan, and the outside reader, Dr. Jayhoon Khodadadi. I also would like to thank Dr. Mike Miller (Department of Biological Sciences) for teaching me how to operate the transmission electron microscope and also for providing me extensive access to the instrument. My gratitude is also extended to Jamie Uertz, from Cytoviva Inc., for his help with the optical microscopic analysis. I also thank appreciate Dr. Khodadadi for providing me giving me access to his thermal analysis laboratory to perform thermal conductivity measurements. We are thankful to to the U.S. Department of Energy for providing funds that supported the nanofluid project under the EPSCoR/DOE award number DE-SC0002470. I would also like to acknowledge Dr. Khodadadi of the Auburn University Mechanical Engineering Department for leading the nanofluid project that resulted in approved this grant. Finally, a great part of thanks will go to my beloved wife who has always been with me with tremendous support.

Table of Contents

List of Tables

List of Figures

List of Abbreviations

PCM	Phase Change Materials
NePCM	Nanostructure enhanced Phase Change Material
TES	Thermal Energy Storage
PEG	Poly(ethylene glycol)
PVP	Poly(vinyl pyrollidone)
TC	Thermal Conductivity
SOA	Sodium Oleate
OS	Oleoyl Sarcosine
BP	Benzophenone
CuL_2	Copper Neo-decanoate
AgL	Silver Neo-decanoate

Chapter I

Introduction

The ongoing growth of economic development depends on the technological advancement and management of energy. Technological advancements include the utilization of alternative energy sources to overcome excessive utilization of fossil fuel and other sources which increases greenhouse gases.[2] Alternative energy sources also include systems devised to extract energy from unconventional resources. Thermal energy from geothermal sources, solar radiation and hot waste stream can be systematically stored by materials for future use. In fact, thermal energy storage (TES) can play an important role to balance the demand and supply of energy. TES systems are primarily of three different types 1) sensible heat storage (SHS) which utilizes the heat capacity of a pure liquid or solid (e.g. water, inorganic salts, sands etc.); 2) latent heat storage (LHS) which absorbs heat during phase change at constant temperature (e.g. hydrocarbons, poly(ethylene glycol) etc.) and 3) thermo-chemical storage (TCS), which involves utilization of chemical reactions in order to store and release thermal energy (e.g. adsorption of water in silica-gel or zeolites).[3] Storage and retrieval of thermal energy in a controllable fashion by any material is of great significance for various thermal-based technologies. Materials which are able to absorb and release thermal energy via the sensible heat and latent heat routes are called phase change materials (PCM).[4] Upon melting, PCM absorb thermal energy, which is stored for future use.

Heat transfer mediated by fluids is one of the most important technical challenges facing numerous industries. Faster cooling is essential to enhance the efficiency of sophisticated machineries. Gases transfer heat by direct collisions between molecules, and as would be

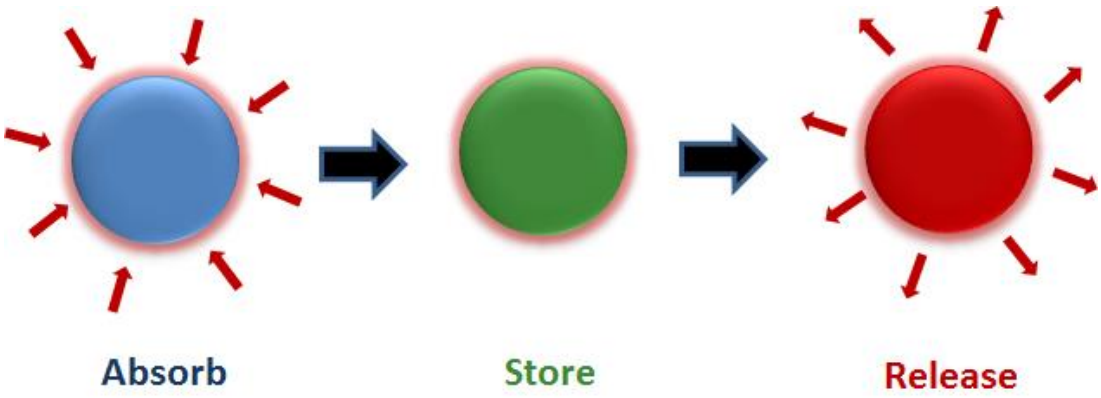

Figure 1.1: A hypothetical PCM showing energy storage capabilities, which includes absorbtion of energy upon melting and releasing the absorbed energy during freezing.

expected, their thermal conductivities are low compared to most solids since they are a dilute media. On the other hand, non-metallic solids transfer heat by lattice vibrations so that there is no net motion of the media as the energy propagates through. Such heat transfer is often described in terms of "phonons", or quanta of lattice vibrations. Metals are much better thermal conductors than non-metals because the same mobile electrons, which participate in electrical conduction, also take part in the transfer of heat. A comparison of thermal conductivity (TC) of base fluids and bulk inorganic materials are given below. Because of the differences in TC introduction of nanoparticles into fluids may result in liquids systems with enhanced thermal conductivities, also known as nanofluids (Table 1.1).

The low thermal conductivity of conventional heat transfer fluids is a serious limitation for improving the performance and compactness of engineering equipment. By considering the fact that metallic solids possess higher TC values than fluids, liquid suspensions of solid particles could be expected to exhibit significantly higher thermal conductivities as compared to conventional heat transfer fluids. Fluids containing millimeter or micrometer size particles are

difficult to deal with due to clogging of narrow passages along the flowing path of the coolant. Also, rapid settling out from ~~the~~ solution of the particulate materials is difficult to prevent.

Table 1.1: Compilation of thermal conductivities and melting enthalpies of common inorganic and organic materials.[5–9]

Material	Melting Temperature (^{0}C)	Melting Enthalpy (kJ/kg)	Thermal Conductivity (W/mK)	Density (g/cc)
PEG 600	17-22	107	0.19 (liquid, 38 ^{0}C)	1.126 (liquid, 25 ^{0}C) 1.232 (solid, 4 ^{0}C)
PEG 6000	55-60, 66	190	-	1.085 (liquid, 70 ^{0}C) 1.212 (solid, 25 ^{0}C)
H_2O	0	333	0.6 (liquid), 2.2 (Solid)	0.997 (liquid, 25 ^{0}C) 0.917 (solid, 0 ^{0}C)
Cu	1085	-	398	8.96 (solid, 25 ^{0}C)
CuO	1326	-	20	6.32 (solid, 25 ^{0}C)
Ag	961.8	-	429	10.49 (solid, 25 ^{0}C)

Due to the large values of the heat of fusion (ΔH_{fus}) possessed by long chain hydrocarbons, these compounds are considered to be best suited for thermal energy storage media.[4] Furthermore, the melting temperature of hydrocarbons can be manipulated by using molecules with ~~of~~ different chain lengths. This interesting possibility provides an opportunity for utilizing hydrocarbons as energy storage materials that can function over a wide temperature range. Although hydrocarbons possess valuable properties for PCM applications, one of their disadvantages is flammability. Another issue associated with hydrocarbons as base fluids is that formation and

long-term stabilization of small particles in alkanes is difficult to achieve because of solubility problems of relevant precursors. Listed below are characteristic thermal properties of PEG's and hydrocarbons relevant to their potential ability as energy storage materials.[10]

Table 1.2: Thermal properties of PEG's as phase change materials.

Material	$\Delta H_{cooling}$(J/g) (solidification)	Temperature range (°C)	$\Delta H_{heating}$(J/g) (melting)	Temperature range (°C)
PEG: 400 MM	48.7	3.7 - 7.3	53.3	5.6 to 10.7
PEG: 600 MM	107.9	20 - 0	112.6	3.6–28
PEG: 1000 MM	102.2	38.2–22.3	107.6	23–44
Octodecane	208.7	28.3–24.8	208.7	27.7–32.5
Dodecane	211	-10.0- (+9)	-	-
Paraffin wax	153.1	56.2–31.2	150.4	31.6–60.6

Dispersion of particles in fluids:

The goal of this study was to achieve enhancements in the thermal conductivity of PCM's not only in the solid phase but also in the liquid phase. In order to achieve enhanced TC, nanoparticles of materials possessing high thermal conductivity were to be incorporated into the fluid form of PCM's. The feasibility of using suspensions of solid particles with sizes in the order of millimeters or micrometers was previously investigated by several researchers and the following significant drawbacks were observed:[11]

1. Rapid sedimentation of the particles with time due to gravity, which reduces the heat transfer capacity of the fluid.

2. Sedimentation of particles is inversely proportional to the fluid circulation rate but erosion of the heat transfer devices, pipelines, etc., increases with increasing circulation rate of the coolant.

3. Particles exhibiting a wide size distribution tend to clog the flow channels especially in the case of narrow channels .

4. Clogging of flow channels radidly increases the pressure drop in the fluid.

5. Eventually, a thermal conductivity enhancement induced by a high particle concentration may be achieved. However, the above mentioned problems become more significant when higher particle volume fraction are used.

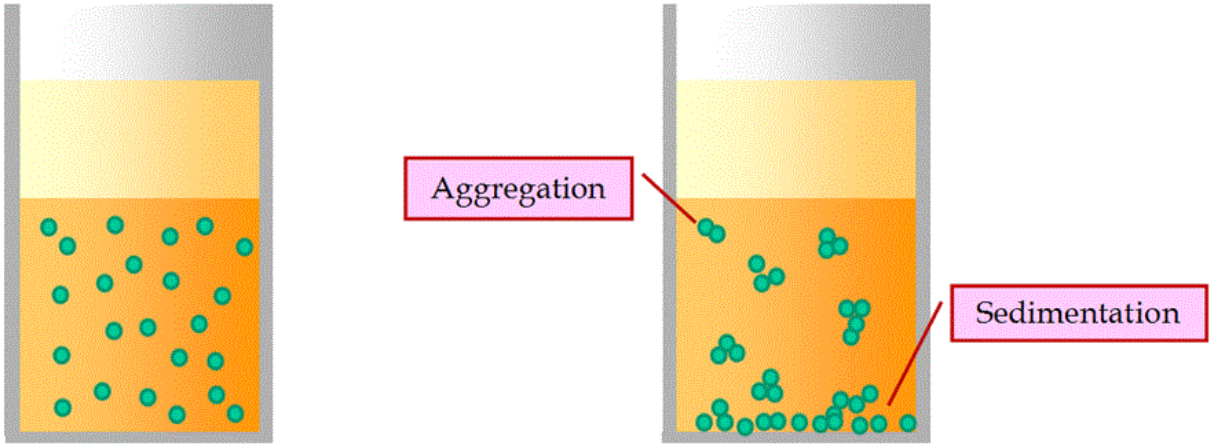

Figure 1.2: Example of stable (left) and unstable (right) colloids.

Nanofluids:

A recent advancement in nanotechnology has been the introduction of nanofluids, that is, suspensions of nanometer-sized solid particles instead of common working fluids.[12] Nanofluids were first proposed by Choi and Eastman in 1995 at ~~the~~ Argonne National Laboratory, USA. These are two-phase systems consisting of a solid phase dispersed into a liquid phase.

Nanofluids have been found to possess enhanced thermophysical properties such as thermal conductivity, thermal diffusivity, viscosity and convective heat transfer coefficients as compared to those of base fluids like oil or water.

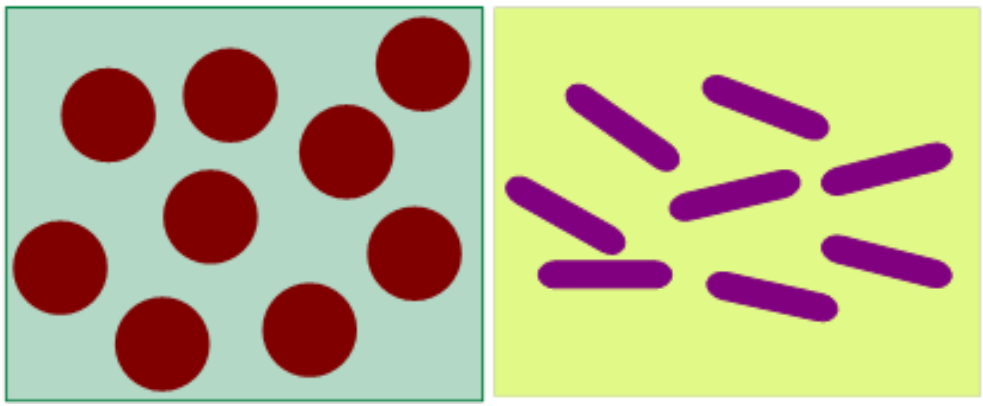

Figure 1.3: Idealized depictions of colloids, or stable suspensions, of colloidal spherical and rodlike particle in fluid media.

Nanofluids have novel properties that make them potentially useful in many applications particularly for efficient heat transfer in several areas, including microelectronics, transportation, and power generation, thermal therapy for cancer treatment, as well as for heating, cooling, ventilation and air conditioning.[2,13]

Basically, metal or metal oxides colloidal particles dispersed in liquid media are used to enhance the thermal conductivity coefficient. For a two-phase system, there are some important issues that need to be considered in order to achieve stability in the solvent medium. One of the most important issues is agglomeration of particles and their subsequent sedimentation. Hence, a big challenge is to avoid particle aggregation as much as possible thereby achieving the desired long-term stability of the dispersed phase in nanofluids. Van der Waals forces between similar particles in a medium are attractive and this force will result in aggregation of most suspensions.

Density differences between the solute particles and the external phase lead to sedimentation or creaming of the aggregated solutes.

Stability of particles in liquid media:

Although colloidal particles in a fluid medium are thermodynamically unstable, they can be made kinetically stable either by charging the particle surface, or by means of steric hindrance. Due to the large surface area to volume ratio, even when stabilizing agents are employed, particle aggregation may be induced by Van der Waals (VDWL) force. If particle stability can be achieved then the enhanced properties of the resulting fluids can be utilized to improve the efficiency of machinery. Individual particles attract each other at short distances due to van der Walls forces. The attraction originates from three contributions: dipole-dipole, dipole-induced dipole and London dispersion forces. If attractions between particles predominate over repulsion forces then particles will adhere and finally coalesce to precipitate out from the colloidal state.

On the other hand, if repulsions predominate over attractions then the system will be stable and a dispersed state will be achieved. There are two major approaches to overcome the attractive forces between particles: electrostatic and steric stabilization.[14] Electrostatic stabilization is based on coulombic repulsions, which counterbalance the VDWL forces. In a two-phase colloidal system, ionic groups can be adsorbed on the particle surface, forming a charged layer next to the dense inner core. In order to balance charge neutrality, an equal number of counter ions with opposite charge will surround the colloidal particles establishing double layers characterized by an overall neutral charge.[15] The mutual repulsion of double layers surrounding the particles provides kinetic stability of the dispersion. Turkevich demonstrated that ~~a~~ mutual

repulsion of electric double layers containing sodium citrate was the main key for the stabilization Au colloids.[16]

Steric stabilization of particles can be achieved by incorporating macromolecules on the surface of the colloidal particles. Grafting or chemisorption of long chain polymer molecules on the dispersed particles is the primary way to stabilize nanoparticles in solution. There are numerous examples of utilization of macromolecules to achieve colloid stabilization. Depending on the interaction between polymer and solid surface, a macromolecule can be classified as either anchored or adsorbed. Anchored polymers bind irreversibly to the colloidal surface whereas adsorbed macromolecules bind at random points along the polymer chain. When two particles with adsorbed polymer chains interact with each other, the macromolecules may overlap with each other, increasing the local segment density. This increase in segment density will eventually increase the osmotic pressure. An increase of local osmotic pressure will result in strong repulsion between particles.[17] Steric stabilization is advantageous over electrostatic stabilization because a very high concentration of particles can be accommodated and the solvent can be completely removed without flocculation of particles. A wide range of studies is available demonstrating steric stabilization of colloids induced by polymers such as PVP[18], PVA[19,20], poly(acrylonitrile)[21], poly(ethylene glycol)[22,23] and polyurea.[24]

Surface active molecules and organic polymers are generally used to induce either electrostatic or steric stabilization of colloidal particles. Surfactants are also often featured in self-assembly processes, where energetic and entropic effects determine the structure and dynamics of complex aggregates. Lyophilic molecules chemically or physically attached to the surface of colloidal particles prevent their aggregation. Overlap of the stabilizing molecules results in an osmotic pressure in the overlap region and the stabilized solutes are pushed apart.

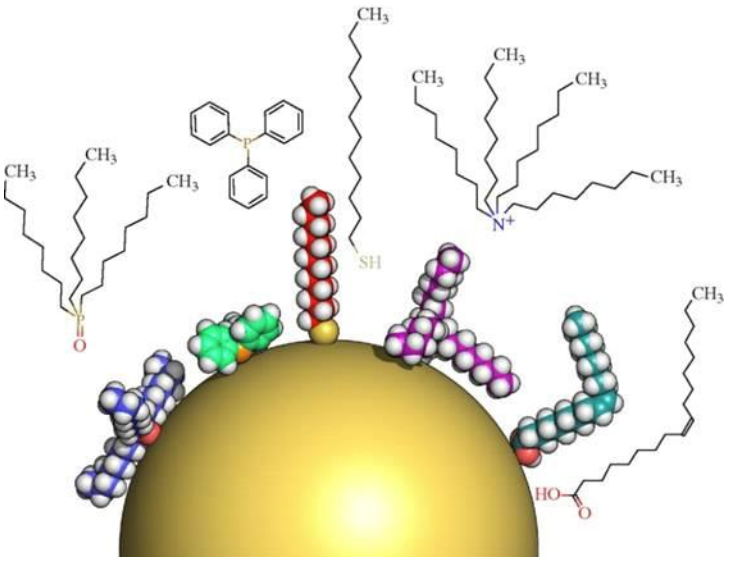

Figure 1.4: Conceptual interaction of organic molecules and surfactants with the surface of colloidal particles in liquid media.

Synthetic strategy of colloidal metal and metal oxide particles:

Numerous procedures are available to obtain nanoparticles of colloidal metals, oxides and sulfides. The formulation of highly monodispersed colloidal particles involves two major steps: a single and short nucleation period followed by slow growth to form colloidal particles.[25] The termination of the growth process may occur through capping of the surface of colloidal particles with the aid of a stabilizer. A short nucleation or seeding is crucial to obtain uniform particles. Otherwise, a second growth process called Ostwald ripening will start to dominate where larger particles will grow further via dissolution of the smaller particles possessing high surface energy to decrease the overall energy of the system.[26] Traditionally, metal nanoparticles are prepared by reducing metal ions in the presence of a suitable particle stabilizer. Reduction of metal ions can be classified into two subdivisions; in the classical chemical approach the redox reaction is induced by strong reducing agents such as sodium borohydride,[27–29] hydrazine and hydrogen[30,31]

etc. Stronger reducing agents are preferable in order to achieve smaller nuclei, which yield narrow size distributions of particles. Sodium citrate and ascorbic acids are commonly used as weak reducing agent to disfavor rapid growth of particles.[32,33]

N, N-dimethyl formamide and alcohols[18–20,34] are also quite extensively used and which act both as solvent as well as electron donors that reduce metal ions. When a strong reducing agent is employed, the reaction is performed at room temperature or even at very low temperatures in order to achieve some control of the rate of reduction and of the rapid particle growth. On the other hand, if a weak reducing agent is employed, the reduction is usually performed at elevated temperatures to achieve fast nuclei formation. Other approaches for reducing metal ions includes introduction of photons or other form of radiation in presence of a chemical sensitizer. A photosensitizer absorbs photons of a particular wavelength and the excited singlet or triplet state of the sensitizer becomes capable of reducing metal ions dissolved in solution. The radiation-chemical approach utilizes solvated electrons generated by ionizing the solvent with the radiation.[35] The reduction procedure of metal salts has been very successful at producing noble metal particles of Ag, Au and Pt. Non-noble metals such as Cu, Fe, Ni and Co cannot be easily prepared by reducing their salts because of their sensitivity towards oxidation by air.

Colloidal metal oxides can be produced by the hot injection method in which transformation of precursor species occurs to form oxidic compounds in presence of a stabilizer or surfactant. Surfactants contain a coordinating head group and an organic long chain; they can adsorb on the surface of oxide particles and thereby induce steric repulsions between particles. The morphology and stability of colloidal metal oxides depend on the reaction time, concentration of precursors and surfactants as well as of the temperature of the reaction medium. Metal oxide

particles with low dispersity and well-defined morphologies can be achieved by judicious adjustment of the reaction parameters.

Thermal conductivity enhancement by particles in fluid from theory to applications:

Over the last decade, nanofluids sparked excitement as well as controversy. The evolution of this field of research has been hindered due to the lack of harmony between theoretical models and experimental data. This has hampered the development of a useful model that describes TC enhancements. In particular, a number of investigations reported that dramatic increases in thermal conductivity were possible by addition of small nanoparticles to liquids, while others showed moderate increases consistent with the effective medium theories of well-dispersed conductive spheres. Maxwell first proposed that a dispersion of metallic particles in a solvent will produce enhanced thermal properties depending on the particle loading of the mixture.[36] According to Maxwell's classical theory, for an inhomogeneous mixture of solid-liquid system the effective thermal conductivity (k) can be described as:

$$k = k_f \frac{2k_f + k_p + 2\phi_p(k_p - k_f)}{2k_f + k_p - \phi_p(k_p - k_f)}$$

where, k_p and k_f are thermal conductivities solid and liquid phases respectively and ϕ_p is the volume fraction of solid particles.

For a nanofluid, the thermal conductivity enhancements beyond the prediction of Maxwell's theory are often regarded to be anomalous or unusual. A wide range of experimental and theoretical studies were reported in the literature to model the thermal conductivity of nanofluids.[36-48] The existing results were generally based on the definition of the effective thermal conductivity of a two-component mixture.

For nanofluids based on dispersions, their heat transfer characteristics are time dependent properties, and their mechanisms are still under investigation. The first classical approach to model thermal conductivity of a colloidal suspension was presented by Maxwell.[36] To model thermal conductivity of a solid–liquid system Maxwell considered a very dilute solution neglecting interactions between particles. Hamilton-Crosser modified Maxwell's model by introducing a shape factor of the particles which is applicable for spherical and cylindrical particles only.[37] The Bruggeman approach addresses the inter-particle collision in a suspension.[38] Bruggerman's model is an extension of Maxwell's model that is applicable for particles of any volume fraction, and matches well Maxwell's model at low concentration of particles. Liquid layering on the nanoparticles surface was also assumed to have an effect on the relative thermal conductivity enhancement as compared with the TC value of the basefluid.[39] The wrapping of liquid molecules on the solid surface acts as a thermal bridge between particles and bulk liquid. The nanolayer thickness of the liquid molecules was also taken into account in order to explain anomalous thermal conductivity enhancements claimed for nanofluids.[40–42] Aggregation of nanoparticles,[43] interfacial thermal resistance,[44,45] Brownian motion followed by micro-liquid convection[46–48] were also suggested to contribute to the overall TC enhancement. Although a plethora of theoretical models are available in literature, none of the models is able to explain some claims of extraordinary experimental TC enhancement single handedly. Accordingly, the mechanism of thermal conductivity enhancement is a hotly debated topic. Efforts to develop nanofluid of long term stability that could yield optimum thermal conductivity enhancements were assessed in several investigations.[13,49,50]

Efforts were made to obtain ideal combinations of nanoparticles and solvents to increase the heat transfer coefficient of the mixture.[12,51–58] Metals are better thermal conductors than non-metals or

oxides. Therefore, particles of metals such as Cu, Fe, Au and Ag dispersed in common basefluids[53] (water, ethylene glycol etc.) were popular components in this research arena. Oxide materials such as CuO, Al_2O_3 and TiO_2 dispersed in water were also considered because of their long term stability and low production cost.[54,57,59] Eastman et al. claimed that the thermal conductivity of ethylene glycol nanofluids containing 0.3% copper particles is boosted by up to 40% in contrast to the TC of the basefluid.[12] Liu et al reported that an introduction of 0.1% Cu particles in water increases TC by up to 23.8%.[60] Also reported was that a TC enhancement of about 150-200% can be achieved using a 1% loading of multi-walled carbon nanotube (MWNT) in poly(α-olefins).[61] A 75% of TC enhancement was also reported for dispersions in ethylene glycol containing 1.2% of diamond particles with diameters of 30-50 nm.[62] Amidst these remarkable observations, there is a considerable number of researchers claiming that nanofluids exhibit no anomalous TC behavior.[63–66] These scientists indicate that their observations can be explained by means of the conventional heat transfer theory. For example, Ag particles coated by oleic acid in chloroform showed an enhancement of TC of about 17% at room temperature.[67]

Thermal conductivity determination for colloidal solutions:

Several methods can be adopted to obtain the thermal conductivity of colloidal solutions; the most common and widely used are the steady state technique (SST), procedures that utilize a transient plane source (TPS) and the transient hot wire (THW) methodology. Transient methods are favored over steady state procedures for liquid samples since the former can determine thermal conductivities in a short period of time, avoiding problems associated with thermal convection. In contrast, the steady state method involves a long- lasting step needed to establish a temperature gradient necessary to obtain thermal conductivity data.

In this work, a transient plane source (TPS) was used for fast and accurate measurements of the thermal conductivity of colloids. The hot disk TPS 500 thermal analyzer can be employed to measure thermal conductivities, within the range of 0.03 – 100 W/mK, as well as thermal diffusivity and specific heat capacity of materials rapidly and with accuracy of better than 5 %. For determinations of solutions a sensor is simply immersed into the liquid sample. This sensor is a flat device consisting of continuous double spiral of electrically conducting Nickel (Ni) metal that can also serve as a resistance thermometer able to measure transient temperatures achieved at different heating times. To ensure electrical insulation and mechanical stability of the sensor this device is coated with thin layer of Kapton polyimide. Thermal conductivities are obtained by passing a constant electrical current through the spiral element of the sensor. As a result, the sensor temperature increases and the generated heat dissipates through both sides of the flat sensor at a rate depending on the transport properties of the surrounding material. The thermal conductivity of the surrounding material can then be calculated from the temperature versus time response of the sensor.

References:

(1) Clary, D. R.; Mills, G. Preparation and Thermal Properties of CuO Particles *J. Phys. Chem. C* **2011**, 1767–1775.

(2) Sharma, A.; Tyagi, V. V.; Chen, C. R.; Buddhi, D. Review on Thermal Energy Storage with Phase Change Materials and Applications. *Renew. Sustain. Energy Rev.* **2009**, *13*, 318–345.

(3) Al Ghossein, R. M.; Hossain, M. S.; Khodadadi, J. M. Experimental Determination of Temperature-Dependent Thermal Conductivity of Solid Eicosane-Based Silver Nanostructure-Enhanced Phase Change Materials for Thermal Energy Storage. *Int. J. Heat Mass Trans.* **2017**, *107*, 697–711.

(4) Pielichowska, K.; Pielichowski, K. Phase Change Materials for Thermal Energy Storage. *Prog. Mater. Sci.* **2014**, *65*, 67–123.

(5) Eapen, J., Rusconi, R., Piazza, R., Yip, S.; The Classical Nature of Thermal Conduction in Nanofluids. *J. Heat Trans.*, **2010**, *132*, 102402.

(6) Kwak, K., Kim, C.; Viscosity and thermal conductivity of copper oxide nanofluid dispersed in ethylene glycol. *Korea-Aust. Rheol. J.* **2005**, *17*, 35–40.

(7) Chung, D. D.; Materials for thermal conduction. *Appl. Therm. Eng.*, **2001**, *21*, 1593–1605.

(8) Bulgrin, R., Naumann, R., Emons, H. H., Holfter, U.; Thermal properties of organic latent cold storage materials. *J. Therm. Anal.* **1991**, *37,* 155–169.

(9) Yaws, C. L. Thermal Conductivity of Liquid – Organic Compounds. *Transport Properties of Chemicals and Hydrocarbons*; Boston: William Andrew Publishing; **2009**, 299–395.

(10) Bentz, D. P.; Turpin, R. Potential Applications of Phase Change Materials in Concrete Technology. *Cem. Concr. Compos.* **2007**, *29*, 527–532.

(11) Eastman, J. a.; Choi, S. U. S.; Li, S.; Yu, W.; Thompson, L. J. Anomalously Increased Effective Thermal Conductivities of Ethylene Glycol-Based Nanofluids Containing Copper Nanoparticles. *Appl. Phys. Lett.* **2001**, *78*, 718–720.

(12) Das, S. K.; Choi, S. U. S.; Patel, H. E. Heat Transfer in Nanofluids — A Review. *Heat Transf. Eng.* **2006**, *27*, 3–19.

(13) Godson, L.; Raja, B.; Mohan Lal, D.; Wongwises, S. Enhancement of Heat Transfer Using Nanofluids - An Overview. *Renew. Sustain. Energy Rev.* **2010**, *14*, 629–641.

(14) Bradley, J. S. The Chemistry of Transition Metal Colloids. *Clust. Colloids From Theory to Appl.* **2007**, 459–544.

(15) Aiken, J. D.; Finke, R. G. A Review of Modern Transition-Metal Nanoclusters: Their Synthesis, Characterization, and Applications in Catalysis. *J. Mol. Catal. A Chem.* **1999**, *145*, 1–44.

(16) Turkevich, J.; Stevenson, P. C.; Hillier, J. A Study of the Nucleation and Growth Processes in the Synthesis of Colloidal Gold. *Discuss. Faraday Soc.* **1951**, *11*, 55–75.

(17) Tadros, T. General Principles of Colloid Stability and the Role of Surface Forces. In *Colloid Stability*; Wiley-VCH Verlag, Weinheim, Germany, 2006; 1–22.

(18) Hirai, H.; Nakao, Y.; Toshima, N. Preparation of Colloidal Transition Metals in Polymers by Reduction with Alcohols or Ethers. *J. Macromol. Sci. Part A - Chem.* **1979**, *13*, 727–750.

(19) Hirai, H.; Nakao, Y.; Toshima, N. Colloidal Rhodium in Polyvinyl Alcohol as Hydrogenation Catalyst of Olefins. *Chem. Lett.* **1976**, 905–910.

(20) Hirai, H.; Nakao, Y.; Toshima, N. Preparation of Colloidal Rhodium in Poly (vinyl Alcohol) by Reduction with Methanol. *J. Macromol. Sci. Part A - Chem.***1978**, *12*,1117–1141.

(21) Demir, M. M.; Gulgun, M. a; Menceloglu, Y. Z.; Abramchuk, S. S.; Makhaeva, E. E.; Khokhlov, A. R.; Matveeva, V. G.; Sulman, M. G. Palladium Nanoparticles by Electrospinning from Poly (Acrylonitrile-Co-Acrylic Acid) - $PdCl_2$ Solutions. Relations between Preparation Conditions, Particle Size, and Catalytic Activity. *Macromolecules*, **2004**, *37*, 1787–1792.

(22) Longenberger, L.; Mills, G. Spontaneous Formation of Gold Particles in Aqueous Polymeric Solutions. In *Nanotechnology*; ACS Symposium Series; American Chemical Society, **1996**; 622, 128–136.

(23) Pillai, U. R.; Sahle-Demessie, E. Phenanthroline-Stabilized Palladium Nanoparticles in Polyethylene Glycol—an Active and Recyclable Catalyst System for the Selective Hydrogenation of Olefins Using Molecular Hydrogen. *J. Mol. Catal. A Chem*. **2004**, *222*, 153–158.

(24) Ley, S. V; Mitchell, C.; Pears, D.; Ramarao, C.; Yu, J.; Zhou, W. Recyclable Polyurea-Microencapsulated Pd(0) Nanoparticles : An Efficient Catalyst for Hydrogenolysis of Epoxides. *Org. Lett*. **2003**, 5, 4665-4668.

(25) LaMer, V.; Dinegar, R. Theory, Production and Mechanism of Formation of Monodispersed Hydrosols. *J. Am. Chem. Soc.* **1950**, *72*, 4847–4854.

(26) Heights, Y. Synthesis and Characterization of Monodisperse Nanocrystals and Close Packed Nanocrystal Assemblies. *Annu. Rev. Mater. Sci.* **2000**, 545–610.

(27) He, S.; Yao, J.; Jiang, P.; Shi, D.; Zhang, H.; Xie, S.; Pang, S.; Gao, H. Formation of Silver Nanoparticles and Self-Assembled Two-Dimensional Ordered Superlattice. *Langmuir* **2001**, *17*, 1571–1575.

(28) Liu, L.; Wei, T.; Guan, X.; Zi, X.; He, H.; Dai, H. Size and Morphology Adjustment of PVP-Stabilized Silver and Gold Nanocrystals Synthesized by Hydrodynamic Assisted Self-Assembly Size and Morphology Adjustment of PVP-Stabilized Silver and Gold Nanocrystals Synthesized by Hydrodynamic Assisted Self-Assembly. *J. Phys. Chem. C.* **2009**, 8595–8600.

(29) Petit, C.; Lixonf, P.; Pileni, M. P. In Situ Synthesis of Silver Nanocluster in AOT Reverse Micelles. *J. Phys. Chem*. **1993**, *97*, 12974–12983.

(30) Rampino, L. D.; Nord, F. F. Preparation of Palladium and Platinum Synthetic High Polymer Catalysts and the Relationship between Particle Size and Rate of Hydrogenation. *J. Am. Chem. Soc.* **1941**, *63*, 2745–2749.

(31) Rampino, L.; Nord, F. Applicability of Palladium Synthetic High Polymer Catalysts. *J. Am. Chem. Soc.* **1941**, *63*, 3268–3268.

(32) Ji, X.; Song, X.; Li, J.; Bai, Y.; Yang, W.; Peng, X. Size Control of Gold Nanocrystals in Citrate Reduction: The Third Role of Citrate. *J. Am. Chem. Soc.* **2007**, *129*, 13939–13948.

(33) Dong, X.; Ji, X.; Wu, H.; Zhao, L.; Li, J.; Yang, W. Shape Control of Silver Nanoparticles by Stepwise Citrate Reduction. *J. Phys. Chem*. C **2009**, *113*, 6573–6576.

(34) Lu, P.; Toshima, N. Catalysis of Polymer-Protected Ni/Pd Bimetallic Nano-Clusters for Hydrogenation of Nitrobenzene Derivatives. *Bull. Chem. Soc. Jpn.* **2000**, *73*, 751–758.

(35) Gutierrez, M.; Henglein, a. Formation of Colloidal Silver By“ push-Pull” reduction of Ag^{+}. *J. Phys. Chem.* **1993**, *97*, 11368–11370.

(36) Maxwell, J. C. *A Treatise on Electricity and Magnetism*. Clarendon Press. Oxford, 1873, 360–366.

(37) Cyanamid, A. Thermal Conductivity of Heterogeneous Two Component Systems. **1959**, *1*, 187–191.

(38) Hui, P. M.; Stroud, D. Thermal Conductivity of Graded Composites : Numerical Simulations and an Effective. *J. Mater. Sci.* **1999**, 3*4*, 5497–5503.

(39) Xue, Q.-Z. Model for Effective Thermal Conductivity of Nanofluids. *Phys. Lett.* A **2003**, *307*, 313–317.

(40) Xie, H.; Fujii, M.; Zhang, X. Effect of Interfacial Nanolayer on the Effective Thermal Conductivity of Nanoparticle-Fluid Mixture. *Int. J. Heat Mass Transf.* **2005**, *48*, 2926–2932.

(41) Murshed, S. M. S.; Leong, K. C.; Yang, C. Thermophysical and Electrokinetic Properties of Nanofluids - A Critical Review. *Appl. Therm. Eng.* **2008**, *28*, 2109–2125.

(42) Leong, K. C.; Yang, C.; Murshed, S. M. S. A Model for the Thermal Conductivity of Nanofluids - The Effect of Interfacial Layer. *J. Nanoparticle Res.* **2006**, *8*, 245–254.

(43) Feng, Y.; Yu, B.; Xu, P.; Zou, M. The Effective Thermal Conductivity of Nanofluids Based on the Nanolayer and the Aggregation of Nanoparticles. *J. Phys. D. Appl. Phys.* **2007**, *40*, 3164–3171.

(44) Bahrami, M.; Yovanovich, M. M.; Culham, R. J. Assessment of Relevant Physical Phenomena Controlling Thermal Performance of Nanofluids. *J. Thermophys. Heat Transf.* **2007**, *21*, 673–680.

(45) Nan, C. W.; Shi, Z.; Lin, Y. A Simple Model for Thermal Conductivity of Carbon Nanotube-Based Composites. *Chem. Phys. Lett.* **2003**, *375*, 666–669.

(46) Xuan, Y.; Li, Q.; Hu, W. Aggregation Structure and Thermal Conductivity of Nanofluids. *AIChE Journal,* **2003**, *49*, 1038-1043.

(47) Keblinski, P.; Phillpot, S. R.; Choi, S. U. S.; Eastman, J. A. Mechanisms of Heat Flow in Suspensions of Nano-Sized Particles (Nanofluid), *Int. J. Heat Mass Transf.* **2002**, *45*, 855–863.

(48) Koo, J.; Kleinstreuer, C. Impact Analysis of Nanoparticle Motion Mechanisms on the Thermal Conductivity of Nanofluids. *Int. Commun. Heat Mass Transf.* **2005**, *32*, 1111–1118.

(49) Saidur, R.; Leong, K. Y.; Mohammad, H. a. A Review on Applications and Challenges of Nanofluids. *Renew. Sustain. Energy Rev.* **2011**, *15*, 1646–1668.

(50) Wong, K. V.; Castillo, M. J. Heat Transfer Mechanisms and Clustering in Nanofluids. *Adv. Mech. Eng.* **2010**, 1-9.

(51) Das, S. K.; Putra, N.; Thiesen, P.; Roetzel, W. Temperature Dependence of Thermal Conductivity Enhancement for Nanofluids. *J. Heat Trans.* **2003**, *125*, 567–574.

(52) Lee, D.; Kim, J. W.; Kim, B. G. A New Parameter to Control Heat Transport in Nanofluids: Surface Charge State of the Particle in Suspension. *J. Phys. Chem.* B **2006**, *110*, 4323–4328.

(53) Xuan, Y.; Li, Q. Heat Transfer Enhancement of Nanofluids. *Int. J. heat fluid flow* **2000**, 21, 58–64.

(54) Murshed, S. M. S.; Leong, K. C.; Yang, C. Enhanced Thermal Conductivity of TiO_2 - Water Based Nanofluids. *Int. J. Therm. Sci.* **2005**, 44, 367–373.

(55) Patel, H. E.; Das, S. K.; Sundararajan, T.; Sreekumaran Nair, a.; George, B.; Pradeep, T. Thermal Conductivities of Naked and Monolayer Protected Metal Nanoparticle Based Nanofluids: Manifestation of Anomalous Enhancement and Chemical Effects. *Appl. Phys. Lett.* **2003**, 83, 2931–2933.

(56) Lee, S.; Choi, S. U. S.; Li, S.; Eastman, J. a. Measuring Thermal Conductivity of Fluids Containing Oxide Nanoparticles. *J. Heat Transfer* **1999**, 121, 280–289.

(57) Xie, H.; Wang, J.; Xi, T.; Liu, Y. Thermal Conductivity of Suspensions Containing Nanosized SiC Particles. *Int. J. Thermophys.* **2002**, *23*, 571–580.

(58) Xie, H.; Lee, H.; Youn, W.; Choi, M. Nanofluids Containing Multiwalled Carbon Nanotubes and Their Enhanced Thermal Conductivities. *J. Appl. Phys.* **2003**, *94*, 4967–4971.

(59) Xie, H.; Wang, J.; Xi, T.; Liu, Y.; Ai, F.; Wu, Q. Thermal Conductivity Enhancement of Suspensions Containing Nanosized Alumina Particles. *J. Appl. Phys.* **2002**, *91*, 4568–4572.

(60) Liu, M. S.; Lin, M. C. C.; Tsai, C. Y.; Wang, C. C. Enhancement of Thermal Conductivity with Cu for Nanofluids Using Chemical Reduction Method. *Int. J. Heat Mass Transf.* **2006**, *49*, 3028–3033.

(61) Choi, S. U. S.; Zhang, Z. G.; Yu, W.; Lockwood, F. E.; Grulke, E. a. Anomalous Thermal Conductivity Enhancement in Nanotube Suspensions. *Appl. Phys. Lett.* **2001**, *79*, 2252–2254.

(62) Kang, H. U.; Kim, S. H.; Oh, J. M. Estimation of Thermal Conductivity of Nanofluid Using Experimental Effective Particle Volume. *Exp. Heat Transf.* **2006**, *19*, 181–191.

(63) Timofeeva, E. V.; Gavrilov, A. N.; McCloskey, J. M.; Tolmachev, Y. V.; Sprunt, S.; Lopatina, L. M.; Selinger, J. V. Thermal Conductivity and Particle Agglomeration in Alumina Nanofluids: Experiment and Theory. *Phys. Rev. E - Stat. Nonlinear, Soft Matter Phys.* **2007**, *76*, 28–39.

(64) Zhang, X.; Gu, H.; Fujii, M. Experimental Study on the Effective Thermal Conductivity and Thermal Diffusivity of Nanofluids. *Int. J. Thermophys.* **2006**, *27*, 569–580.

(65) Zhang, X.; Gu, H.; Fujii, M. Effective Thermal Conductivity and Thermal Diffusivity of Nanofluids Containing Spherical and Cylindrical Nanoparticles. *Exp. Therm. Fluid Sci.* **2007**, *31*, 593–599.

(66) Zhang, X.; Gu, H.; Fujii, M. Effective Thermal Conductivity and Thermal Diffusivity of Nanofluids Containing Spherical and Cylindrical Nanoparticles. *Exp. Therm. Fluid Sci.* **2007**, *31*, 593–599.

(67) Li, D.; Hong, B.; Fang, W.; Guo, Y.; Lin, R. Preparation of Well-Dispersed Silver Nanoparticles for Oil-Based Nanofluids. *Ind. Eng. Chem. Res.* **2010**, *49*, 1697–1702.

Chapter II

Synthesis of Concentrated Spherical Ag Colloidal Particles in Liquid Polyethylene Glycol

Introduction:

Fluids typically possess lower thermal conductivities as compared to those of solids, which limits their thermal performance. Cooling induced by fluids is crucial for improved performances and compactness of sophisticated equipment.[1] Metallic solids possess much higher thermal conductivities than those of conventional heat transfer fluids. Hence, liquids containing suspended metal particles are anticipated to exhibit enhanced thermal conductivities in comparison with conventional fluids, particularly at higher concentrations of dispersed particles. The dispersion of small solid metal or metal oxide particles in liquid media may be useful for improving thermal transport and thereby, can help to solve cooling problems in industry.[2–4] However, the thermodynamic instability of dispersions of solid particles in fluids usually hampers their long term stability needed for practical applications. This problem arises when the dispersed particles collide with each other and fuse to form aggregated particles, which eventually precipitate out of solution due to the gravitational force. However, kinetically controlled long term stability of the particles can be achieved via selection of a stabilizers that can decrease the frequency of collisions between particles.

In the last few decades, considerable research has been carried out to investigate thermo-physical properties of nanofluid systems. Dispersion of nanoparticles in fluid systems has been reported to enhance the thermal conductivity of the liquids beyond expectation values derived using the

theoretical framework of Maxwell.[5–18] These dispersions, called nanofluids, were claimed to reach enhancements in thermal conductivity that do not depend exclusively on the particle volume fraction.[6,13,16,18] The origin of the reported enhancements remains unclear since particle size, shape, inter-particle distance, solid-liquid interfacial thermal resistance and viscosity of the solution were ~~are~~ anticipated to exert a significant effect on the overall thermal conductivity.[19–22] Most of the properties and applications of dispersed metal or metal oxides colloidal particles are governed by their size, stability and concentration in solution. The low content of particles and their restricted stability in the liquid phase are limitations that restrict possible utilization of colloids in various fields of applications such as photocatalysis, heat transfer and nanolubrication.[23–25] Synthesis of Ag particles in non-aqueous media is common but their long-term stabilization at high concentration is challenging.[26–29] Colloidal Ag particles are commonly produced via reduction of Ag ions using a suitable reducing agent such as sodium borohyride, ascorbic acid etc.[30–34]

Many researchers have been trying to develop hydrocarbon-based nanofluid systems because of their alleged impressive thermal properties.[35–37] However, hydrocarbons are flammable and therefore risky to use for high temperature applications. Another disadvantage of hydrocarbons is to find a suitable method to synthesize nanoparticles in these media because of the solubility problems of the available precursors. Achieving long term particle stability against precipitation is also difficult in hydrocarbons since efficient stabilizers that dissolve in such solvents are scarse. These drawbacks were the main reason for choosing PEG to serve as solvents and phase change materials (PCM) for nanofluid applications. Potential uses of PEG macromolecules as PCM has been investigated frequently in the last two decades particularly for thermal energy storage.[38,39] As shown in Tables 1 and 2 of the Introduction section, the polymers exhibit thermal

properties relevant to PCM applications that are only slightly inferior to those of commonly used hydrocarbons. In addition, blending of PEG macromolecules with different molar masses enables to widen considerably the range of accessible temperatures in which melting and freezing takes place.

The maximum nanoparticle loading achieved in aqueous systems was 0.1 M with a polydispersity of 53%.[2] No procedure for the synthesis of highly concentrated Ag colloids in PEG have been reported. An earlier study demonstrated that PEG of high molar mass was useful as a particle stabilizer and, at the same time, served as reductant of Ag^+ ions forming Ag crystalites in water.[40] The stabilization of metal nanoparticles is often achieved by various ligands and polymers, specially natural or synthetic polymers with a certain affinity toward metals. The most frequently used stabilizer for metal nanoparticles in polar solvents is poly(vinyl pyrollidone), PVP.[23,25] In this work, a procedure will be presented enabled the successful synthesis of highly concentrated and stable Ag particles in poly(ethylene glycol) with an average molar mass of 600 g/mol, or PEG 600, which is a liquid at room temperature. Metal concentrations of up to 10% by weight (1 M) in PEG 600 were accomplished via reduction of Ag(I) ions. PEG acted as both solvent and reducing agent whereas poly(vinyl pyrollidone) served as particle stabilizer. The crystallites consisted of fcc silver and exhibited a nearly spherical shape with an average diameter of 5.6 nm but crystallite aggregates with a mean diameter of 0.33 micron were also present in concentrated colloids. Only modest TC enhancements were determined at high particle concentrations but the Ag colloids exhibited excellent lubrication properties.

Experimental

$AgNO_3$ and $(NH_4)_2HPO_4$ were purchased from Fisher Scientific, - Carbowax PEG 600 (M.W. of 600 g/mol) was received from Electron Microscopy Sciences, poly(vinyl pyrollidone) with a molar mass of 10^4 g/mole was obtained from Polysciences and methyl acetate was from Alfa Aesar.

Absorption spectra were obtained using Shimadzu spectrophotometers models UV-2450 and UV-2501 PC. Direct imaging of colloidal particles in PEG was performed by means of a Cytoviva optical instrumentation. Images were captured with an an Olympus BX53 microscope equipped with a CytoViva 150 Darkfield condenser, a Solarc 24 light source together with CitoViva and Hyperspectral software; data analysis employed the Image J program. Liquid samples were placed between two specially cleaned Nexterion glass B microslides that were positioned in the microscope. This high resolution optical microscope possesses improved alignment and focus of dark-field illumination which enhances the signal-to-noise ratio and enables imaging of nanoscale materials. Transmission electron microscopy (TEM) measurements were carried out on dried colloidal samples using a ZEISS EM10 instrument operating at 80 kV. Samples were prepared by first precipitating the PVP coated particles using acetone. The coagulated particles were rinsed repeatedly with water and acetone to remove excess PEG 600, and then redispersed in methanol to a final concentration of 0.05 mM (dilution factor = 4000). A small droplet of the methanolic Ag solution was placed onto a carbon coated TEM grid and dried under vacuum. Samples were also prepared via first polymerization of the colloid in the presence of a resin called LR White, followed by slicing the resulting solid sample with a microtoming knife.

For XRD measurements particles were collected by precipitation with methyl acetate without removal of the PVP coating. Treatment of PVP coated particles with methyl acetate induces a decrease in the solubility of PVP, thereby precipitating the polymer out of the solution along with the particles. Redispersion of PVP coated particles can be achieved again in water or any other suitable solvents such as methanol, acetonitrile etc. The precipitated particles were collected and washed thoroughly several times with methyl acetate and dried before XRD measurements. Thermal conductivity (TC) tests were carried out using a TPS 500 hot disk thermal analyzer. Ethylene Glycol (EG) was used as a reference since this liquid possesses similar values of TC and viscosity as PEG. For TC measurements a sample of 6 mL was introduced into a glass pan during each measurement and with the aid of an Al stage the sample was placed into a temperature-controlled bath, followed by immersing perpendicularly a hot disk thermal probe . A HH11B thermocouple (Omega) with a k-type probe was used to record the measuring temperature. Viscosity determinations carried out by placing 20 mL of sample into the spindle holder of a Brookfield (DV-II+pro) viscometer.

Results and Discussion

A typical colloid synthesis involved first preparation of 18.5 mL of a 0.97 M solution of PVP (in terms of monomer concentration), which was accomplished via dissolving the polymer in PEG 600 at 40 ^{0}C for 20 min in an oil bath. Then the temperature of the PVP/PEG solution was raised to 110 ^{0}C followed by rapid addition of 2 mL of 3.13 M $AgNO_3$ dissolved in a mixture of ethylene glycol and water (1:1 volume ratio). The resulting solution, consisting of 0.2 M Ag and 0.9 M PVP in 20 mL, turned immediately dark red and total reduction of the silver ions was completed within 4 min. Silver colloids of a concentration of 1 M were also prepared following a

similar procedure except that the solutions contained 1.25 M PVP and that silver nitrate was dissolved in 4 mL of a ethylene glycol/water mixture with a 1:1 volume ratio.

Shown in Figure 2.1 are UV-Vis spectra recorded during the formation of silver particles via reduction of Ag^{+} ions in PEG 600 solutions containing PVP as a particle stabilizer. The spectra were acquired using solutions prepared by withdrawing samples from the hot reaction mixture and quenching them quickly in a water/ice mixture, followed by a 200 fold dilution with

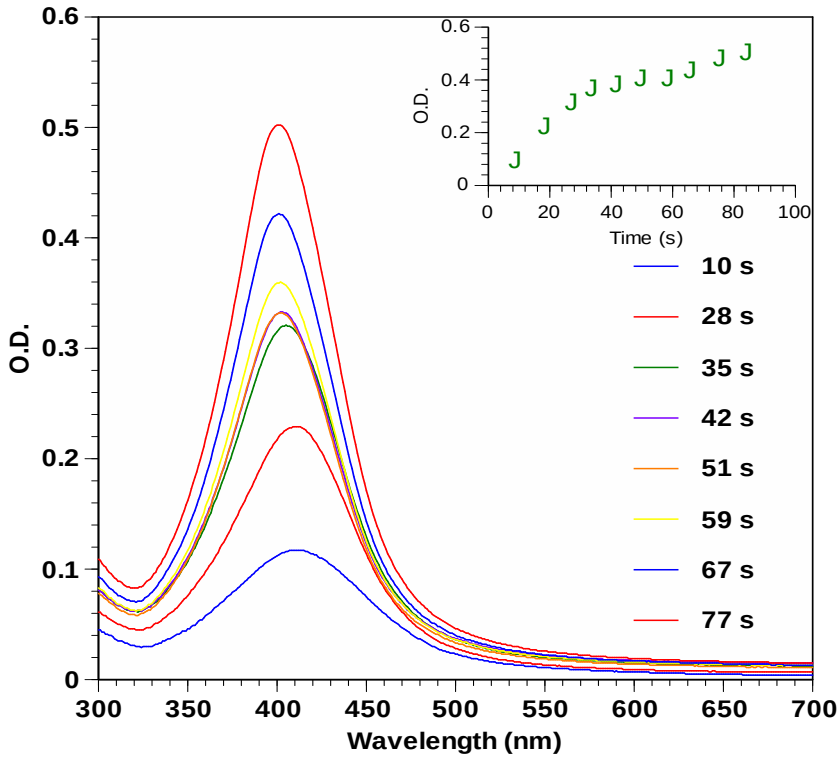

Figure 2.1: Spectral evolution with time during formation of Ag particles at 110 ^{0}C in a solution with 0.2 M $AgNO_3$ determined in a 1 cm quartz cell. Spectra were recorded after quenching samples withdrawn at different times and dilution by a factor of 200 with PEG 600.Inset shows the evolution of the optical density at 417 nm with time.

a solution of 0.9 M PVP in PEG 600. As illustrated in Figure 2.1 the optical signal was initially centered at a wavelength of maximum absorbance (λ_{max}) of about 417 nm. However, the absorbance shifted to shorter wavelength and gained in strength as the reduction proceeded, resulting in a signal with λ_{max} = 402 nm at the reaction end. Further evidence of the optical changes during the reaction is provided in the inset of Figure 2.1 depicting a non-linear evolution of the optical density recorded at 417 nm. Optical signals with λ_{max} in the range of 420-400 nm are frequently observed during the reduction of Ag^+ ions, which have been ~~is~~ attributed to the surface plasmon resonance due to collective oscillations of surface electrons. Blue shifts of λ_{max} together with a narrowing of the plasmon are also frequently detected,[39] which are similar to the spectral changes illustrated in Figure 2.1.

An unusual feature concerns the extinction coefficient (ε) of the colloids determined at λ_{max} = 402 nm after the particle formation process was completed. The value of the extinction coefficient varied significanltly for solutions with different initial [Ag^+]. For instance, colloids prepared from 10^{-2} M Ag^+ solutions resulted in ε = 10792 M^{-1} cm^{-1} after dilution within the range of 5 x $10^{-5} \leq [Ag] \leq 5 \times 10^{-4}$ M. On the other hand, colloids made from 0.2 M Ag^+ solutions yielded an ε value of 652 M^{-1} cm^{-1} when diluted to 5 x $10^{-4} \leq [Ag] \leq 2 \times 10^{-3}$ M. These findings suggested that at high concentrations the Ag particles experienced a change that altered their surfaces given that the plasmon signal is related to a collective oscillation of surface electrons. The origin of such changes will be discussed later in conjunction when the results of optical microscopy.

The completion of the reduction was tested by precipitating the particles from the solution at reaction times of 2, 3 and 4 min with the aid of methyl acetate. Particle precipitation resulted in clear solutions, which were then treated with an aqueous NaCl solution. Formation of a white

AgCl powder was noticed for samples collected after 2 and 3 minutes of heating. No such precipitation was observed from the samples retrieved after 4 min of heating, confirming the completion of the Ag^+ reduction process. The formation and growth of Ag nanoparticles are processes sensitive to the reaction temperature. If fact, after a very short period of reaction time nucleation and growth of silver particles may occur simultaneously. Determinations of the kinetics of particle formation using optical methods were not possible due to the ε variations mentioned before. In view of the high metal concentrations used during the colloid preparations, gravimetric determinations of the Ag mass generated allowed collection of kinetic data. For this purpose, samples were withdrawn from the hot reaction mixture at various time intervals and then cooled down by solidification with liquid nitrogen to stop further reaction. After melting the solids at room temperature, particle precipitation was accomplished via mixing with an aqueous $(NH_4)_2HPO_4$ solution followed by washing several times with water and acetone. Such method enabled selective particle precipitation without PVP, which remained disssolved in the water-PEG mixture. The samples were dried in a vacuum chamber and the mass of metallic silver was determined gravimetrically.

Reduction of Ag^+ was anticipated to occur according to reaction 1,

$$e^- + Ag^+ \rightarrow Ag\ (s) \qquad (1)$$

If Ag formation is described by a first-order rate law then:

$$d[Ag]/dt = -d[Ag^+]/dt = k\,[Ag^+] \qquad (2)$$

Since $[Ag^+] = [Ag^+]_0\, e^{-kt}$ and $[Ag] = [Ag^+]_0 - [Ag^+]$ then

$$\ln\{1- ([Ag]/[Ag^+]_0)\} = -kt \qquad (3)$$

According to this analysis a plot of ln{1- ([Ag]/[Ag^+]$_0$)} versus time was expected to yield a straight line with no intercept. As illustrated in Figure 2.2 a straight line was obtained from such a plot but the data followed the equation; y = -8 ×10^{-3} x - 0.25, r^2 = 0.99. Equation (3) predicts no intercept in contrast to results shown in the Figure, which can be traced to a systematic problem of the experimental procedure. The times utilized in the plot corresponds to the t values at which the samples were withdrawn from the hot solutions. However, about 20 s passed before the samples were completely frozen, meaning that some additional Ag^+ reduction took place during that period of time. Unfortunately the contribution of this additional reduction step is difficult to estimate given that the solution temperature remained undetermined. Nevertheless, the kinetic results are consistent with a first-order reaction that proceeded with a rate constant of 8 ×10^{-3} 1/s.

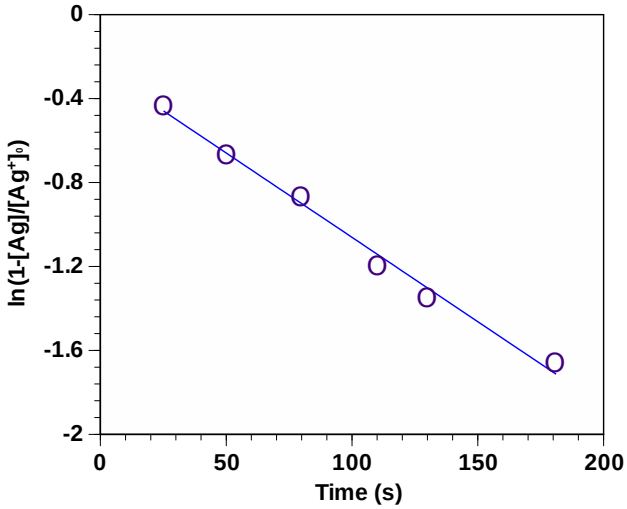

Figure 2.2; First-order plot of the formation of colloidal Ag. Particles produced at different time interval were precipitated using $(NH_4)_2HPO_4$ and the metal mass determined gravimetrically. The data followed the straight line equation: y = -8 ×10^{-3} x - 0.25, r^2 = 0.99.

XRD experiments were carried out to determine the nature of the solid obtained via precipitation of colloids utilizing methyl acetate as a coagulation agent. Cleaning of the precipitated solid was accomplished by rinsing them several times with H_2O and acetone. The presence of the (111), (200), (220) and (311) reflections from the fcc Ag crystal lattice in the XRD pattern depicted in Figure 2.3 confirmed that the precipitated material consisted of metallic silver crystallites. Small particles usually exhibit boad diffraction signals but only sharp diffraction peaks were detected, suggesting that crystallite agglomeration occurred during the precipitation process yielding large particles. Although no efforts were made to isolate the particles from PVP the diffractometer trace shown in Figure 1.3 was free from any other signals probably because of the amorphous nature of the polymer.

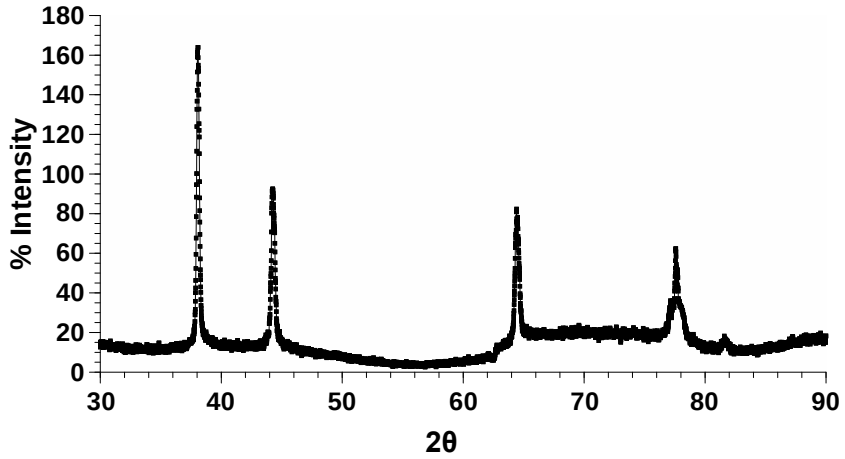

Figure 2.3: XRD pattern from a powder sample obtained via precipitation of a 0.2 M Ag colloid. The signals correspond to refelections from the Ag fcc crystal lattice structure listed on JCPDF card #4-783.

Since the number of Ag aggregates prevails over individual small particles at high concentration (Figure 2.4), the presence of aggregates were anticipated to be the reason for small extinction

value of AgPEG colloids at higher concentration. The aggregated particles may bind with PVP more efficiently and lower the intensity of Plasmon band of Ag particles.

Confirmation that the colloids consisted of small Ag particles was obtained from TEM analysis of samples prepared as described in the Experimental section. TEM images of the samples show that nearly spherical crystallites in the size range of 3-9 nm were present, see Figure 2.4. A histogram of size distribution was obtained by measuring the diameters of about 200 crystallites, yielding an average particle size of 5.6 nm. No significant deviations from the results of Figure 1.4 were obtained from TEM images of samples prepared by slicing the solid materials made via polymerization of the resin in the presence of dilute colloids. Furthermore, analogous particle diameters and size distributions were obtained when colloids prepared from either 200 or 10 mM Ag^+ solutions.

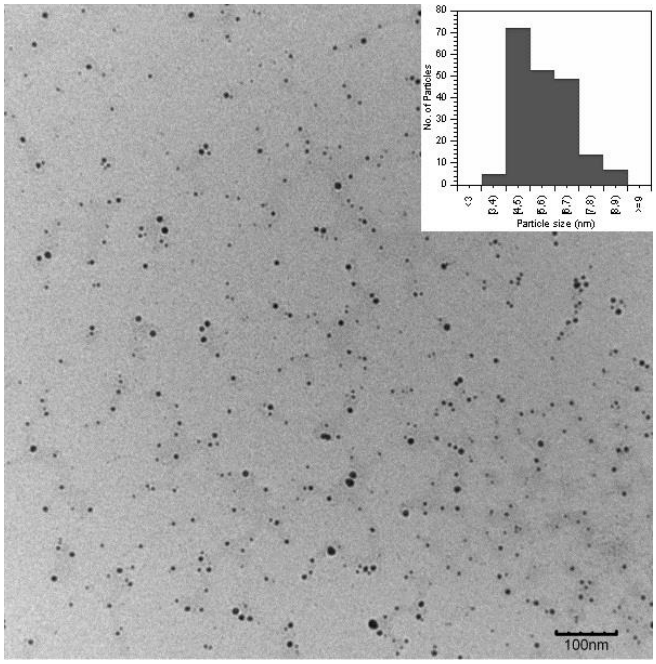

Figure 2.4: Transmission electron micrograph of Ag particles precipitated using acetone depicting a nearly spherical crystallite shape. The size bar equals 100 nm; inset shows the corresponding size histogram.

Analysis of the colloids was also attempted using CytoViva optical microscopy since this technique enables imaging liquid samples directly without the laborius sample preparation procedures needed for TEM measurements. Although the detection limit of this technique is about ≈ 10-20 nm for noble metals as described by manufacturer, colored spots resulting from light scattering due to metallic aggregates can be imaged.

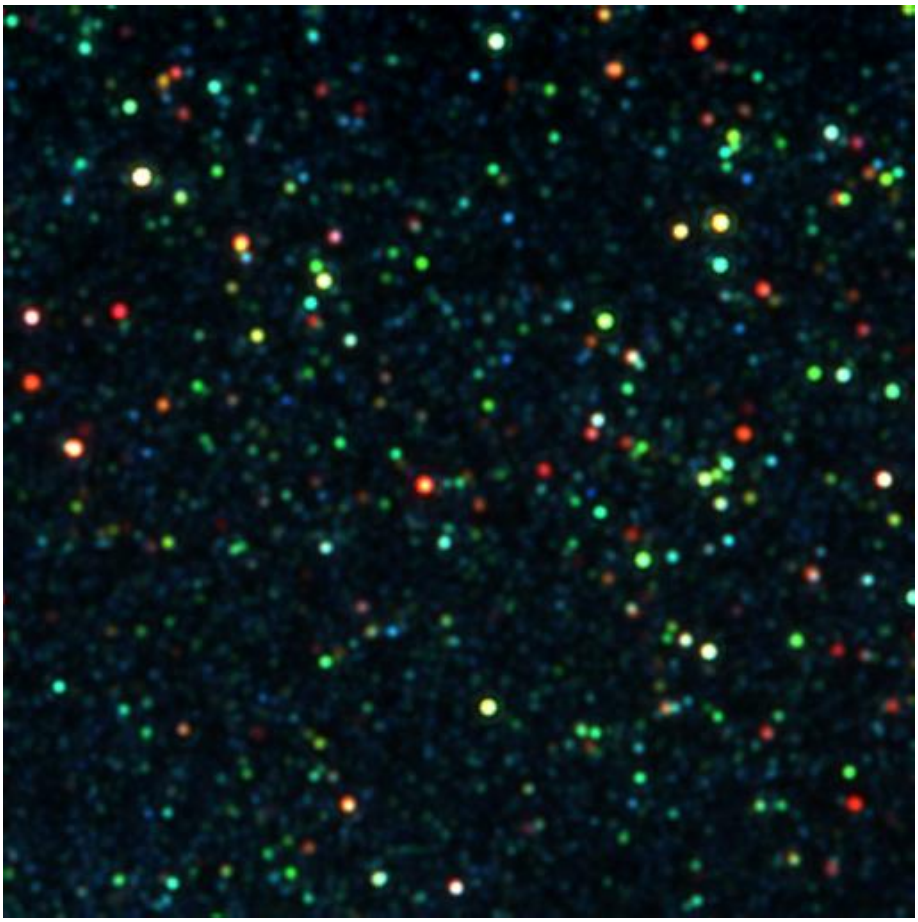

Figure 2.5: Dark field cytoviva optical image of a colloid prepared using 10 mM Ag^{+} solution, magnification 60X, the scale bar is 30 μm.

Figure 2.5 shows direct optical image obtained by placing a droplet of 10 mM freshly prepared colloid in a ultraclean microscopic slide. A typical optical image reveals several dots of different

colors. In dark field images the aggregates appeared as roughly spherical spots exhibiting blue, red, yellow and green colors. The appearance of different colors was due to light scattering from objects of different size. The blue colors was due to the objects of small size and larger objects shows green or red colors. Determination of the spot diameters was restricted to the smaller blue objects present in dark field images. The reason for such limitation is that larger colored spots showed a significant amount of glare that impeded precise determination of their diameters. Figures 2.6 (c) and (d) are size histograms for the smaller objects found in Figures 2.6 (a) and (b); an average size of 360 nm was determined for both colloids.

Hence, while the CytoViva technique is unable to produce images such as the one depicted in

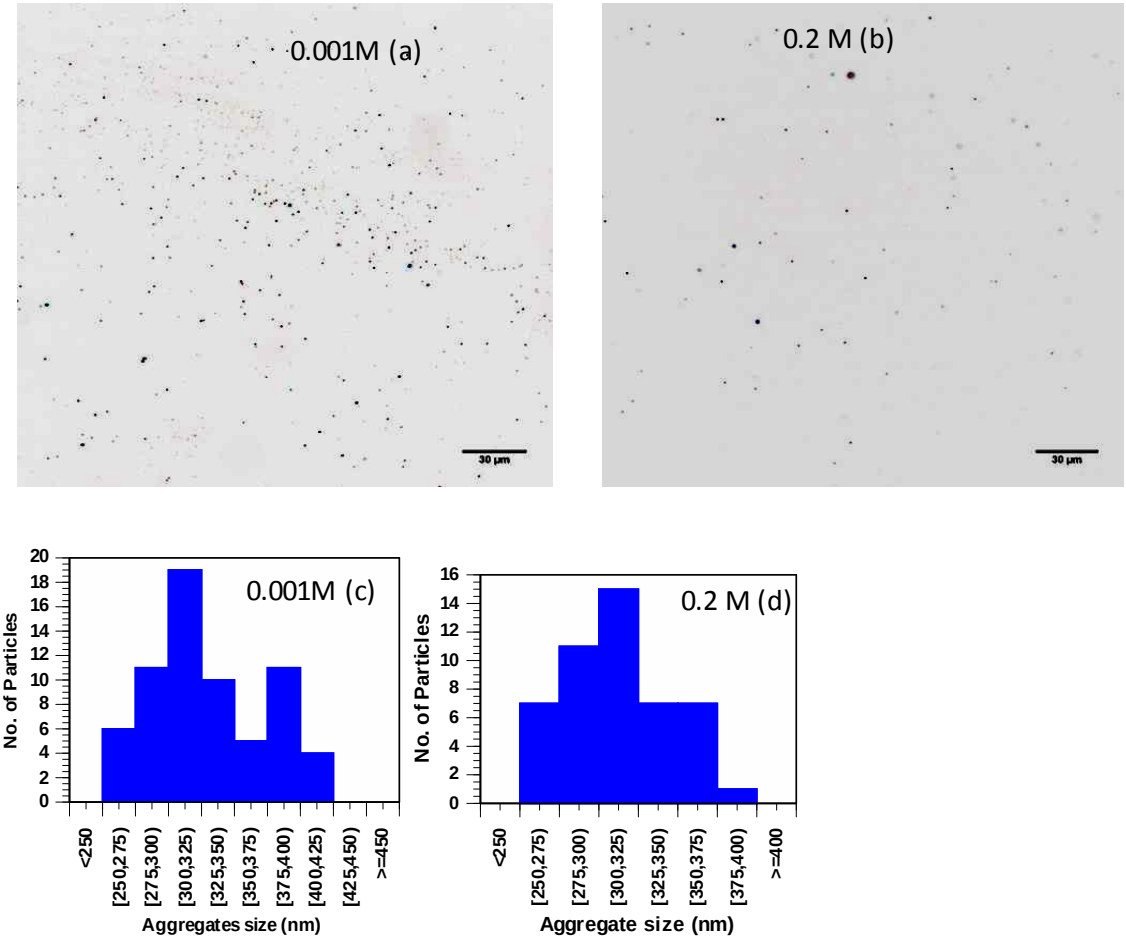

Figure 2.6: Bright field CytoViva images of (a) a colloid prepared using a 1 mM Ag^+ solution, magnification = 100X, the scale bar corresponds to 30 μm; (b) a colloid made from a 0.2 M Ag^+ solution, magnification = 40X, scale bar = 30 μm. Corresponding size histograms derived by analyzing about 200 aggregates: (c) derived from image (a), and (d) obtained from image (b).

figure 2.4, detection of particle aggregates seemed feasible. Shown in Figures 2.6 (a) and (b) are images obtained from two different colloids made via reduction of Ag^+ in solutions containing initially 1 and 200 mM $AgNO_3$. To facilitate visualization of the aggregates the images are presented in the bright field mode, which revealed the presence of objects with diameters in the hundreds of nm that were stable for more than eight months.

An obvious and significant difference of the CitoViva images shown in Figure 2.6 is that the number of objects noticed for the 1 mM colloid was considerably larger as compared to the case of the 200 mM sol. In fact, most of the aggregates detected in images captured from dilute sols appeared as smaller blue spots whereas concentrated colloids contained objects exhibiting mainly other colors. Such difference can be explained under the assumption that much higher concentrations of the smaller aggregates (with a blue color) were produced during preparation of concentrated colloids. Further aggregation of such small objects ensued, resulting in a preferential formation of larger aggregates. Experiments were, therefore, conducted in which concentrated colloids were diluted by a factor of 100 with a solution of PVP in PEG 600. Images very similar to that shown in Figure 2.6 (a) resulted from such experiments, supporting the idea that aggregation of the smaller Ag aggregates took place mainly in concentrated solutions.

The results from the dilution experiments also implied that the larger aggregates transformed (de-aggregated) into smaller objects upon dilution; Figure 2.7 is a scheme representing such a

process. The de-aggregation process is quite unusual given that aggregation of small metal crystallites is frequently irreversible, yielding large particles that precipitate out of solution.

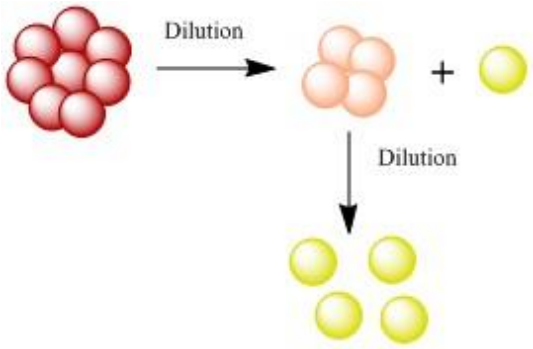

Figure 2.7: Scheme depicting the proposed fragmentation of large particle aggregates to form smaller aggregates as well as individual particles upon dilution.

Further confirmation that large aggregates were present in concentrated Ag colloids was provided by centrifugation experiments carried out between 1.5 to 3 x 10^4 rpm. Only large particle aggregates were anticipated to separate from solution and a small amount of metal was indeed precipitated at 3 x 10^4 rpm but only for concentrated colloids. As mentioned before, such Ag colloids exhibited an extinction coefficient of the plasmon with λ_{max} = 402 nm about 17 times smaller than the ε value of dilute sols. This difference persisted even after dilution of the concentrated sols to concentrations also accessible from the dilute colloids. An explanation for these results involves occurrence of chemical interface damping (CID), which has been documented extensively in the case of nm-sized Ag crystallites.[41] CID originates when the plasmon absorption is disrupted by adsorption of, for instance, oxidizers on the surface of the metal particles. Preparation of concentrated Ag colloids involved reduction of large amounts of Ag^+, resulting in high concentrations of oxidized reductant. Adsorption of the oxidized material

on the Ag surface would be favored under such conditions. Hence, the smaller ε value of concentrated colloids may result because of a CID effect derived from the experimental conditions required to generate concentrated colloids.

Both PEG and PVP have been used in water as reducing agents for the transformation of Ag^+ ions into metal crystallites.[42,43] Ag^+ can be reduced by polyethylene glycol directly at high temperature, but the reaction was significantly slower than in PEG 600 solutions also containing PVP. In fact, Ag^+ ions were reduced efficiently by PVP at room temperature whereas the equivalent reaction induced by PEG was very slow even at 40 ^{0}C. PVP contains a strong polar function (pyrollidone) and both the oxygen and nitrogen atoms of such group possess strong affinity toward metal ions and are available for coordination.[44] Hence, both PEG and PVP molecules may have acted as reducing agents that transformed Ag^+ into metal crystallites in the polymeric solvent.

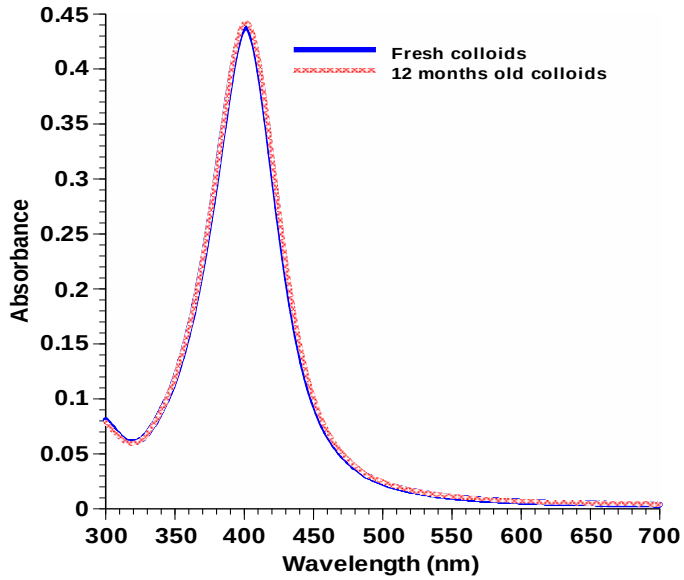

Figure 2.8: Spectra of the 1.0 M Ag colloids (dilution factor = 10^3) in PEG 600 at different time interval showing the particles stability in polymer solvent in presence of PVP.

The concentration of Ag particles can be increased up to 1.0 M (9.6 % by weight) in the PEG/PVP system. Such highly concentrated Ag colloids were still stable after 12 months (Figure 2.8). TEM analysis of the colloidal particles confirmed that the size distribution of the particles remained unchanged in such highly concentrated colloids although the were made with the same amount of stabilizer (PVP) as employed for the more dilute.

Upon heating 110 ^{0}C of 0.2 M AgPEG colloids for longer time, the yellowish red colloids changed in color to pink and further heating yielded green sols (Figure 2.9). TEM images obtained from the pink and green sols are presented in Figure 2.10. Analysis of the image shown in Figure 2.10(a) indicates that the heating process induced the particles within aggregates present in the original AgPEG colloids to fuse with each other, yielding the larger particles with irregular shapes noticed in the pink sols. Further heating of the pink colloids induced further particle growth, leading to the formation of semi-spherical or non-spherical Ag particles, Figure

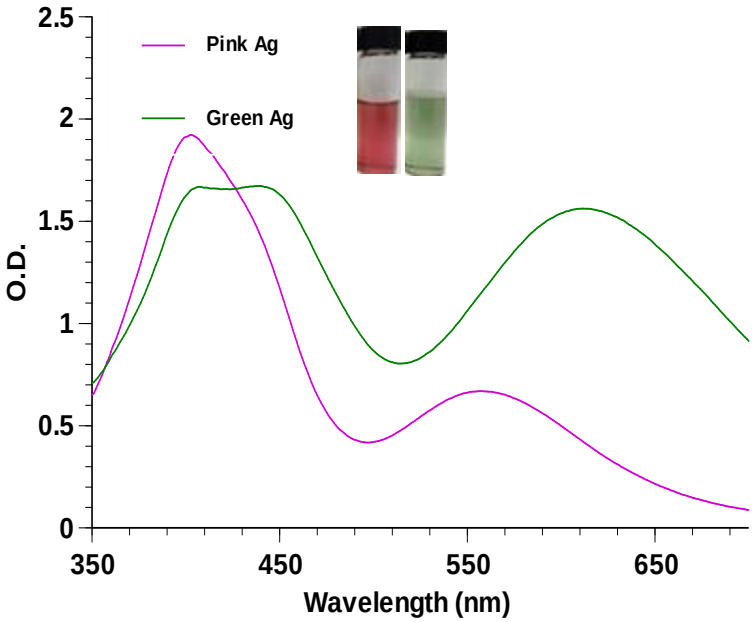

Figure 2.9: Evolution spectra offormation of pink Ag colloid (50 min at 110 ^{0}C) and green Ag colloid (70 min at 110 ^{0}C); Initial Conc. of $AgNO_3$ was 0.2M, Dilution Factor=200).

2.10(b). The color changes of Ag colloids due to the size and shape transformations has been reported previously.[45,46]

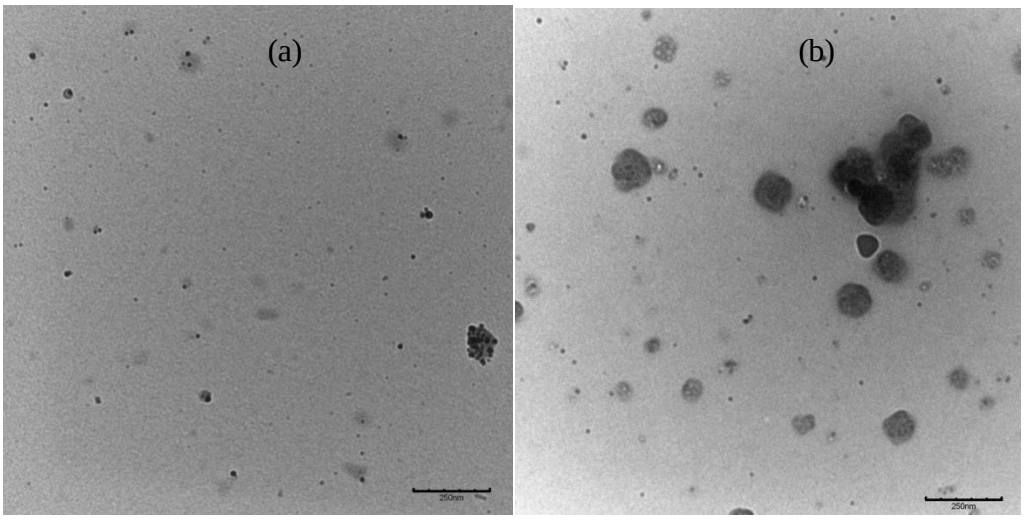

Figure 2.10:TEM images of pink (a) Ag colloids and (b) green Ag colloids formed at 110^0 C by heating 0.2 M AgPEG colloids for (a) 50 minutes and (b) 70 minutes.

Thermal conductivity (TC) tests were carried out by using the TPS 500 thermal analyzer. At each concentration and temperature, several measurements were carried out and the average values of thermal conductivity were taken to calculate overall TC enhancement. The data presented in Figure 2.11(a) indicates that the enhancement of TC depends linearly up to 0.2 M Ag. The subsequent decrease in TC at higher concentrations is attributed to the large increase in viscosity of the AgPEG colloidal system. The maximum TC enhancement obtained with the 0.2 M AgPEG system was 12.34 % at 25^{0}C (Figure 2.11 (a). Presented in Figure 2.11 (b) is the temperature dependence of the TC enhancement for 0.2 M and 1.0 M AgPEG colloids. For 0.2 M AgPEG colloids, the enhancement increases linearly with temperature and the maximum value was found to be 18.4% at 55 ^{0}C. Such values agree, within a factor of 2, with predictions

based on the classical formulations from Maxwell for dispersed metal particles.[3] With 1.0 M AgPEG colloids, the thermal conductivity is surprisingly very low and the TC value increases initially with temperature and then decreases. This unexpected decrease in thermal conductivity ~~is~~ may be due to the viscosity increase of 1.0 M Ag/PEG system or the interfacial thermal resistance offered by the solid Ag particles and liquid PEG medium.

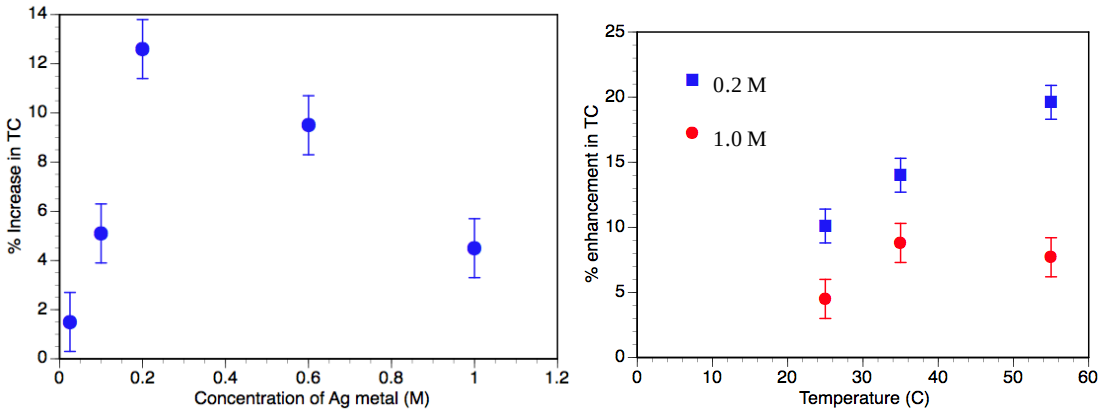

Figure 2.11: a) Variation of the percent increase in TC with Ag concentration at 25 ^{0}C. b) Temperature dependence of the percent increase in TC for 0.2 M and 1.0 MAgPEG colloids.

Figure 2.12 is a plot of viscosity against the concentration of Ag colloids. To determine the effect of PVP on the overall viscosity several PVP/PEG solutions were also used for viscosity measurements. Such blank experiments served elucidate if the viscosity increase was induced by the metal particles or by PVP. The results from Figure 2.12 clearly indicate that PVP induced a ~~has~~ negligible effect on the overall viscosity increase of the colloidal solution. A nonlinear relationship between shear viscosity and particle concentration exists, and the viscosity increases dramatically at very high concentrations of Ag particles. The dramatic increase of viscosity with particles concentration may be the reason for very low thermal conductivity at higher concentration of Ag particles in PEG600 solutions.

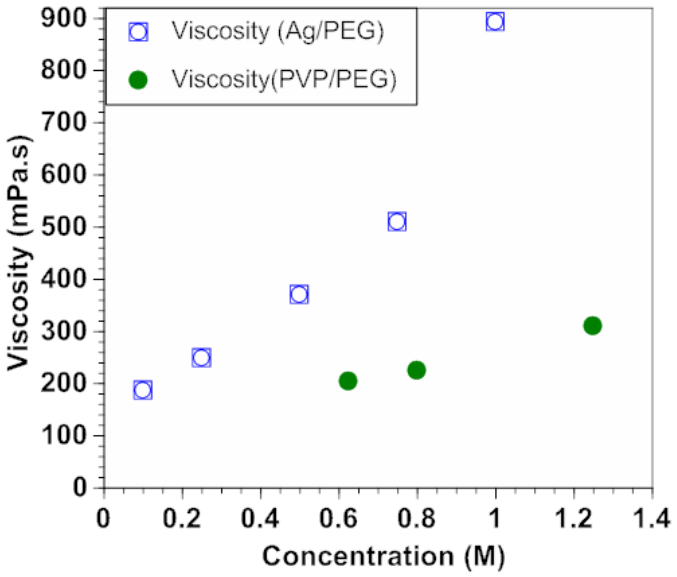

Figure 2.12: Viscosity increase with concentration of Ag (blue) and PVP (Green) at 25 ^{0}C.

Although the thermal conductivity enhancement by Ag colloids in PEG was found to be small, these sols were found to exhibit excellent tribological characteristics. PEG itself is considered as a good lubricant because of its low volatility and non-toxicity; incorporation of Ag particles induced a substantial decrease of both friction and wear coefficient (~ 35%). A thorough investigation on the promising lubrication properties of the colloids have been presented in a recent publication.[47]

Conclusions:

Ag Colloids containing large particle concentrations can be prepared using solutions of PVP in PEG600. The stabilization of highly concentrated colloidal particles was achieved mainly due to the stabilizing ability of Polyvinyl Pyrollidone whereas PEG600 served as the solvent. At very high concentrations aggregates of particles coexist at equilibrium with individual small

crystallites. The large amounts of crystallites and particle aggregates present in the colloids excerted a small increase in the overall thermal conductivity of nanofluids, which are within the exhancement anticipated according to Maxwell formulations.. However, at very high concentrations (> 0.2 M), the thermal conductivity of these nanofluid systems was found to decreased perhaps due to the combined effects of increase in viscosity and interfacial thermal resistance between solid-liquid interfaces. At high concentrations, the number of particles is large and therefore, interfacial thermal resistance will also increase accordingly. However, Ag PEG colloids exhibit excellent lubrication properties even at low concentration of particles.

References:

1. Garimella, S. V, Sobhan, C. B. Transport in Microchannels – a critical review. *Annu. Rev. heat transf.;* **2003**, 13, 1-50.
2. Wang, W.; Gu, B. Preparation and Characterization of Silver Nanoparticles at High Concentrations. *ACS Symposium Series***,** Wahington DC, **2004**, 1–14.
3. Eapen, J.; Rusconi, R.; Piazza, R.; Yip, S. The Classical Nature of Thermal Conduction in Nanofluids. *J. Heat* Transfer **2010**, *132*, 102402.
4. Ozerinc S.; Kakac, S.; Yazicloglu, A. G. Enhanced Thermal Conductivity of Nanofluids: A State-of-the-Art Review. *Microfluid. Nanofluid.* **2009**, *8*, 145–170.
5. Chopkar, M.; Das, P. K.; Manna, I. Synthesis and Characterization of Nanofluid for Advanced Heat Transfer Applications. *Scr. Mater.* **2006**, *55*, 549–552.
6. Eapen, J.; Li, J.; Yip, S. Beyond the Maxwell Limit: Thermal Conduction in Nanofluids with Percolating Fluid Structures. *Phys. Rev. E - Stat. Nonlinear, Soft Matter Phys.* **2007**, *76*, 1–4.
7. Eastman, J. A.; Choi, S. U. S.; Li, S.; Yu, W.; Thompson, L. J. Anomalously Increased Effective Thermal Conductivities of Ethylene Glycol-Based Nanofluids Containing Copper Nanoparticles. *Appl. Phys. Lett.* **2001**, *78*, 718–720.
8. Hong, T.; Yang, H.; Choi, C. Study of the Enhanced Thermal Conductivity of Fe Nanofluids. *J. Appl. Phys.* **2005**, *97*, 64311.

9. Jana, S.; Salehi-Khojin, A.; Zhong, W. H. Enhancement of Fluid Thermal Conductivity by the Addition of Single and Hybrid Nano-Additives. *Thermochim. Acta* **2007**, *462*, 45–55.
10. Jang, S. P.; Choi, S. U. S. Role of Brownian Motion in the Enhanced Thermal Conductivity of Nanofluids. *Appl. Phys. Lett.* **2004**, *84*, 4316–4318.
11. Kang, H. U.; Kim, S. H.; Oh, J. M. Estimation of Thermal Conductivity of Nanofluid Using Experimental Effective Particle Volume. *Exp. Heat Transf.* **2006**, *19*, 181–191.
12. Keblinski, P.; Phillpot, S. R.; Choi, S. U. S.; Eastman, J. A. Mechanisms of Heat flow in Suspensions of Nano-Sized Particles (Nanofluids). **2002**, *45*, 855–863.
13. Patel, H. E.; Sundararajan, T.; Das, S. K. A Cell Model Approach for Thermal Conductivity of Nanofluids. *J. Nanoparticle Res.* **2008**, *10*, 87–97.
14. Philip, J.; Shima, P. D.; Raj, B. Evidence for Enhanced Thermal Conduction through Percolating Structures in Nanofluids. *Nanotechnology* **2008**, *19*, 305706.
15. Prasher, R.; Bhattacharya, P.; Phelan, P. E. Thermal Conductivity of Nanoscale Colloidal Solutions (Nanofluids). *Phys. Rev. Lett.* **2005**, *94*, 3–6.
16. Prasher, R.; Evans, W.; Meakin, P.; Fish, J.; Phelan, P.; Keblinski, P. Effect of Aggregation on Thermal Conduction in Colloidal Nanofluids. *Appl. Phys. Lett.* **2006**, *89*, 143119.
17. Shaikh, S.; Lafdi, K.; Ponnappan, R. Thermal Conductivity Improvement in Carbon Nanoparticle Doped PAO Oil: An Experimental Study. *J. Appl. Phys.* **2007**, *101, 064302*.
18. Wang, B. X.; Zhou, L. P.; Peng, X. F. A Fractal Model for Predicting the Effective Thermal Conductivity of Liquid with Suspension of Nanoparticles. *Int. J. Heat Mass Transf.* **2003**, *46*, 2665–2672.

19. Choi, S. U. S. The Role of Interfacial Layers in the Enhanced Thermal Conductivity of Nanofluids: A Renovated Maxwell Model. *J. Nanoparticle Res.* **2003**, *5*, 167–171.

20. Warrier, P.; Teja, A. Effect of Particle Size on the Thermal Conductivity of Nanofluids Containing Metallic Nanoparticles. *Nanoscale Res. Lett*. **2011**, *6*, 247.

21. Timofeeva, E. V.; Routbort, J. L.; Singh, D. Particle Shape Effects on Thermophysical Properties of Alumina Nanofluids. *J. Appl. Phys.* **2009**, *106*, 1–10.

22. Sundar, L. S.; Singh, M. K.; Ramana, E. V.; Singh, B.; Gracio, J.; Sousa, A. C. M. Enhanced Thermal Conductivity and Viscosity of Nanodiamond-Nickel Nanocomposite Nanofluids. *Sci. Rep.* **2014**, *4*, 4039.

23. He, B.; Tan, J. J.; Liew, K. Y.; Liu, H. Synthesis of Size Controlled Ag Nanoparticles. *J. Mol. Catal. A Chem*. **2004**, *221*, 121–126.

24. He, S.; Chen, H.; Guo, Z.; Wang, B.; Tang, C.; Feng, Y. High-Concentration Silver Colloid Stabilized by a Cationic Gemini Surfactant. *Colloids Surfaces A* **2013**, *429*, 98–105.

25. Pastoriza-Santos, I.; Liz-Marzan, L. M. Formation of PVP-Protected Metal Nanoparticles in DMF. *Langmuir*, **2002**, 2888–2894.

26. Singh, A. K.; Raykar, V. S. Microwave Synthesis of Silver Nanofluids with Polyvinylpyrrolidone (PVP) and Their Transport Properties. *Colloid Polym. Sci.* **2008**, *286*, 1667–1673.

27. Sharma, P.; Baek, I.-H.; Cho, T.; Park, S.; Lee, K. B. Enhancement of Thermal Conductivity of Ethylene Glycol Based Silver Nanofluids. *Powder Technol.* **2011**, *208*, 7–19.

28. Chang, G.; Luo, Y.; Lu, W.; Liao, F.; Sun, X. Hydrothermal Synthesis of Ultra-Highly Concentrated, Well-Stable Ag Nanoparticles and Their Application for Enzymeless Hydrogen Peroxide Detection. *J. Nanoparticle Res.* **2011**, *13*, 2689–2695.

29. Lee, B.-H.; Hsu, M.-S.; Hsu, Y.-C.; Lo, C.-W.; Huang, C.-L. A Facile Method To Obtain Highly Stable Silver Nanoplate Colloids with Desired Surface Plasmon Resonance Wavelengths. *J. Phys. Chem.* C **2010**, *114*, 6222–6227.

30. Nickel, U.; Castell, A.; Po, K.; Schneider, S. A Silver Colloid Produced by Reduction with Hydrazine as Support for Highly Sensitive Surface-Enhanced Raman. *Langmuir,* **2000**, 9087–9091.

31. Leopold, N.; Lendl, B. A New Method for Fast Preparation of Highly Surface-Enhanced Raman Scattering (SERS) Active Silver Colloids at Room Temperature by Reduction of Silver Nitrate with Hydroxylamine Hydrochloride. *J. Phys. Chem.* B **2003**, *107*, 5723–5727.

32. Khanna, P. K.; Subbarao, V. V. V. S. Nanosized Silver Powder via Reduction of Silver Nitrate by Sodium Formaldehydesulfoxylate in Acidic pH Medium. *Mater. Lett.* **2003**, *57*, 2242–2245.

33. Sondi, I.; Goia, D. V; Matijevic, E. Preparation of Highly Concentrated Stable Dispersions of Uniform Silver Nanoparticles. *J. Colloid Interface Sci.* **2003**, *260*, 75–81.

34. Li, D.; Xie, W.; Fang, W. Preparation and Properties of Copper-Oil-Based Nanofluids. *Nanoscale Res. Lett*. **2011**, *6*, 373.

35. Fang, X.; Fan, L.-W.; Ding, Q.; Wang, X.; Yao, X.-L.; Hou, J.-F.; Yu, Z.-T.; Cheng, G.-H.; Hu, Y.-C.; Cen, K.-F. Increased Thermal Conductivity of Eicosane-Based Composite Phase Change Materials in the Presence of Graphene Nanoplatelets. *Energy &* Fuels **2013**, *27*, 4041–4047.

36. Nabil, M.; Khodadadi, J. M. Experimental Determination of Temperature-Dependent Thermal Conductivity of Solid Eicosane-Based Nanostructure-Enhanced Phase Change Materials. *Int. J. Heat Mass Transf*. **2013**, *67*, 301–310.

37. Qi, G.-Q.; Liang, C.-L.; Bao, R.-Y.; Liu, Z.-Y.; Yang, W.; Xie, B.-H.; Yang, M.-B. Polyethylene Glycol Based Shape-Stabilized Phase Change Material for Thermal Energy Storage with Ultra-Low Content of Graphene Oxide. *Sol. Energy Mater. Sol. Cells* **2014**, *123*, 171–177.

38. Meng, Q.; Hu, J. A Poly(ethylene Glycol)-Based Smart Phase Change Material. *Sol. Energy Mater. Sol. Cells* **2008**, *92*, 1260–1268.

39. Panacek, A.; Kvitek, L.; Prucek, R.; Kolar, M.; Vecerova, R.; Pizurova, N.; Sharma, V. K.; Nevecna, T.; Zboril, R. Silver Colloid Nanoparticles: Synthesis, Characterization, and Their Antibacterial Activity. *J. Phys. Chem*. B **2006**, *110*, 16248–16253.

40. Longenberger, L.; G. Mills; Formation of Metal Particles in Aqueous Solutions by Reactions of Metal Complexes with Polymers. *J. Phys. Chem*. **1995**, *99*, 475-478.

41. Kreibig U.; Vollmer, M. *Optical Properties of Metal Clusters*; Springer-Verlag: Berlin, 1995; pp. 380-387.

42. Hoppe, C. E.; Lazzari, M.; Pardiñas-Blanco, I.; Lopez-Quintela, M. A. One-Step Synthesis of Gold and Silver Hydrosols Using poly(N-Vinyl-2-Pyrrolidone) as a Reducing Agent. *Langmuir* **2006**, *22*, 7027–7034.

43. Kan, C.; Cai, W.; Li, C.; Zhang, L. Optical Studies of Polyvinylpyrrolidone Reduction Effect on Free and Complex Metal Ions. *J. Mater. Res.* **2011**, *20*, 320–324.

44. Pileni, M.-P. The Role of Soft Colloidal Templates in Controlling the Size and Shape of Inorganic Nanocrystals. *Nat. Mater.* **2003**, *2*, 145–150.

45. Zielińska, A.; Skwarek, E.; Zaleska, A.; Gazda, M.; Hupka, J. Preparation of Silver Nanoparticles with Controlled Particle Size. *Procedia Chem.* **2009**, *1*, 1560–1566.

46. Barlak, S.; Sara, O. N.; Karaipekli, A.; Yapıcı, S. Thermal Conductivity and Viscosity of Nanofluids Having Nanoencapsulated Phase Change Material. *Nanoscale Microscale Thermophys. Eng.* **2016**, *20*, 85–96.

47. Ghaednia, H.; Hossain, M. S.; Jackson, R. L. Tribological Performance of Silver Nanoparticle-Enhanced Polyethylene Glycol Lubricants. *Tribol. Trans.* **2015**, *2004*, 585-592.

Chapter III

Stable Colloidal CuO Nanorods in Alkanes and Their Transformation to Spherical Metallic Copper

Introduction

The ability to dissipate heat quickly has become an important technical challenge with the current fast progress in technological development. Faster cooling is essential for both solid state devices and industrial reactors in order to achieve better efficiency.[1] One of the most important limiting factors to achieve faster cooling in various industries is the poor thermal properties such as thermal storage and conductivity of conventional heat transfer fluids. For example, the thermal conductivity of paraffin wax is very low, amounting to only 0.21-0.24 W/mK.[2]

Materials with high enthalpy of fusion can absorb tremendous amount of heat during melting and then releases stored energy when they solidify. Such energy storage media are called phase change materials (PCM),[3] which possess impressive thermal properties in the solid state including high thermal conductivity and thermal diffusivity. Numerous different PCM are available for thermal energy storage including organic materials (such as paraffin and fatty acids/esters) and inorganic compounds including hydrates.[3,4] However, application of PCM in numerous fields has been constraint because of their poor thermal conductivity in the fluid form. Since solid materials possess extremely high thermal conductivities as compared to conventional fluids, liquids containing suspended small solid particles were expected to show higher thermal conductivity than in the absence of the dispersed material.[5,6] Such dispersions are called nanostructure enhanced phase change materials (NePCM)[7]. The nanoparticles additives are expected to enhance thermal conductivity of the PCM not only when present as solids but also during phase change and in the fluid region.

Introduction of small particles into fluids can be achieved by various physical[2,8] and chemical[9–11] approaches. An example of a physical method is ultrasound vibration, often used to maintain homogeneity of the dispersions but this procedure requires repetitive use of an external power source. Moreover, such particle dispersions are both thermodynamically and kinetically unstable due to particle-particle clustering or aggregation and eventually precipitation out of solution due to gravity. Colloidal small particles dispersed in liquid media are expected to be a reasonable alternative to overcome this issue.[6] Small colloidal particles of metal or metal oxide are also thermodynamically unstable in fluids but they can be stabilized kinetically for a certain period of time by means of a third entity which interacts with solid-liquid interfaces. To be most effective, kinetic stabilization of colloidal particles requires extremely low concentrations of the dispersed material. At high concentrations particle aggregation is prominent due to increased effective interparticle collisions that lead to aggregation.

Utilization of highly concentrated colloids were neglected because of the difficulty of stabilization of particles at high concentration and thought to be unfeasible. Clary *et al*, [12] showed that a very high concentration of suspended spherical CuO particles in alkanes (that function as PCM) can be achieved provided that the particles are highly pure and well coated by organic ligands.[12] They found that particles of high concentration (5 wt%) can be stabilized for more than a year. Despite the promising properties of the resulting colloids, these NePCM showed little enhancement of thermal conductivity (~7%).

Furthermore, the morphology of small colloidal particles was assumed to also exert an effect on overall thermal conductivity enhancement of NePCM. To date, CuO particles of different sizes and shapes, such as spheres[12], rods[13,14], wires[15], sheets[16] and hollow structure,[17] were produced in laboratories using a wide variety of chemical and physical methods. Experiments with unstable

suspensions seemed to indicate that nanorods, nanorhombics or nanowires showed exceedingly better TC enhancement as compared to spherical particles[18]. There is no single model able to explain the wide spectrum of thermal conductivity data for solid-liquid systems. Nevertheless, nanorods, or any other (one-dimensional) 1D nanostructures, were expected to yield higher TC enhancements in fluids as compared to spheres because 1D nanostructures would provide a directional force field for effective thermal conduction.

Synthesis of colloidal nanorods of long term stability is extremely difficult to achieve and has only been observed for rods with minute lengths and at very low concentrations[19]. Herein, we provide a combined physical and chemical approach to produce colloidal CuO nanorods that remained stable in solution for up to 2 months. A useful starting point for the synthesis of CuO nanorods was the work of Li and Chang, which produced mixtures of spherical and rod-shaped crystallites.[81]. Modification of the procedure was necessary to obtain clean and stable rods with ~~of~~ ~ 100% yield. Synthesis of sodium oleate (SOA) coated rodlike CuO particles involves three steps: (1) preparation of bare CuO particles, (2) synthesis of an anionic surfactant via a two-phase reaction of oleic acid (OA) and NaOH, followed by particle stabilization using the SOA surfactant as stibilizer in basic solution, and (3) post-processing together with purification for subsequent re-dispersion of well-coated CuO rods (CuO/SOA) in alkane-based solvents. Octane and tetradecane (TD) were selected as dispersion media for CuO rods, because they are short-chain analogues of paraffins used for PCM applications. Another simple approach employed ~~of~~ oleoyl sarcosine (OS) as a stabilizer yielding coated CuO (CuO/OS) in tetradecane, but this method produced irregular rodlike particles with high aspect ratio. Attempts were also made to achieve stable metallic Cu nanorods via *in situ* reduction of CuO/SOA rods prepared in TD by means of the an organometallic reagent sodium bis(2-methoxyethoxy) aluminumhydride, known

as Red-Al that is soluble in alkanes. Although the reduction tales place this reaction induced a shape change of the oxide nanorods forming spherical metal particles.

The resulting colloids were characterized using UV-Visible spectral measurements, which also served to test the long term stability of rods. Further characterizations of the CuO rods employed transmission electron microscopic (TEM) and X-ray diffraction (XRD) methods. Thermal conductivity (TC) enhancements induced by the rods were found to be better as compared to the changes noticed with spherical particles but still poor in terms of the increases needed for high temperature applications.

Materials and methods:

Copper (II) nitrate hemi-pentahydrate (> 98%) was purchased from Acros Organics, OS was from TCI America, oleic acid was from Fisher Scientific, tetradecane was from Alfa Aesar, sodium hydroxide micropills (> 98.5 %) and anhydrous octane (> 99%) were obtained from Sigma Aldrich.

Absorbance spectra were recorded on a Shimadzu UV- 2450 spectrophotometer using 1 cm quartz cells. TEM measurements were carried out using dried colloidal samples on a ZEISS EM10 instrument operating at 80 kV. XRD determinations were performed on a Rigaku Ultima diffractometer without removal of the strongly bound oleate ligands. Thermal conductivity tests were carried out by means of a TPS 500 hot disk thermal analyzer. Atomic absorption analysis of the particles was carried out by using a Varian AA240 atomic absorption spectrometer.

(a) Preparation of bare CuO particles:

The synthesis of bare CuO particles proceeded according the following reaction:

$$Cu(NO_3)_2\ (aq) + 2\ NaOH\ (aq) \rightarrow CuO\downarrow + 2\ NaNO_3\ (aq) + H_2O\ (l) \quad (3.1)$$

An Erlenmeyer flask containing 100 mL of DI water was submerged in a hot oil bath at 90°C followed by addition of 10 g of $Cu(NO_3)_2 \cdot 2.5H_2O$. The solution was heated for ~10 min until the temperature returned to ~90 °C (the dissociation of the cupric salt is endothermic), followed by addition of 3.61 g NaOH to yield a Cu (II) : NaOH mole ratio of 2.1:1. The resulting mixture was allowed to react at that temperature for 45 min. After removing the flask from the oil bath the solution was cooled to room temperature prior to filtering with a Hirsch funnel equipped with #4 Whatman filter paper (diameter = 15 cm). The filtrate was rinsed three times with 50 mL aliquots of DI water then dried at room temperature under air. After drying, the product was ground to a fine powder with a mortar and pestle prior to storage.

(b) Preparation of Sodium Oleate (SOA) and CuO/SOA

Sodium oleate was prepared by a simple two-phase equimolar reaction of oleic acid and sodium hydroxide. (OA is abbreviated as R—COOH):

$$R—COOH + NaOH \rightarrow R—COO^-Na^+ + H_2O \quad (3.2)$$

100 mL of DI water were placed in a 125 mL Erlenmeyer flask and 0.298 g of NaOH (74.5 mM) were then dissolved. The flask was brought to ~90 °C in the oil bath whereupon 2.0 g of OA (70.8 mM) were added directly. OA does not dissolve in water but forms water soluble sodium oleate by reacting with NaOH; this reaction required 30 minutes to reach completion at 90 °C.

This was followed by addition of 1.0 g of finely ground black CuO powder to the above basic surfactant solution. A chocolate-brown color immediately appeared but after continued stirring, small, brown particles were observed (~2-3 min). Surfactant-coated CuO particles were generated after heating at 90 °C for 40 min; the resulting mixture was then cooled down to room temperature. The coated particles were found to be stable in basic solution indefinitely.

(c) Purification & re-dispersion in Alkane:

A subsequent step consisted of adding 300 mL of methanol into 100 mL of the solution that contained the surfactant-coated CuO particles. Addition of methanol helps to reduce solvent polarity and induced the surfactant-coated CuO particles to form flakes, which precipitated out of the solution upon vigorous stirring. The precipitate was separated and washed several times first with ethanol and then with water to remove excess ions. Addition of 50 mL of chloroform enabled re-dispersion of the coated particles. The chloroform-based solution was then taken into a separatory funnel and 200 mL of water were added, followed by shaking the resulting mixture to remove possible remnant ions adhered to the particles. Complete separation of the aqueous and chloroform phases was achieved by leaving the biphasic solution in the funnel for an hour.

The chloroform-based solution of coated particles was then separated and dried at room temperature under air. Dispersion of cleaned, coated CuO particles can be easily achieved by dissolving a certain amount of powder in a known amount of alkane via sonication for 5 minutes.

Presented in Figure 3.1 is a diagram of the complete synthetic and purification process that yielded CuO/SOA rods.

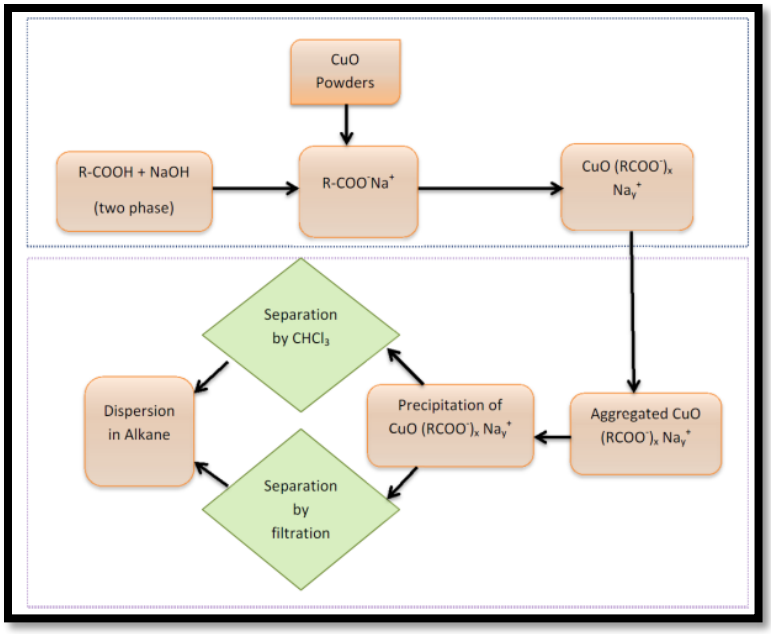

Figure 3.1: Synthetic and purification protocol for CuO/SOA rods and dispersion in alkanes.

The concentration (as mass %) of Cu present in colloids containing CuO/SOA rods was determined using atomic absorption (AA) spectroscopy. In order to perform the compositional analysis 4 standard samples of $CuCl_2$ were used to prepare a calibration curve. As shown in Figure 3.2, an excellent linearity of the absorbance versus Cu^{2+} concentration was obtained upon dissolving $CuCl_2$ in HCl within the range of 1 to 11 ppm of metal ion. To assay the amount of metal ions present in the colloid an aliquot was precipitated by acetone and washed. In a subsequent step a known amount of CuO/SOA powder was dissolved in 0.1 M HCl to yield 7.31 ppm of Cu^{2+}. This procedure assumed that the mass of CuO/SOA corresponded mainly to CuO, meaning that the amount of SOA present in the sample was considered negligible as compared with the quantity of oxide present. Included in the data of Figure 3.2 is the result obtained during the assay of a CuO/SOA colloid, corresponding to 6.31 ppm (red symbol) of Cu^{2+}. Thus, the difference between the theoretical value (7.31), which neglected the contribution of the

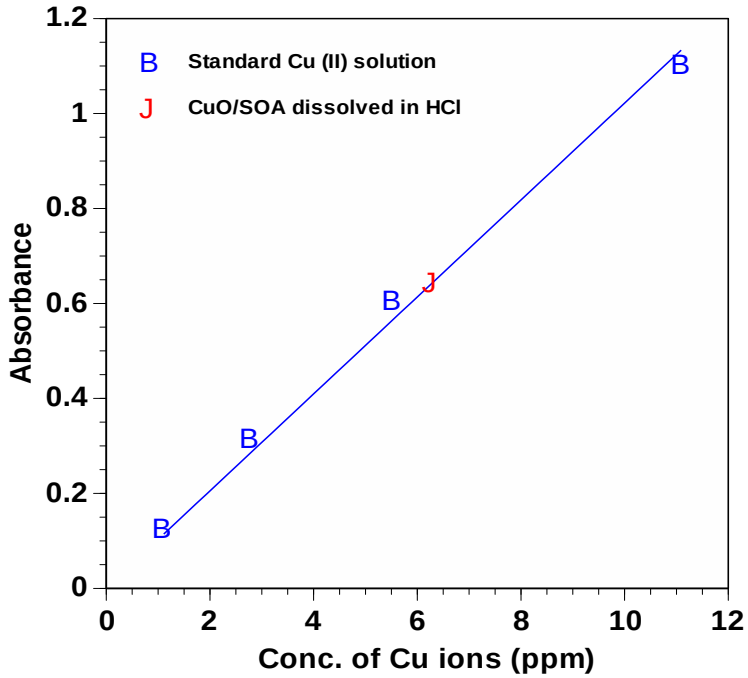

Figure 3.2: AA calibration curve and determination of the Cu^{2+}content in the CuO/SOA colloid.

surfactant, and the experimental finding corresponded to the mass of bound oleate ligands.

Synthesis of OS coated CuO rods:

Bare CuO particles were synthesized using a method similar to the one mentioned above. A 30.0 mL of a 0.25 M OS solution in tetradecane was kept in an oil bath at 180 ^{0}C for 30 min. To obtain a 0.1 M CuO colloid, 0.239 g of clean, dried and meshed CuO powder were introduced in the OS solution and left at 180 ^{0}C for 40 min, then the flask was cooled to room temperature. Similarly, colloids with 0.5 M and 1.0 M CuO were prepared keeping a constant concentration ratio of OS to CuO equal to 2.5.

Results and discussion:

The synthesized CuO rods were first characterized by UV-Visible spectrophotometry. The rods were found to absorb at two distinct wavelengths unlike spherical particles. Spheres absorb only at 285 nm reported before[12] which was characteristic absorption band for CuO particles regardless of size and shape. However, an additional exciton band was observed in the absorption spectrum of the newly synthesized rod-shaped particles at 350 nm. This optical signal is easily recognized in Figure 3.4, which depicts a comparison of the optical spectra

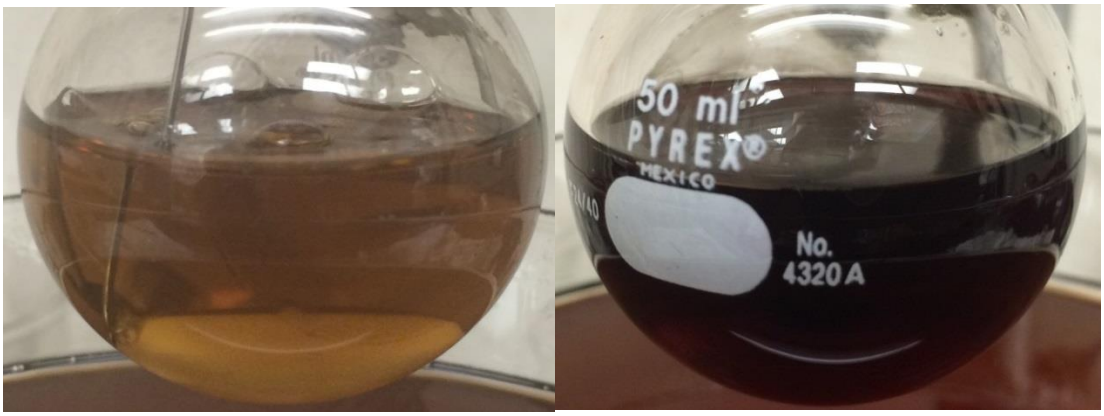

Figure 3.3: Visual color change during reduction of brownish CuO rods (left) into dark red metallic Cu (right).

measured for spherical (blue curve) and rod-shaped CuO crystallites, red curve. These results clearly indicate that the particles formed by means of the new synthetic process exhibit a shape other than spherical. The nominal composition of coated CuO/SOA colloids, calculated to be 84.11% by mass of CuO and 15.89% of oleate, was confirmed experimentally using AA analysis (Figure 3.2).

The crystallinity of the CuO material was tested by means of powder XRD after floculation of the colloidal particles from TD. Acetone was employed as the precipitating agent but this

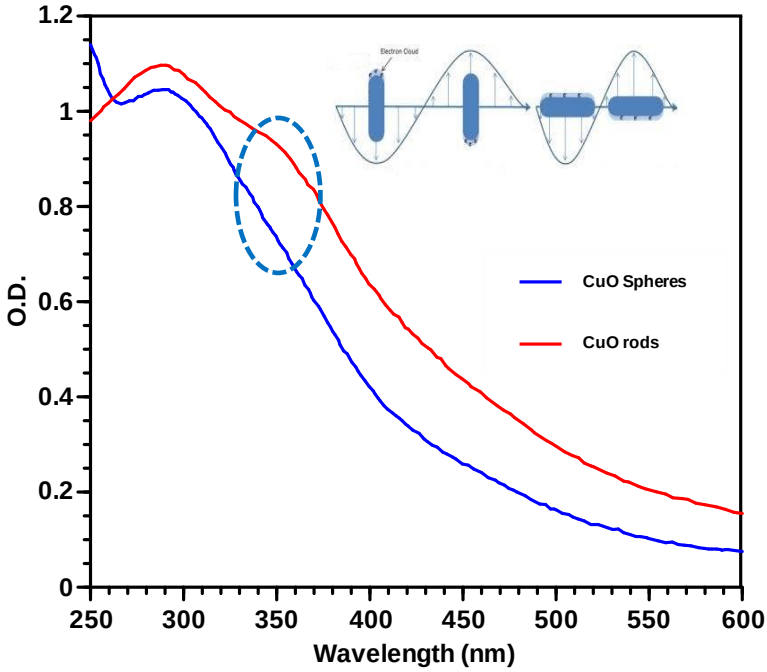

Figure 3.4: Comparison between absorbance spectra of 2.75 × 10^{-3} M CuO/SOA rods and CuO/SOA spheres[12] in Octane depicting a new exciton band at 350 nm characteristic for only rodlikeCuO particles.

chemical had no effect on the SOA coating present on the CuO surface. The presence of such surface coating decreased the signal to noise ratio and made the XRD measurements difficult. Presented in Figure 3.4 is a typical diffractometer trace recorded using the $\theta/2\theta$ geometry with 2θ ranging from 3^{o} to 80^{o}. The diffraction pattern demonstrates the crystallinity of the oxide rods since the reflections correspond to the monoclinic structure of CuO listed in the JCPDS card No. 41-0254.

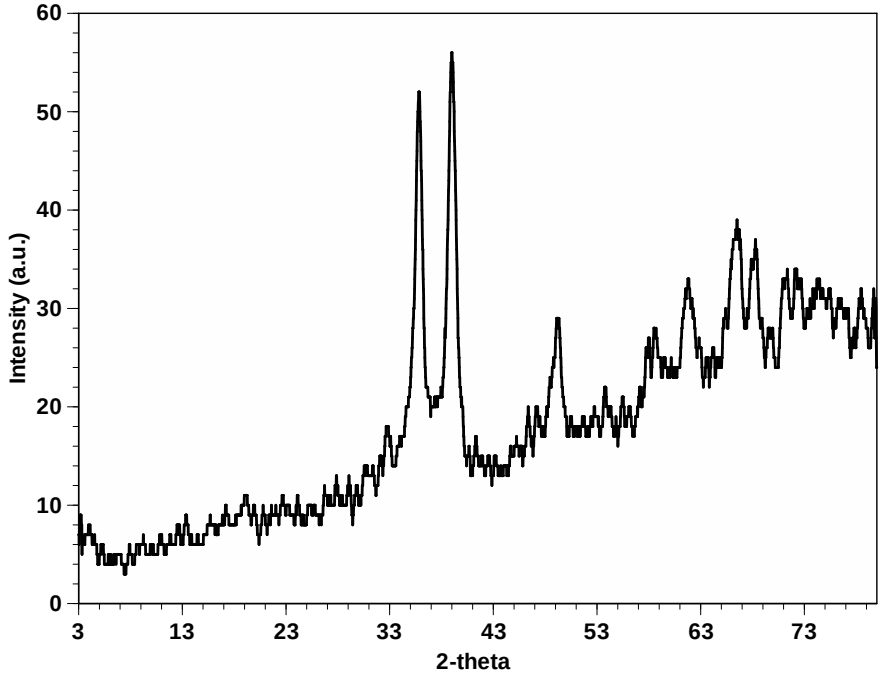

Figure 3.4: XRD pattern of CuO particles coated with oleate groups. The signals match well the reflections of monoclinic CuO (JCPDS card 48-1548).

Tests to determine the stability of CuO-SOA rods against precipitation were performed via dispersion of the particles in octane. UV-Visible spectral analysis was employed to determine stability of the particles. Initially, the crystallites were dispersed in alkanes after purification from remanent ions bound to the particle surfaces. Dispersion tests were carried out by adding a known amount of SOA coated CuO into a desired alkane and sonication for 10 min. After this dispersion step loosely coated particles precipitated within a time period but approximately 50% particles remained in the solution for a long time, see Figures 3.6 (a) and (b).

Well-coated rods were then separated from loosely coated or uncoated particles and spectral analyses was carried out to ascertain the stability of these particles. According to the optical spectrum presented in Figure 3.4, CuO rods exhibit two absorption maxima at 285 and 350 nm. If both of these signals are due to the anisotropic CuO rods, then their precipitation was

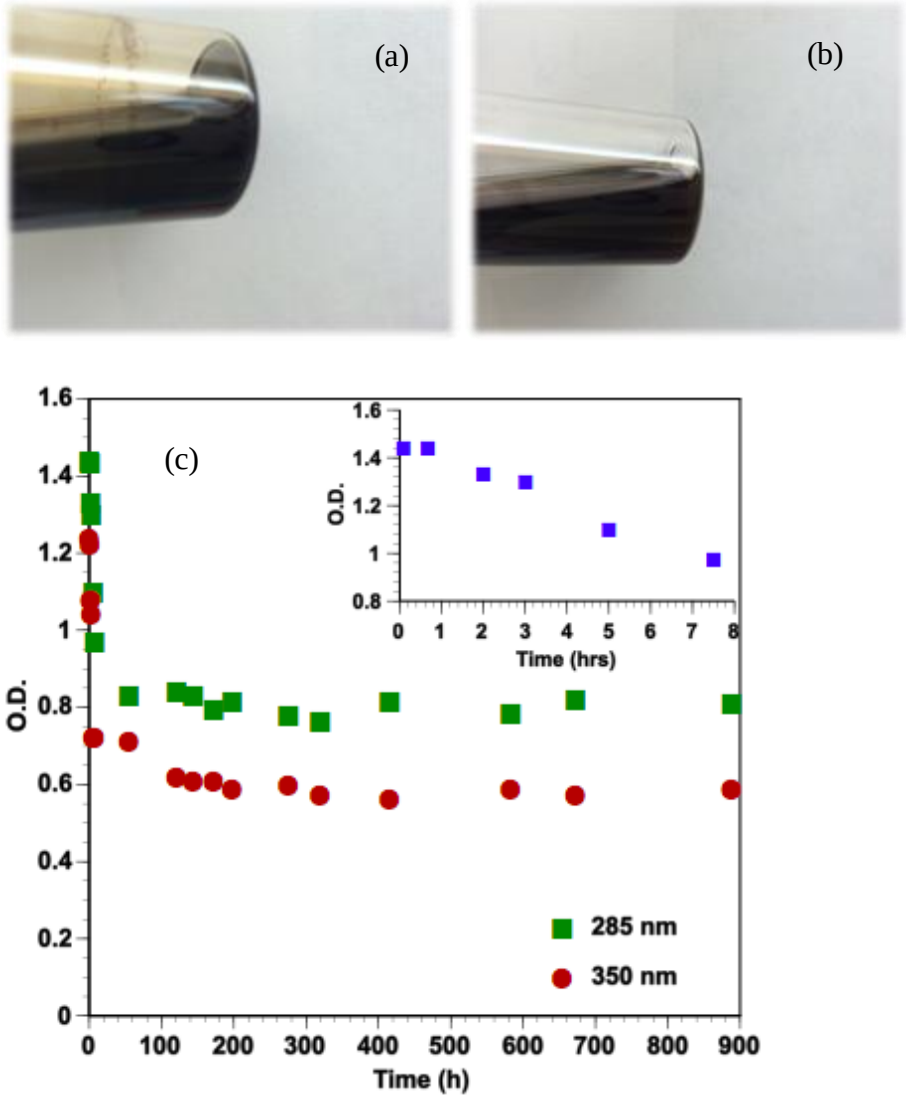

Figure 3.5: photograph of (a) dispersed CuO/SOA rods in octane after sonication, and (b) after separation of precipitated material leaving only rods with strongly bound SOA. (c) Stability tests based on changes in optical density at 285 nm and 350 nm as a function of time for a colloid containing 0.5 wt% of CuO in octane. Inset is showing the initial precipitation of rods after dispersion.

anticipated to induce a decrease of the optical density at both wavelengths. As depicted in Figure 3.5(c) such a decrease in optical density at both 285 and 350 nm was observed. The spectral data

also shows that the optical density remains constant over a long period of time following the initial particle precipitation. Obviously colloids exhibiting unchanged optical properties are those stable against precipitation.

Transmission electron microscopic analysis was performed for both CuO/SOA and CuO/OS. A very dilute suspension of CuO rods was prepared by mixing a colloid with a large amount of hexane. Then a small droplet was placed gently on a TEM grid followed by drying overnight under air. The dried grid was then analyzed placed with the TEM instrument; a typical image is presented in Figure 3.6(a). Clearly the generated particles exhibited preferentially a rod-like shape but significant variations in length and diameter were noticed. A number of TEM images were analyzed from different sections of the grid and more than 99% of the particles were present as somewhat irregular rods. These results are quite different from the particles obtained by most procedures that yielded rods. The reason is that procedures to produce stable colloids result in at most 50% of the particles exhibiting a rod shape. Depicted in Figure 3.6(b) is a 3D

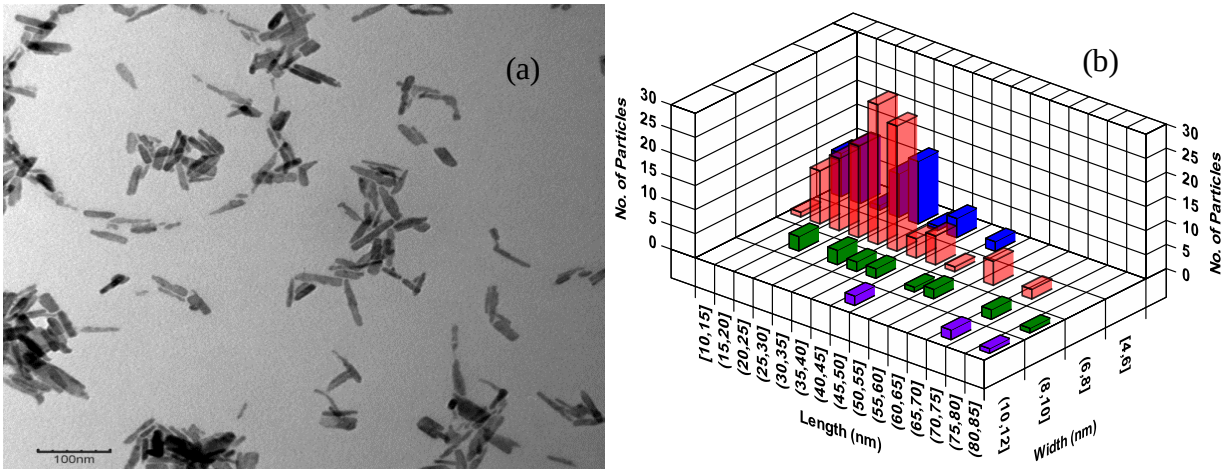

Figure 3.6: (a) TEM image of a CuO-SOA colloid and (b) the corresponding 3D histogram. The scale bar corresponds to 100 nm.

histogram of particles length and diameter. The most frequent length and diameter were found to be 35 nm and 7 nm respectively. The reason that the rod-like shape became prevalent is still unclear but it was assumed that the mechanical force employed to grind and mesh the initial bare CuO particles before coating induced preferential grain boundary growth in terms of size and shape.

CuO particles were also coated with OS to ascertain if the nature of the stabilizer had an effect on the shape of the particles. The resulting 0.1 M CuO/OS colloid was diluted with hexane to 1×10^{-4} M CuO and a small droplet was placed and dried on a TEM grid. Images of such colloid are presented in Figures 3.7(a) and (b). CuO/OS colloids also consist of rods but their shape is significant more irregular than the crystallites generated using SOA as a stabilizer. The distribution of lengths was found to be broad and ranges mostly between 20-140 nm whereas the width was narrower ranging between 2 and 14 nm.

Thermal conductivity determinations on CuO/SOA and CuO/OS colloids of rods were performed using a KD2 probe. Illustrated in Figure 3.8 is the percent enhancement of thermal conductivity at room temperature determined for colloids in tetradecane as a function CuO concentration. The TC value of tetradecane were experimentally determined to be 0.137 W/mK, which agrees well with previous reported data.[20] In both cases TC increases continuously as the CuO concentration is augmented. Although a very high concentration of stable oxide material was achieved for CuO/SOA colloids, the resulting maximum TC enhancement was very modest amounting to only 9.5 %. The CuO/OS colloids on the other hand, exhibited a higher enhancement of TC at room temperature with a maximum of 25 % at 0.25 M CuO. The improved TC performance exhibited by the CuO/OS colloids was assumed to derive from the fact that the length of the rods in these systems is larger than that of the particles present in CuO/SOA sols.

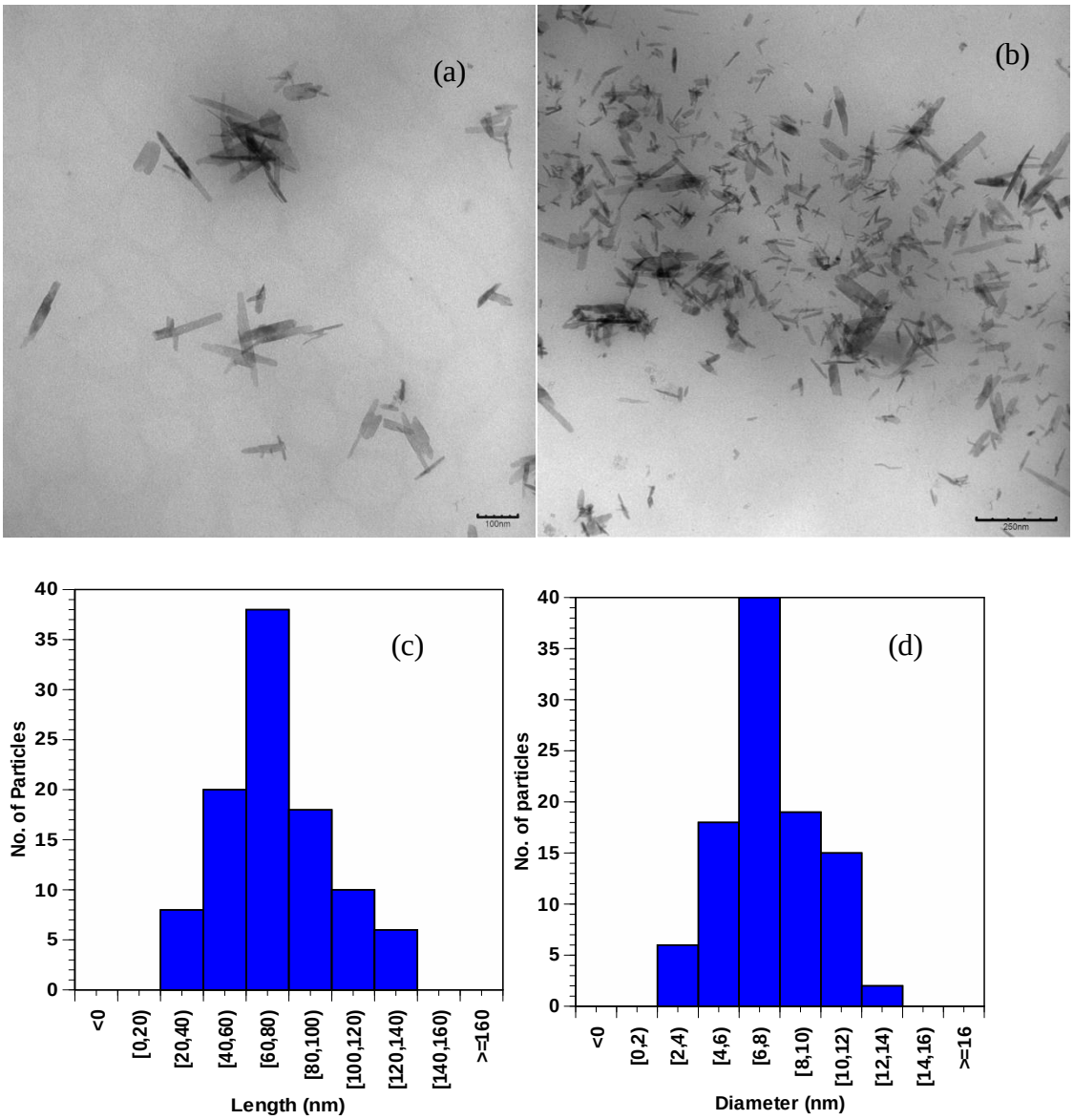

Figure 3.7: (a) and (b) TEM images of CuO/OS, the scale bars correspond to 100 and 250 nm, respectively. Figures 3.7(c) and (d) are the corresponding histogram of: (c) length and (d) diameter of the rod-like particles.

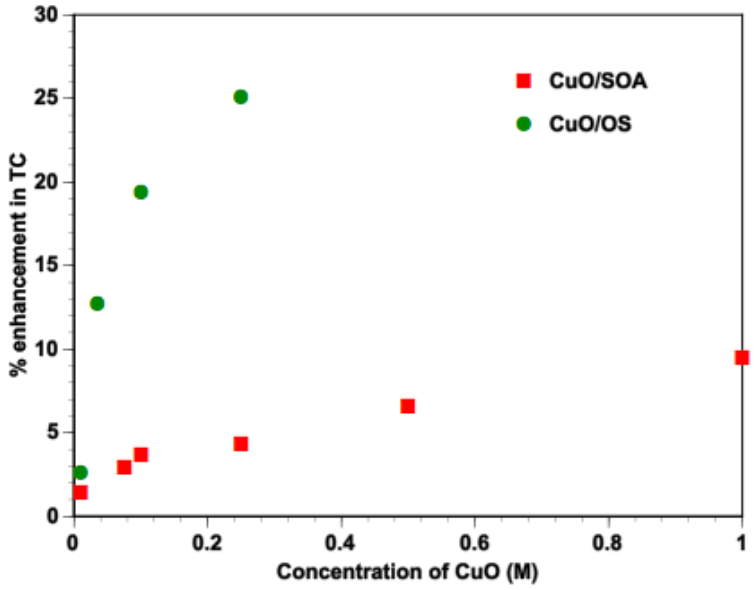

Figure 3.8: Thermal conductivity enhancement by CuO/SOA and CuO/OS rods at various concentrations. All the measurements were performed at 22 ^{O}C.

Reduction of CuO/SOA rods into metallic Cu:

Red-Al was used to reduce CuO in alkane since this reductant can be easily dissolved in organic non-polar solvents. Due to the sensitivity of Red-Al towards oxygen the reduction of CuO rods was performed in a sealed flask under a continuous flow of Argon. The purpose of the reduction was to determine if the original rod-like shape would be retained during slow transformation of CuO into metallic Cu.

CuO/SOA and CuO/OS colloids containing 0.1 M copper were reduced by stoichiometric amounts of Red-Al at 150 °C for 90 minutes. During the reaction a visual color change from light brown to dark red color indicates the transformation of CuO to metallic Cu. Since both Red-Al and the desired product, metallic Cu, are oxygen sensitive the reaction was carried out

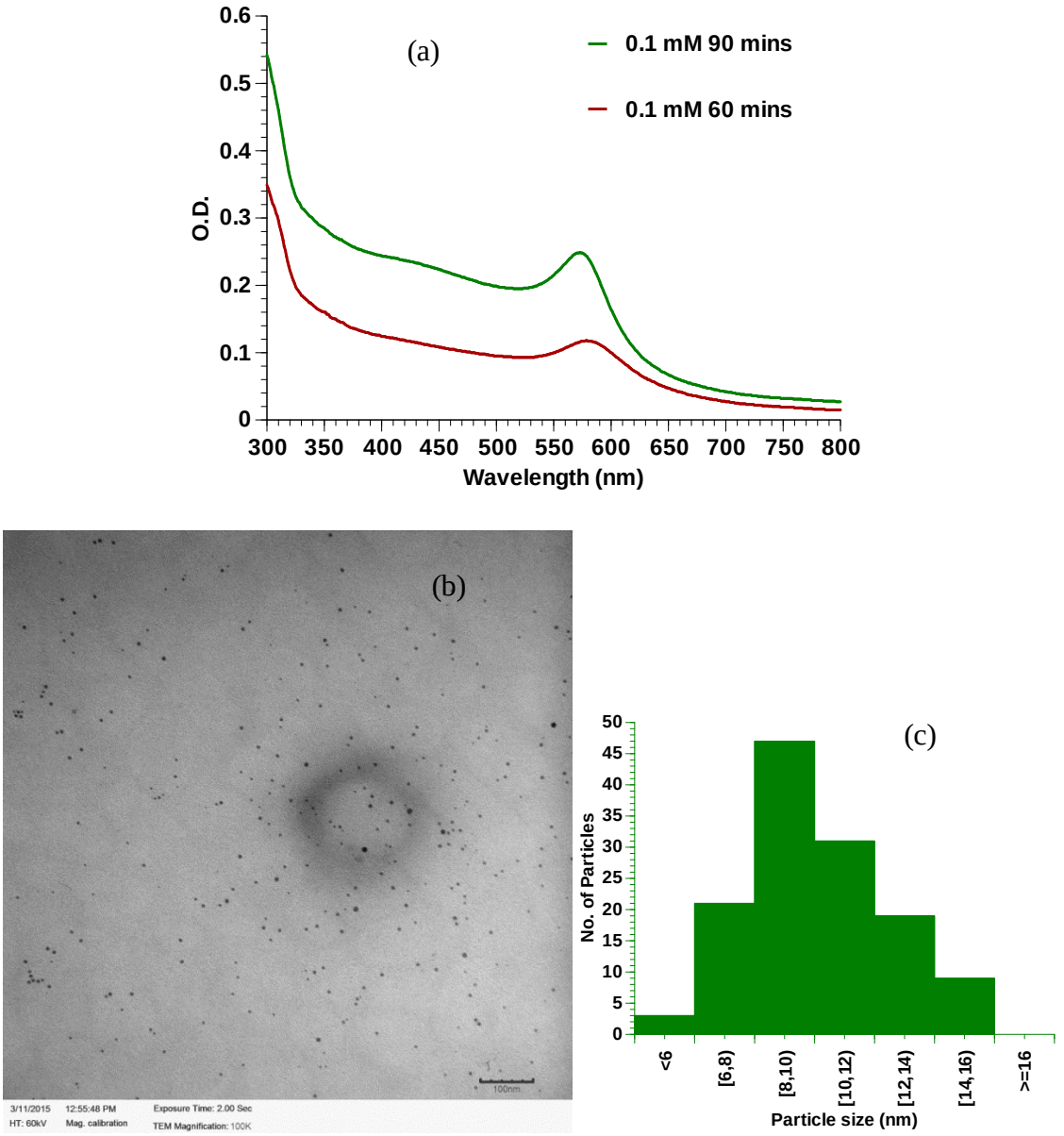

Figure 3.9: (a) Evolution spectra of formation of 0.1 M Cu colloid diluted to 1×10^{-4} M from a colloidal rod-like CuO/SOA solution showing the characteristic absorption maxima of the plasmon band corresponding to metallic Cu at 580 nm, (b) TEM micrograph shows uniform and spherical metallic copper formed by disrupting original rodlike shape of CuO and (c) a histogram made from TEM micrograph showing particles size distribution.

in a glove-bag under an Ar atmosphere.

As illustrated in Figure 3.3 the synthesized metallic copper was visually recognized from the color change from dark brown to dark red that took place during the reaction. Presented in Figure 3.9(a) are two optical spectra obtained during the reduction (60 min) and at the end of the reaction (90 min). Both spectra exhibit absorbance maxima at 580 nm corresponding to the well known plasmon of metallic Cu.[21,22] The resulting metallic Cu colloid has remained stable in tetradecane for more than 12 months after preparation when air was excluded. A TEM image of the Cu crystallites and the corresponding size histogram are presented in Figure 3.9(b) and (c), respectively. The results indicate that the particles are fairly spherical exhibiting a somewhat narrow size distribution with an average diameter of 9.8 nm. These observations mean that the original rod-like CuO particles break apart during reduction, generating new seeds of metallic Cu leading to a spherical shape.

Conclusions:

CuO rods were produced and stabilized in alkane-based fluids analogous to paraffins PCM. The rod-like CuO particles were stabilized using either SOA or OS ligands. Although OS coated rods were found to be irregular in size and shape, they exhibited a more pronounced TC enhancement as compared to CuO/SOA rods. The oxide rods were subjected to *in situ* reduction in order to achieve metallic copper without hampering the shape. Instead of retaining the original shape, the rods were reduced and produced new seeds that formed spherical crystallites. The spherical metallic copper particles were found to be stable in absence of air for more than a year. This reduction method constitutes a novel procedure for the synthesis of highly concentrated Cu colloids in alkanes, which were not accessible utilizing conventional approaches.

References:

(1) Keblinski, P.; Eastman, J. a.; Cahill, D. G. Nanofluids for Thermal Transport. *Mater. Today* **2005**, *8*, 36–44.

(2) Jesumathy, S.; Udayakumar, M.; Suresh, S. Experimental Study of Enhanced Heat Transfer by Addition of CuO Nanoparticle. *Heat Mass Transf.* **2011**, *48*, 965–978.

(3) Sharma, A.; Tyagi, V. V.; Chen, C. R.; Buddhi, D. Review on Thermal Energy Storage with Phase Change Materials and Applications. *Renew. Sustain. Energy Rev.* **2009**, *13*, 318–345.

(4) Jegadheeswaran, S.; Pohekar, S. D. Performance Enhancement in Latent Heat Thermal Storage System: A Review. *Renew. Sustain. Energy Rev.* **2009**, *13*, 2225–2244.

(5) Kakac, S.; Lui, H. Heat Exchangers; Selection, Rating and Thermal Design, Third edition, Boca Raton, **2012**.

(6) Shima, P. D.; Philip, J. Role of Thermal Conductivity of Dispersed Nanoparticles on Heat Transfer Properties of Nanofluid. *Ind. Eng. Chem. Res.* **2014**, *53*, 980–988.

(7) Fan, L.; Khodadadi, J. M. Thermal Conductivity Enhancement of Phase Change Materials for Thermal Energy Storage: A Review. *Renew. Sustain. Energy Rev.* **2011**, *15*, 24–46.

(8) Dey, K. K.; Kumar, A.; Shanker, R.; Dhawan, A.; Wan, M.; Yadav, R. R.; Srivastava, A. K. Growth Morphologies, Phase Formation, Optical & Biological Responses of Nanostructures of CuO and Their Application as Cooling Fluid in High Energy Density Devices. *RSC Adv.* **2012**, *2*, 1387–1403.

(9) Zhu, H.; Han, D.; Meng, Z.; Wu, D.; Zhang, C. Preparation and Thermal Conductivity of CuO Nanofluid via a Wet Chemical Method. *Nanoscale Res. Lett*. **2011**, *6*, 181-186.

(10) Brust, M.; Walker, M.; Bethell, D.; Schiffrin, D. J.; Whyman, R. Synthesis of Thiol-Derivatised Gold Nanoparticles in. *Chem*. *Commun*. **1994**, 7, 801–802.

(11) Zhu, H. T.; Zhang, C. Y.; Tang, Y. M.; Wang, J. X. Novel Synthesis and Thermal Conductivity of CuO Nanofluid. *J. Phys. Chem*. *C* **2007**, *111*, 1646–1650.

(12) Clary, D. R.; Mills, G. Preparation and Thermal Properties of CuO Particles. *J. Phys. Chem*. *C* **2011**, 115, 1767–1775.

(13) Cao, M.; Hu, C.; Wang, Y.; Guo, Y.; Guo, C.; Wang, E. A Controllable Synthetic Route to Cu, Cu2O, and CuO Nanotubes and Nanorods. *Chem*. *Commun*. **2003**, *15*, 1884–1885.

(14) Chen, H.; Zhao, G.; Liu, Y. Low-Temperature Solution Synthesis of CuO Nanorods with Thin Diameter. *Mater. Lett*. **2013**, *93*, 60–63.

(15) Jiang, X.; Herricks, T.; Xia, Y. CuO Nanowires Can Be Synthesized by Heating Copper Substrates in Air. *Nano Lett*. **2002**, *2*, 1333–1338.

(16) Zhang, F.; Zhu, A.; Luo, Y.; Tian, Y.; Yang, J.; Qin, Y. CuO Nanosheets for Sensitive and Selective Determination of H 2 S with High Recovery Ability. *J. Phys. Chem*. *C* **2010**, *114*, 19214–19219.

(17) Qin, Y.; Zhang, F.; Chen, Y.; Zhou, Y.; Li, J.; Zhu, A.; Luo, Y.; Tian, Y.; Yang, J. Hierarchically Porous CuO Hollow Spheres Fabricated via a One- Pot Template-Free Method for High Performance Gas Sensors Hierarchically Porous CuO Hollow

Spheres Fabricated via a One-Pot Template-Free Method for High Performance Gas Sensors. *J. Phys. Chem. C* **2012**, *116*, 11994–12000.

(18) Farbod, M.; Kouhpeymaniasl, R.; Noghrehabadi, A. R. Morphology Dependence of Thermal and Rheological Properties of Oil-Based Nanofluids of CuO Nanostructures. *Colloids Surfaces A Physicochem. Eng. Asp.* **2015**, *474*, 71–75.

(19) Park, S. J.; Kim, S.; Lee, S.; Khim, Z. G.; Char, K.; Hyeon, T. Synthesis and Magnetic Studies of Uniform Iron Nanorods and Nanospheres. *J. Am. Chem. Soc.* **2000**, *122*, 8581–8582.

(20) Li, C. C.; Chang, M. H. Colloidal Stability of CuO Nanoparticles in Alkanes via Oleate Modifications. *Mater. Lett.* **2004**, *58*, 3903–3907.

(21) Vargaftik, N. B.; Filippov, L.P.; Tarzimanov, A. A. Totskii, E. E. *Handbook of Thermal Conductivity of liquids and gases*, Boca Raton, **1995**; 304-305

(22) Salzemann, C.; Lisiecki, I.; Brioude, a.; Urban, J.; Pileni, M. P. Collections of Copper Nanocrystals Characterized by Different Sizes and Shapes: Optical Response of These Nanoobjects. *J. Phys. Chem. B* **2004**, *108*, 13242–13248.

(23) Clary, D. R.; Mills, G. Photochemical Generation of Nanometer-Sized Cu Particles in Octane. *J. Phys. Chem. C* **2011**, *115*, 14656–14663.

Chapter IV

Formation of Ag Nanoclusters in Alkanes

Introduction:

Metal nanoclusters composed of ten to hundred atoms have received much attention due to their novel size-dependent properties. Metal nanoparticles can be categorized into two distinct groups: plasmonic nanoparticles and molecular-like nanoparticles. Metal nanoparticles with dimensions exhibit continuous electronic band structures and are now known as plasmonic nanoparticles. The reason for this is that larger particles of several metals (for instance Ag, Au and Cu) exhibit strong optical transitions, called plasmons, in the visible induced by collective oscillations of surface electrons.[1] Metal particles with dimensions of < 2 nm (2-100 atoms) possess a molecular-like discrete electronic structure presumably due to some quantum confinement. These molecular-like small objects are simply known as metal nanoclusters.[2] Therefore, nanoclusters are considered as a class of materials with some properties that are somewhat different from those of atoms and also of larger nanoparticles. Considerable research interest exists in the field of noble metal clusters because of their novel physical and chemical properties. For instance, objects comprising of only a few atoms are able to display strong electronic transitions and fluorescence.[3] Unlike fluorescent quantum dots such as CdSe, light-emitting metal nanoclusters were expected to be less toxic and posses better stablility in solution.

A wide variety of applications were proposed for Ag clusters, including the detection of ions such as Hg^{2+}, Cu^{2+} and NO_3^-.[4–6] Ag clusters have also been used for the detection of thiols,[7] ochratoxin A,[8] melamine,[9] as well as protein, miRNA.[10,11] Furthermore, Ag clusters have been claimed to be useful for many other biological applications such as bio-imaging.[12,13] tracing drug delivery,[14] enhanced antimicrobial activities,[15] and as a probe for DNA-drug interaction.[16]

Ag nanoclusters were previously prepared by radiolytic reduction of Ag ions in presence of polyphosphate or polyacrylate as stabilizers.[17–20] Clusters formed this way do not exhibit the characteristic plasmon band of metallic Ag, but display discrete electronic transitions that depend on the number of Ag atoms present in the cluster.[17] Solvated electrons together with primary and secondary radicals produced from the solvent or stabilizers are the main reactive species responsible for the ultrafast nucleation and growth process of isolated Ag atoms that eventually generate the clusters.[3] Chemical reduction processes were also utilized to obtain small Ag nanoclusters.[19,21] Materials with poor affinity toward Ag are not suitable as stabilizers during the Ag^+ reduction with strong reducing agents. The reason is that fast Ag^+ reduction ensues under such conditions and chemicals interacting only weakly with the formed Ag atoms are unable to prevent them from aggregating all to way into large particles.

Fluorescent Ag clusters free of nanoparticles were synthesized by reduction of Ag^+ ions with $NaBH_4$ in the presence of DNA.[21] Highly fluorescent and photo-stable Ag clusters were also obtained in the presence if single stranded DNA.[22,23] A photochemical approach employed photoreduction of Ag^+ ions to obtain Ag nanoclusters was developed by Dickson *et al* on AgO films.[24] Analogous procedures were subsequently demonstrated using a wide variety of photosensitizers, for instance, water-soluble Ag clusters exhibiting high emission intensity were obtained in presence of dendrimers.[25] Other examples of photochemical pathways to produce clusters involved polymer microgels, poly(styrene sulfonate) capsules, polyglycerol-b-polyacrylic acid copolymers, polyelectrolytes and organic fluorophore thioflavin.[26–28]

Although significant progress has been achieved for the preparation of water-soluble Ag nanoclusters, there is a scarcity of knowledge about their formation in organic media. Such knowledge may be helpful to understand the role that solvent molecules play in the cluster

photoluminescence, a property not observed for the larger nanoparticles. In fact, no methods for the generation of stable Ag clusters in non-polar solvents have been reported thus far. This is not surprising given that Ag clusters are thermodynamically much less stable than nanoparticles, although the latter tend to grow spontaneously toward bulk metal. Kinetic stabilization enables preparation of colloidal particles that can persist in solution for long times. No such stabilization of neutral metal clusters in liquids has been possible because their tendency to grow is highly favored. Only charged silver clusters consisting of Ag^+ ions bonded to Ag atoms have been isolated in polar media due to their strong binding to anionic ligands.

Interestingly, a recent investigation on the photoreduction of Ag(I) neodecanoate sensitized by benzophenone (BP) in octane containing oleoyl sarcosine (OS) as a particle stabilizer yielded metal crystallites together with a species exhibiting a absorptions with a maximum wavelength (λ_{max}) of 325 nm and also a broad signal centered at about 510 nm.[29] The data seemed to suggest that an Ag cluster was responsible for such optical signal and that such species remained adsorbed on the surface of silver particles. However, the products were not always stable and seemed to be affected by the presence of adventitious H_2O and air in the hydrocarbon. Surprisingly, unusual optical signals centered at 460 and 510 nm were noticed during the initial stages of the thermal particle formation in mineral oil containing 1.1 x 10^{-2} M Ag(I) lactate and 2 x 10^{-2} M OS.[30] These signals were erroneously assigned to higher multipole optical transitions originating from very large Ag particles. However, as the reaction proceeded both signals merged and blue-shifted to about 420 nm, which is essentially the λ_{max} of the Ag plasmon from small particles discussed in Chapter 2. Thus, the explanation proposed originally required large Ag particles to shrink somehow during the course of a reaction that generated smaller metal crystallites as final products, a process that is unlikely from the thermodynamic viewpoint.

Broad optical signals red-shifted from the plasmon signal have been noticed frequently during the early stages of the formation process leading to Ag crystallites,[29] and correspond to optical transitions from particles not large enough to possess a plasmon.[1] However, the initial absorptions observed by Bonnemann et al were different as they showed maxima, suggesting that these signals may have originated from clusters. Because of such possibility, efforts were made to generate similar species via thermal and photochemical reactions of Ag(I) neodecanoate in alkanes containing OS.

Presented here is a simple photochemical procedure for the formation of Ag clusters in pentane, octane, dodecane and tetradecane using 350 and 420 nm photons. The sensitizer was presumably a complex of Ag(I) with OS, and simultaneously generated Ag particles seemed to have aided stabilization of the clusters. Interestingly, the clusters were stable in the presence of air for several days and some of them exhibited a strong fluorescence signal during the early stages of their formation.

Experimental Section

Ag neodecanote was purchased from Strem, OS was obtained from TCI, dodecane was from Alfa Aesar whereas, pentane, octane and tetradecane were supplied by Sigma Aldrich. Illuminations were carried out inside a Rayonet circular photochemical reactor equipped with 16 lamps producing either 350 or 420 nm photons. The temperature inside the illuminated Rayonet was 29 °C; Aberchrome 540 was used to determine the light intensity (I_0) in the forward direction for 350 nm photons, and in the reverse direction for 420 nm light.[31] Optical spectra were collected on a Shimadzu UV-Vis PC2501 spectrophotometer. Transmission electron

microscopy (TEM) measurements were carried employing a Zeiss EM 10CR instrument operating at 60 kV.

Experiments were performed in pentane, octane, dodecane and tetradecane, the same results were obtained with air or after degassing the solutions with N_2. In a typical cluster synthesis, a solution with 1.0 mM of Ag(I) neodecanoate was prepared in a certain alkene via dissolution of the metal complex by means of sonication or heat (50 ^{O}C) in the case of high molecular weight solvents. This solution was mixed, using equal volumes, with another prepared in the same solvent containing 1.0 mM of OS. The resulting mixture was then heated or placed in a 3.0 mL quartz cuvette and irradiated inside the Rayonet under continuous stirring.

Results and Discussions:

Considering the unusual optical signals detected in the earlier study on the thermal reduction of 1.1 x 10^{-2} M Ag(I) lactate in mineral oil, analogous experiments were conducted in dodecane solutions. For that purpose, a solution containing 0.1 M Ag(I) neodecanoate and 0.125 M OS was heated at 160 °C under stirring. A red solution was obtained after 1 min of heating, at which point an aliquot was separated cooled quickly and diluted to [Ag] = 33 μM. The spectrum of this solution is represented by the blue curve of Figure 4.1 and exhibited two broad signals centered at about 540 and 420 nm, respectively. Such signals were somewhat similar to those detected in the earlier study using mineral oil.[30] Further darkening of the concentrated Ag(I) neodecanoate occurred upon continuous heating up to 11 min, at which point a dark brown coloration resulted. Cooling and dilution of the reaction mixture to [Ag] = 67 μM yielded a yellow solution with an absorption spectrum represented in Figure 4.1 by the green curve. The spectrum exhibits only

one strong absorption with λ_{max} = 414 nm corresponding to the surface plasmon signal characteristic of spherical Ag crystallites with dimensions in the range of 2-10 nm.[1]

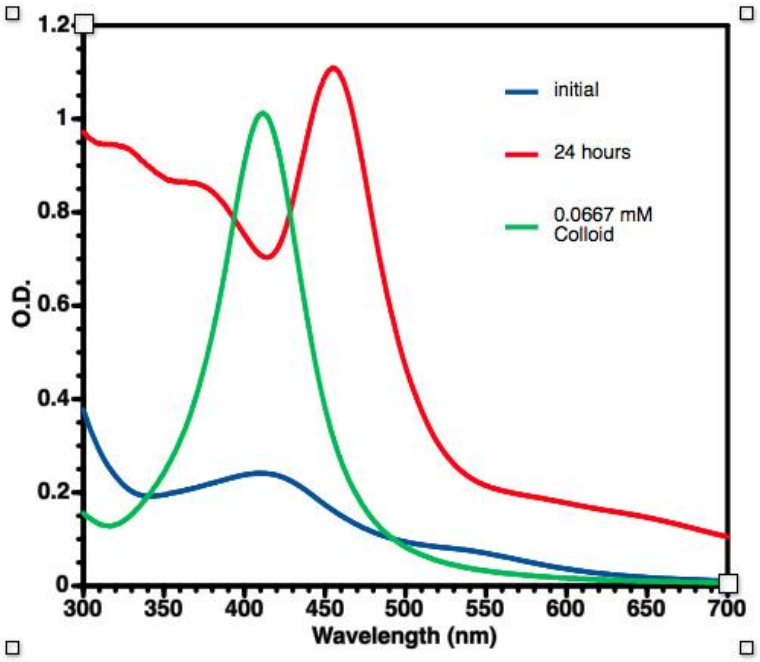

Figure 4.1: Spectra collected from dodecane solution with 0.1 M Ag(I) neodecanoate and 0.125 M OS. Initial spectrum (blue line) was obtained after heating the solution for 1 min at 160 °C followed by dilution to [Ag] = 33 μM. Red line: spectrum obtained from the solution heated after 1 min and then aged under laboratory light for 24 h without dilution. The green spectrum resulted after heating the solution for 11 min and then diluted to [Ag] = 67 μM.

No additional optical changes resulted upon further heating, indicating that the thermal reaction ended in about 11 min. Mixing of the resulting concentrated Ag colloid with 2-propanol or acetone completely precipitated the photogenerated metal and gravimetric analysis of the product confirmed the completeness of the thermal reduction. Additional changes were experienced by

the aliquot retrieved after 1 min of heating. Exposure of such concentrated sample to ambient laboratory light for 24 h yielded a red solution; depicted by the blue line in Figure 4.1 is the corresponding spectrum. Two broad signals centered at about 320 and 375 nm were observed in addition to a very strong signal with λ_{max} = 475 nm. In contrast, no spectral changes occurred when the dilute solution exhibiting the spectrum represented by the blue line was exposed to ambient light. Further experiments showed that spectra changes could also be induced via exposure of an unheated solution with 0.1 M Ag(I) neodecanoate and 0.125 M OS to ambient light but not upon aging in the dark. Comparison of the red spectrum with that of colloidal Ag (green curve) showed that species other than spherical Ag crystallites dominated the optical properties of the heated solution exposed subsequently to light.

Considering that the unusual optical signals were noticed prior to detection of the plasmon from silver particles, a logical possibility involved non-metallic Ag clusters as possible chromophores. This, in turn, implied that Ag clusters were accessible either by heating or exposing concentrated solutions of Ag(I) neodecanoate and OS to ambient light. The possibility of preparing somewhat stable Ag clusters in alkanes was intriguing as such species were not anticipated to survive in nonpolar media. Systematic tests performed to assess if such an approach was feasible showed that thermal transformations suffered from reproducibility issues and were not further used. On the other hand, direct photolysis of solutions containing Ag(I) neodecanoate and OS provided a simple and reproducible route for cluster formation. Additionally, the new photolytic method no longer required rigorous drying of solvents/reagents and exclusion air was, in contrast to the previously used and more complex procedure where BP served as a sensitizer.[29]

Initial experiments showed that formation of species with optical signals different from the plasmon resulted when either 420 or 350 nm photons were employed. These tests also showed

that the same photoinduced optical changes were achieved for solutions with and without a short heating step prior to illumination. Hence, all subsequent experiments were performed with solutions not heated before exposing them to light. Another important observation was that efficient photochemical transformations occurred only for solutions containing both Ag(I) neodecanoate and OS. Illumination of solutions without OS resulted in slow photoreductions of the silver complex. Obviously, interactions between the Ag(I) complex and OS resulted in a species able to act as a sensitizer that initiated the photoreactions. Unfortunately the spectrum of the sensitizer was very similar to that of the Ag(I) complex given that no spectral changes were noticeable in the presence and absence of OS.

Presented in Figure 4.2 are spectra recorded during photolysis with 420 nm photons of a solution

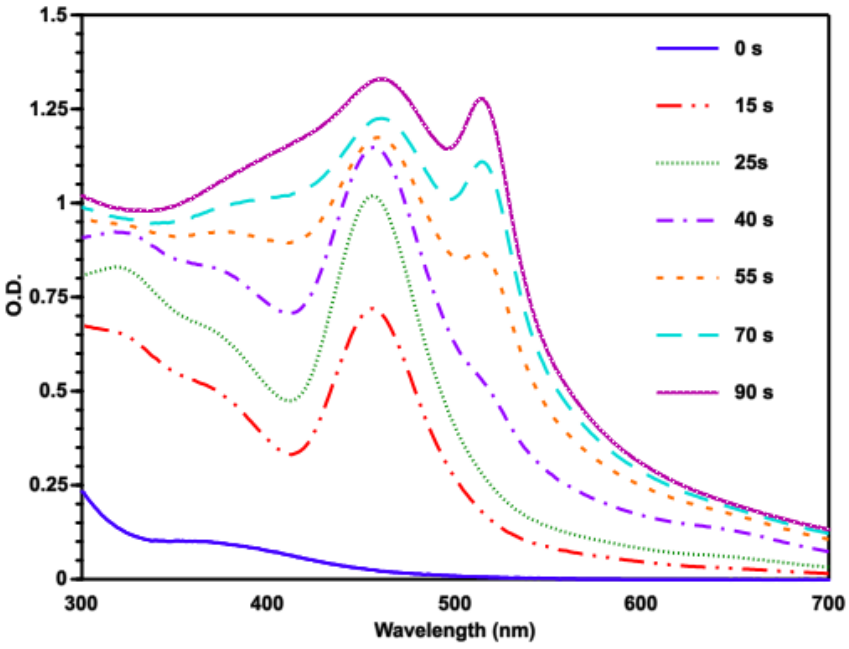

Figure 4.2: Spectral evolution during exposure to 420 nm photons of a solution with 0.5 mM Ag neodecanote and 0.5 mM OS in dodecane, $I_0 = 4.1 \times 10^{-5}$ M/s.

with 0.5 mM Ag(I) neodecanote and 0.5 mM OS in dodecane. Lower concentrations were employed since the highly concentrated system utilized to obtain the data of Figure 4.1 was plagued by reproducibility problems. The unirradiated solution exhibited a weak and broad absorption in the wavelength range of 350 and 420 nm. Photolysis for 15 s yielded a weak signal centered at about 320 nm, a shoulder at 375 nm and a prominent absorption with λ_{max} = 457 nm.

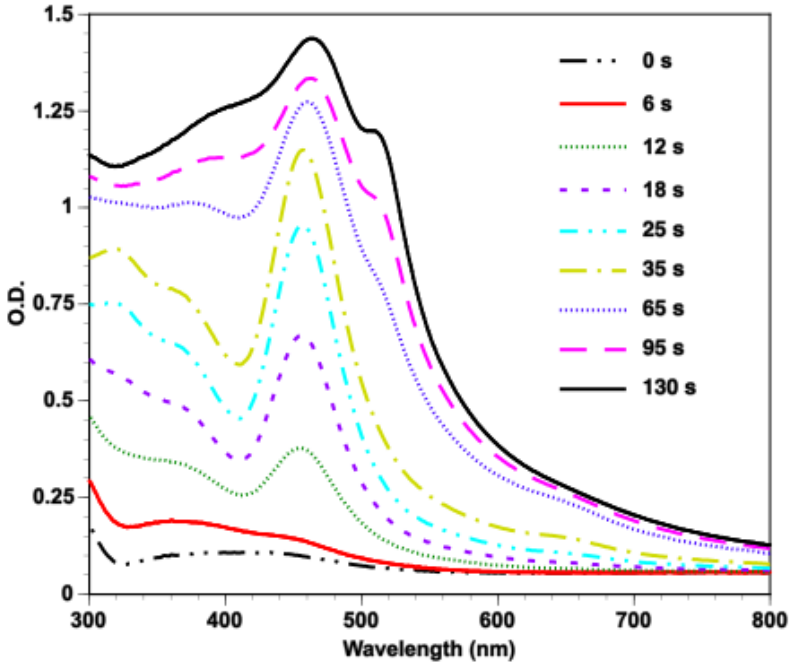

Figure 4.3: Evolution of optical spectra during photolysis of a solution containing 0.5 mM Ag neodecanote and 0.5 mM OS in dodecane to 350 nm photons with $I_0 = 5 \times 10^{-5}$ M/s.

This spectrum is strongly reminiscent of the one shown in Figure 4.1 that resulted from exposure to ambient light of a concentrated solution heated briefly. Further illumination strengthened all three signals but new absorptions with maxima at about 520 and 650 nm emerged. Longer exposures increased the strength of the signals at 375 nm, 457 nm and 520 nm whereas the other absorption bands were no longer detectable. As illustrated in Figure 4.3, analogous changes were

obtained upon photolysis using 350 nm, and the photoreactions proceeded with similar rates because the photons fluxes at both wavelengths were close to each other. The only significant difference is that a higher intensity of the 520 nm signal was achieved with 420 nm photons than using 350 nm light. Identical results were obtained in other alkanes including pentane, octane, and tetradecane.

A comparison of the optical data shown in Figures 4.1 through 4.3 shows that the Ag plasmon was less intense when contrasted with the strength of the signals with maxima at 457 and 520 nm. Obviously, the latter absorptions originate from species different from Ag crystallites, which most probably consist of small Ag clusters. Indeed, an absorption with a maximum at around 320 nm was assigned to a transition taking place in single Ag atoms.[32,33] Interestingly, two absorption bands at around 385 and 442 nm are believed to originate from the dimeric silver cluster (Ag_2) prepared in Argon matrices.[33] In a different study an absorption with λ_{max} = 450 nm was assigned to dimeric Ag clusters.[34] Claims have also been made that trimeric Ag species absorb near 500 nm.[33] Similar observation of clusters showing three absorption bands were reported before in aqueous medium using PMMA template to stabilize the clusters although the position of the absorption maxima differs from 5-20 nm.[35] These assignments are useful as starting points to rationalize the photogenerated optical signals. Fir instance, the shoulder with λ_{max} = 320 nm noticed at intermediate times in Figures 4.2 and 4.3 could originated from Ag atoms stabilized temporarily. On the other hand, both bands at 375 and 457 nm seemed to evolve synchronously during photolysis, suggesting that they originate from the same species, namely.

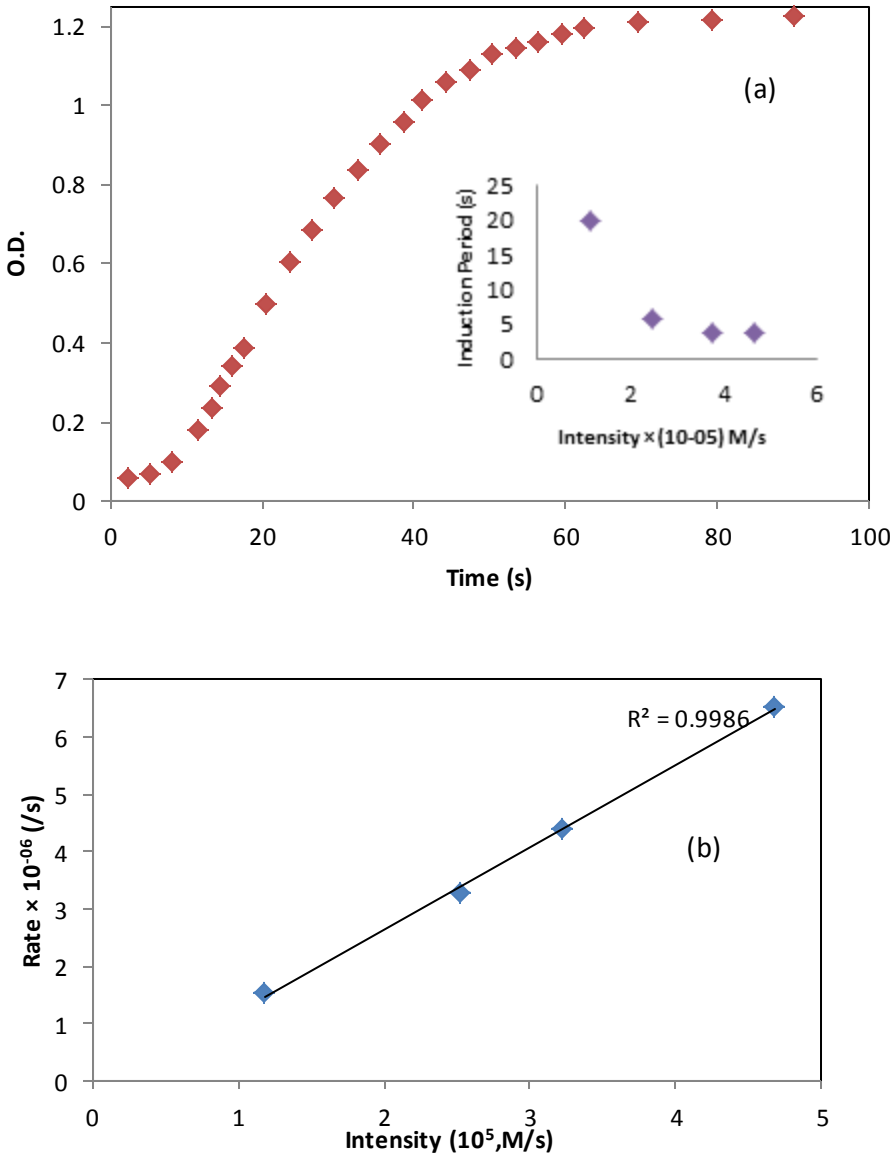

Figure 4.4: (a) Plot of optical density at 457 nm during photolysis with 420 nm photons of an air-saturated dodecane solution with 0.5 mM Ag neodecanote and 0.5 mM OS; $I_0 = 4.7 \times 10^{-5}$ M/s. Shown in the inset is the dependence of induction period on the photon flux. (b) Linear dependence of initial formation rate of clusters (determined at 457 nm) on light intensity.

an Ag_2 cluster. Another reasonable possibility is that the absorption centered at around 520 nm is probably due to the presence of a trimeric Ag cluster, Ag_3.

The kinetics of the Ag_2 cluster formation was monitored spectrophotometrically both in the absence and presence of air. Plotted in Figure 4.4(a) is the growth in intensity of the 457 nm signal as a function of time. The only difference between experiments performed with and without air is that the presence of O_2 retarded the onset of cluster formation resulting in a short induction period. This is noticeable in Figure 4.4(a) since only a small increase in the optical density (O.D.) at 457 nm was observed during the first 8 s of the reaction, followed by a much faster cluster formation at longer times after most to the O_2 was consumed. As shown in the inset of Figure 4.4(a) the length of the induction period was inversely proportional to the light intensity. This means that a reductant (•RH) was generated photochemically, which reacted with Ag(I) but was also scavenged by O_2. However, the latter reaction yielded a products unable to reduce Ag(I), thereby retarding the cluster formation. Illuminations with higher light intensities generated larger [•RH], consuming O_2 faster and decreasing the length of the induction period.

Initial rates of reaction (in terms of Δ(O.D.)/s since the cluster extinction coefficient remained unknown) were evaluated from the steep increase in absorbance after the induction period. Figure 4.4(b) demonstrates that the initial rate of cluster formation was a linear function of light intensity, which is consistent with the idea that Ag(I) was reduced via a reaction with •RH formed photochemically. The results of Figure 4.4(a) indicate that formation of the Ag_2 cluster became increasingly less efficient at times longer than 30 s. Inspection of Figure 4.2 reveals that the signal centered at 520 nm started to emerge in that time range, suggesting that Ag_2 was subsequently transformed into the Ag_3 cluster.

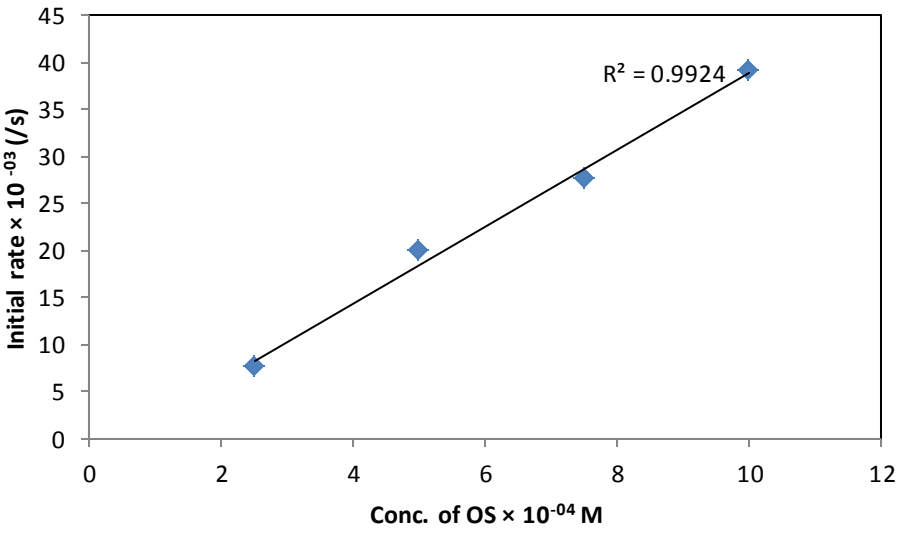

Figure 4.5: Initial formation rate of the signal at 475 nm as a function of [OS] for air-saturated solutions containing 0.5 mM Ag neodecanote exposed to 420 nm light, $I_0 = 4.1 \times 10^{-5}$ M/s.

Illumination of solutions without OS resulted in vey slow reductions of the silver complex, meaning that the sarcosine molecule participated in the photoreaction. The data of Figure 4.5 support such interpretation given that the initial rate of Ag_2 formation increased linearly with [OS], implying that the photoreaction was first-order with respect to sarcosine concentration. Only broad and weak absorptions are present in the spectra of Figures 4.2 and 4.3 collected prior to illumination and the spectra hardly changed when OS was excluded from the solutions. Taken together these observations indicate that interactions between the Ag(I) complex and OS were not particularly strong but, nevertheless, resulted in a species able to initiate photochemical transformations.

Another important observation was that the Ag_3 cluster was were considerable less stable than Ag_2. After the optical changes induced by 90 s of exposure to 420 nm light presented in Figure 4.2 the spectrum of the solution solution with 0.5 mM Ag neodecanote and 0.5 mM OS in

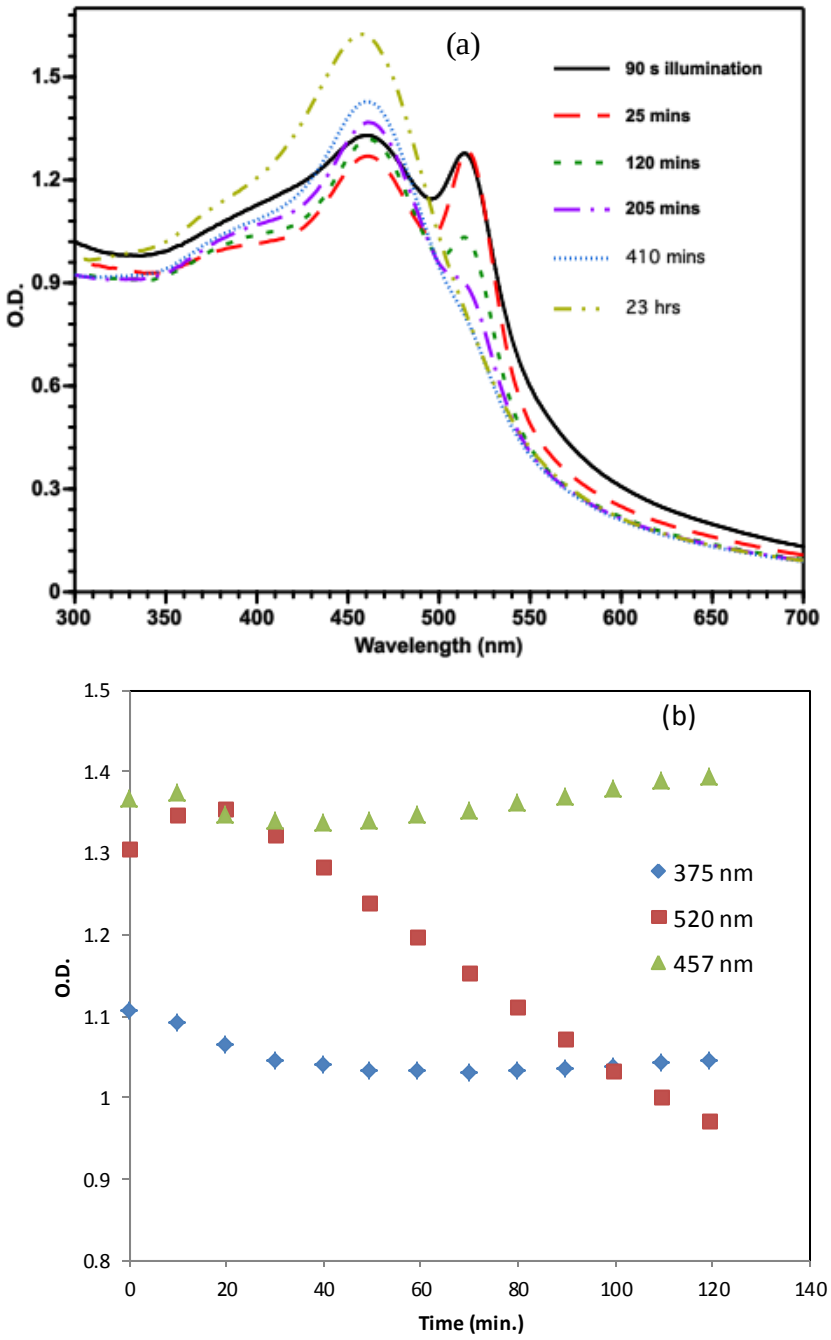

Figure 4.6: (a) Thermal evolution of optical spectra recorded after illumination of a solution with 0.5 mM Ag neodecanote and 0.5 mM OS in dodecane with 420 nm photons for 90 s, I_0 = 4.1 × 10^{-5} M/s. (b) Plot of O.D. changes at different wavelengths resulting from the dark reaction after 90 s of photolysis.

dodecane continued to evolve in the dark. The subsequent post-irradiation evolution of the spectrum is depicted in Figure 4.6(a). After 25 min of terminating the photolysis a slight increase in O.D. at 375, 475 and 520 was detected suggesting that a slow cluster formation step continued in the dark. At longer times the signal with λ_{max} = 520 nm decreased in intensity and completely vanished after 410 min. During that period of time the signals centered at 375 and 475 nm first decreased slightly but then increased in intensity. However, both signals turned significantly stronger after 23 h of dark reaction. Presented in Figure 4.6(b) is the evolution of the absorbance at 375, 475 and 520 nm as a function of time for the first 120 min of the dark reaction. The initial decay at 375 and 475 nm can be easily understood under the assumption that Ag_3 also absorbed significantly at these two wavelengths. As Ag_3 decayed thermally in the dark, the intensity of all the optical decreased. Interestingly after about 50 min the intensities of the absorptions of Ag_2 intensified slightly whereas the signal of Ag_3 continued to weaken. These transformations suggested that Ag_3 was significantly less stable than Ag_2, and that the trimer eventually converted, at least in part, into the dimer within a day. Since the conversion of Ag_3 than Ag_2 was not affected by air, a simple oxidation of the trimer via reaction with O_2 was not a reasonable pathway. Disproportionation of Ag_3 was expected to proceed through a second-order reaction, which was inconsistent with the kinetic data shown in Figure 4.6(b). According to these results the trimer followed a zero-order rate law, which seemed to suggest a disproportionation taking place on a surface, perhaps that of a metal particle.

To test the possibility that the clusters were generated simultaneously with Ag crystallites, during the photochemical reaction, a solution irradiated for 90 s showing the optical spectra displayed in Figure 4.2 was used to prepare a TEM specimen. Presented in Figure 4.7 is a typical TEM

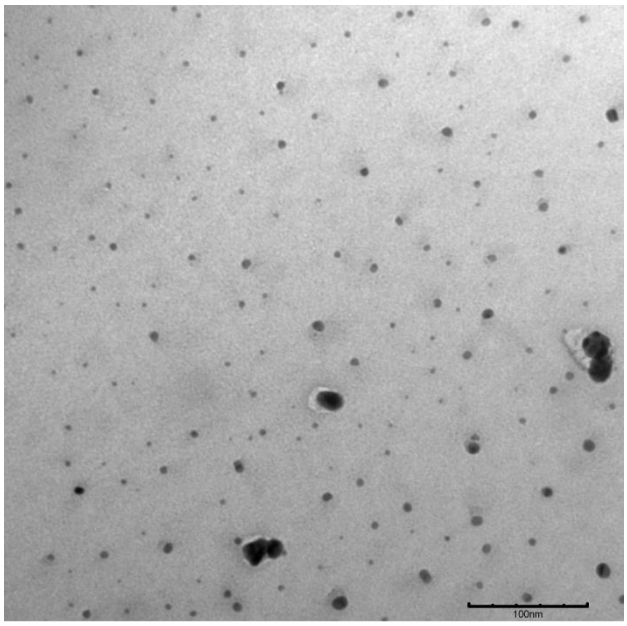

Figure 4.7: TEM image of Ag nanoparticles formed during cluster formation, the size bar corresponds to 100 nm.

image showing the presence of numerous nearly spherical Ag crystallites. A size histogram constructed by sizing about 300 crystallites revealed that the dimensions ranged between 1-20 nm with an average diameter (d_{av}) of 6 nm. An analogous experiment with the colloid showing the spectrum displayed in Figure 4.1 yielded a size range of 1-18 nm with d_{av} = 7 nm. Efforts to isolate the clusters via precipitation of the colloidal particles resulted in a complete disappearance of the optical signals corresponding to the clusters. Similar observations were made during the photochemical generation of Ag colloids in octane, and suggested that formation of the clusters occurred on the surface of exisitng Ag particles.[29]

Titration experiments of Ag clusters and particles:

Ag clusters were expected to be more reactive as compared to large nanoparticles, meaning that they would be oxidized more easily than silver crystallites. A set of weak oxidizing agents were

considered for oxidation of cluster without affecting the coexisting metallic particles. The basic idea was that weak oxidizing agent will first oxidizes the clusters first and then the Ag particles due to their different reactivities. The goal of such experiments was to determine the concentration of clusters generated by the photochemical reaction. Long chain carboxylic acids are considered to be very weak oxidizers particularly in non-polar solvents. Initial attempts to oxidize the clusters formed via a 90 s illumination of a solution with 0.5 mM Ag neodecanoate and 0.5 mM OS, exhibiting the spectrum shown in Figure 4.2, with octanoic acid were unsuccessful. These observations were not surprising because octanoic acid is an extremely weak oxidizer that remains undissociate in non-polar solvents. However, drastic optical changes were noticed upon titration with I_2 of a cluster solution prepared via photolysis of 2.5 mL of dodecane containing 0.25 mM Ag neodecanote and 0.25 mM OS, illuminated with 350 nm for 180 s. The corresponding spectral alterations are shown in Figure 4.8; I_2 was selected as a oxidizer given that this chemical is soluble in alkanes. The optical signals were partially bleached during addition of I_2; such process was completed after addition of 422.4 nmol of oxidizing equivalents. The spectrum recorded after the titration was over fits well with that reported for AgI particles exhibiting a maximum at 420 nm.[36] An interesting result was that oxidized not only the clusters but also the Ag crystallites and the number of oxidizing equivalents needed (422.4 nmol) implies that 1.7×10^{-4} M of the Ag(I) ions were reduced during the photochemical step. Using the absorption of the starting material at 350 nm together with the light intensity and exposure time a quantum yield of 0.09 is calculated for the overall photoreduction of Ag(I). This number is only a lower limit since according to results from the I_2 titration experiments, only one third of initial

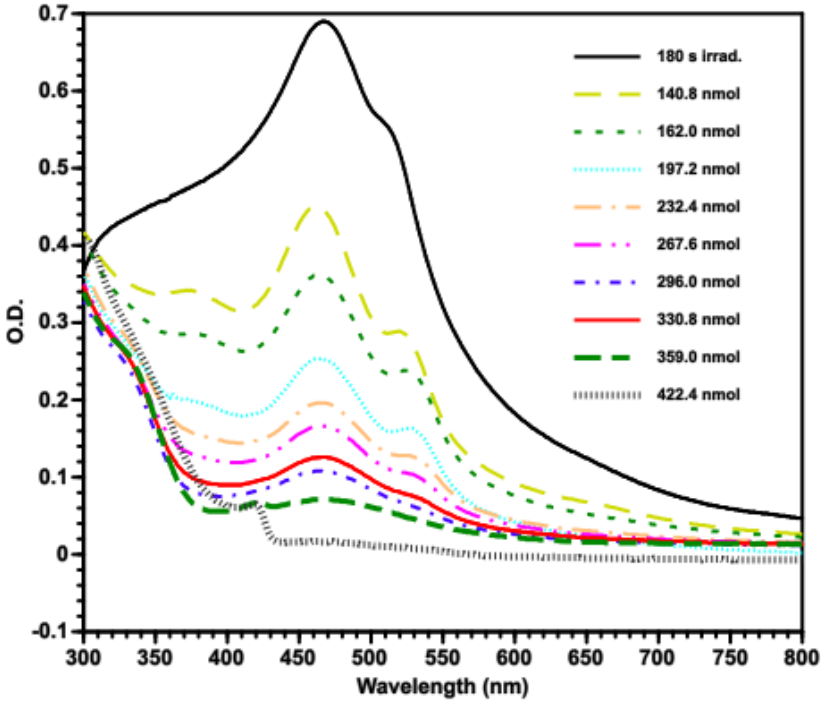

Figure 4.8: Spectra recorded during titration with a 3.52 mM I_2 solution of 2.5 mL of a dodecane solution containing 0.25 mM Ag neodecanote and 0.25 mM OS, photolyzed for 180 s with 350 nm photons, $I_0 = 5 \times 10^{-5}$ M/s.

Ag neodecanoate was reduced after 90 s irradiation. In fact, the reduction process became extremely slow after 90 s illumination probably because a large number of photons was absorbed by the metallic particles, which yielded no photochemical transformation .

Further titration experiments were conducted using ferrocenium hexafluorophosphate since this chemical is a weak oxidizing agent. The basic idea was to attempt exclusive oxidation of the clusters without attacking the metal particles. Titration of Ag clusters were performed under nitrogen due to the sensitivity of the ferrocene and ferrocenium complexes towards oxygen and

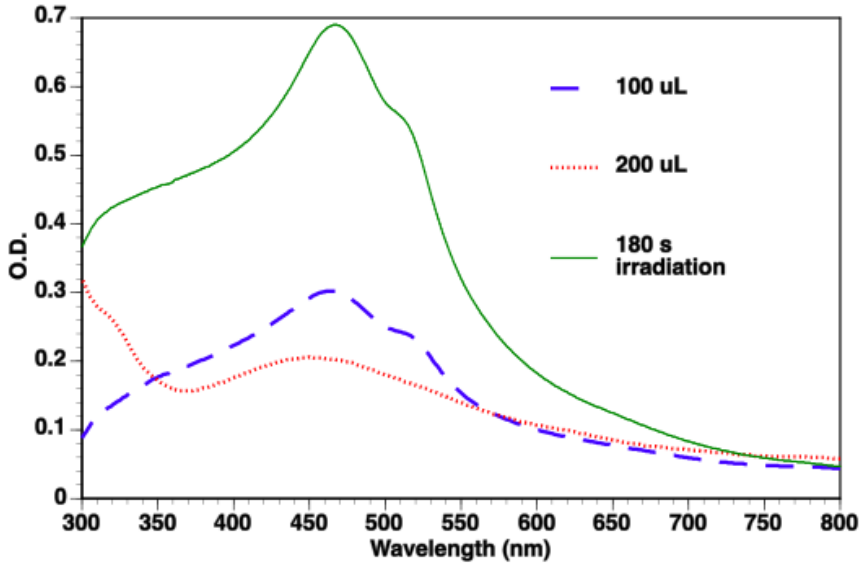

Figure 4.9: Spectra acquired during titration under N_2 with a 1.5 mM solution of ferrocenium hexafluorophosphate of a solution containing 2.5 mL of 0.25 mM Ag neodecanote and 0.25 mM OS, photolyzed for 180 s with 350 nm photons, $I_0 = 5 \times 10^{-5}$ M/s.

leaving behind a broad absorption centered at about 450 nm. The broadening of the optical signal of the colloid is probably because the iron (II) products induced some aggregation of the Ag crystallites. The amount of oxidizer required to bleach the signals of the clusters indicated that 1.1×10^{-4} M of the Ag(I) ions were reduced forming clusters. Combination of the results shown in Figures 4.8 and 4.9 implies that 2/3 of the Ag(I) ions reduced were present as clusters and that only 1/3 was represented by Ag particles. An interesting conclusion was that the clusters completely dominated the optical properties of the solutions. This is not unexpected if the clusters were present on the surface of the particles, where they effectively dampened the plasmon of the metal particles according to the CID meachnism.[1]

Fluorescence of Ag clusters:

Numerous studies on the synthesis of Ag clusters in water have reported that they exhibit luminescent properties.[21–28] Therefore, experiments were conducted to test if the Ag clusters photogenerated in alkanes were also luminescent. In these experiments the flurescence of Ag(I) and of neodecanote were tested separately followed by determinations in which both components were present as well as of illuminated solutions. Shown in Figure 4.10(a) are emission spectra obtained via excitation of the solutions with 475 nm photons. As shown in Figures 4.2 or 4.3 the Ag_2 cluster exhibits a strong absorption band centered at that wavelength. Emission spectra were also acquired from solutions containing of 0.25 mM Ag(I) neodecanote and 0.25 mM OS, and also after different irradiation periods (0 s, 15 s and 90 s). As illustrated in Figure 4.10, only weak signals were detected when solutions containing only Ag(I) neodecanote or OS. Analogous results were obtained after with an unirradiated solution containing both Ag(I) neodecanote or OS. Howver, a strong fluorescence signal centered at 560 nm was recorded after 15 s of irradiation. The same signal resulted using either 375 or 457 nm as the excitation wavelengths, which correspond to the maxima noticed in the absorption spectrum of Ag_2. The results shown in Figure 4.10(b) indicate that illuminations for longer times diminished the intensity of the fluorescence, yielding an emission spectrum that coincided with that determined for silver(I) neodecanoate. According to Figure 4.2, short irradiation times generated mostly Ag_2 clusters exhibiting the strong absorption bands centered at 375 and 457 nm, which are the species responsible for the emission with a maximum at 560 nm. Longer illumination times generated additional A particles together with clusters on their surfaces. However, higher concentrations of products resulting either from the OS oxidation or that of the solvent also accumulated. Hence, the observed decrease in the emission intensity at linger photolysis times is probably a results of

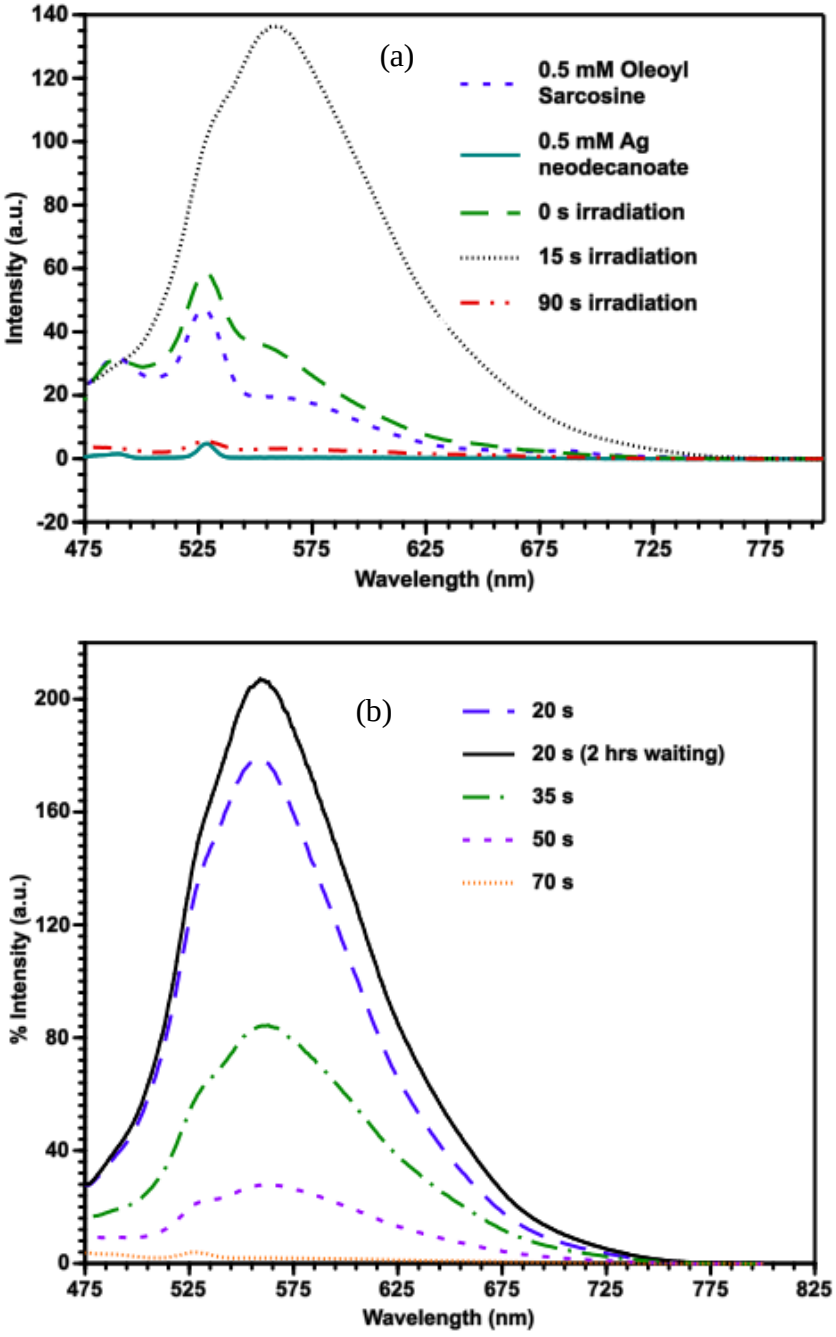

Figure 4.10: (a) Fluorescence spectra of different samples in presence or absence of Ag neodecanoate at different irradiation time; excitation wavelength: 457 nm, slit width: 10 nm. (b) Decay of the luminescence from Ag clusters at longer illumination times due to the formation of nanoparticles which inhibits fluorescence of clusters (bottom).

quenching by the oxidation products. Interestingly, the data shown in Figure 4.10(b) indicated that the emission of clusters formed during short irradiation periods remained fairly constant even under exposure to air for several h.

Conclusions:

This present study showed that report Ag clusters can be easily produced using a simple photochemical approach. We also report that the concentration of Ag clusters can be determined via a straightforward titration procedure based on their selective oxidation. Separation of clusters from nanoparticles with precise number of atoms has not yet been explored. The predominant clusters seem to consist of dimers and trimers located on to the surface of large metal particles.

Fluorescent Ag clusters have already shown a wide variety of potential applications including chemical sensing, bio-detection and bio-imaging. Preparation of analogous cluster systems in organic solvents may result new potential applications.

References:

(1) Kreibig U.; Vollmer, M. *Optical Properties of Metal Clusters*; Springer-Verlag: Berlin, 1995; 380-387.

(2) Zheng, J.; Nicovich, P. R.; Dickson, R. M. Highly Fluorescent Noble-Metal Quantum Dots. *Annu. Rev. Phys. Chem.* **2007**, *58*, 409–431.

(3) Xu, H.; Suslick, K. S. Water-Soluble Fluorescent Silver Nanoclusters. *Adv. Mater.* **2010**, *22*, 1078–1082.

(4) Adhikari, B.; Banerjee, A. Facile Synthesis of Water-Soluble Fluorescent Silver Nanoclusters and HgII Sensing. *Chem. Mater.***2010**, *22*, 4364–4371.

(5) Lan, G. Y.; Huang, C. C.; Chang, H. T. Silver Nanoclusters as Fluorescent Probes for Selective and Sensitive Detection of Copper Ions. *Chem. Commun.* **2010**, *46*, 1257–1259.

(6) Dhanya, S.; Saumya, V.; Rao, T. P. Synthesis of Silver Nanoclusters, Characterization and Application to Trace Level Sensing of Nitrate in Aqueous Media. *Electrochim. Acta* **2013**, *102*, 299–305.

(7) Huang, Z.; Pu, F.; Lin, Y.; Ren, J.; Qu, X. Modulating DNA-Templated Silver Nanoclusters for Fluorescence Turn-on Detection of Thiol Compounds. *Chem. Commun.* **2011**, *47*, 3487–3489.

(8) Chen, J.; Zhang, X.; Cai, S.; Wu, D.; Chen, M.; Wang, S.; Zhang, J. A Fluorescent Aptasensor Based on DNA-Scaffolded Silver-Nanocluster for OchratoxinA Detection. *Biosens. Bioelectron.* **2014**, *57*, 226–231.

(9) Han, S.; Zhu, S.; Liu, Z.; Hu, L.; Parveen, S.; Xu, G. Oligonucleotide-Stabilized Fluorescent Silver Nanoclusters for Turn-on Detection of Melamine. *Biosens. Bioelectron.* **2012**, *36*, 267–270.

(10) Shah, P.; Thulstrup, P. W.; Cho, S. K.; Bhang, Y.-J.; Ahn, J. C.; Choi, S. W.; Bjerrum, M. J.; Yang, S. W. In-Solution Multiplex miRNA Detection Using DNA-Templated Silver Nanocluster Probes. *Analyst* **2014**, *139*, 2158–2166.

(11) Shah, P.; Cho, S. K.; Thulstrup, P. W.; Bhang, Y.-J.; Ahn, J. C.; Choi, S. W.; Rorvig-Lund, A.; Yang, S. W. Effect of Salts, Solvents and Buffer on miRNA Detection Using DNA Silver Nanocluster (DNA/AgNCs) Probes. *Nanotechnology* **2014**, *25*, 45101- 45107.

(12) Antoku, Y.; Hotta, J.; Mizuno, H.; Dickson, R. M.; Hofkens, J.; Vosch, T. Transfection of Living HeLa Cells with Fluorescent Poly-Cytosine Encapsulated Ag Nanoclusters. *Photochem. Photobiol. Sci.* **2010**, *9*, 716–721.

(13) Byers, R. J.; Hitchman, E. R. Quantum Dots Brighten Biological Imaging. *Prog. Histochem. Cytochem.* **2011**, *45*, 201–237.

(14) Su, S.; Wang, H.; Liu, X.; Wu, Y.; Nie, G. IRGD-Coupled Responsive Fluorescent Nanogel for Targeted Drug Delivery. *Biomaterials* **2013**, *34*, 3523–3533.

(15) Wang, X.; Gao, W.; Xu, S.; Xu, W. Luminescent Fibers: In Situ Synthesis of Silver Nanoclusters on Silk via Ultraviolet Light-Induced Reduction and Their Antibacterial Activity. *Chem. Eng. J.* **2012**, *210*, 585–589.

(16) Yuan, J.; Guo, W.; Wang, E. Oligonucleotide Stabilized Silver Nanoclusters as Fluorescence Probe for Drug-DNA Interaction Investigation. *Anal. Chim. Acta* **2011**, *706*, 338–342.

(17) Henglein, A. Non-Metallic Silver Clusters in Aqueous Solution: Stabilization and Chemical Reactions. *Chem. Phys. Lett.* **1989**, *154*, 473–476.

(18) Linnert, T.; Mulvaney, P. Long-Lived Nonmetallic Silver Clusters in Aqueous Solution: Preparation and Photolysis. *J. Am. Chem. Soc.* **1990**, *112*, 4657–4664.

(19) Henglein, A. Physichochemical Properties of Small Metal Particles in Solution: "Microelectrode" Reactions, Chemisorption, Composite Metal Particles, and the Atom-to-Metal Transition. *J. Phys. Chem.* **1993**, *97*, 5457–5471.

(20) Ershov, B. G.; Henglein, A. Reduction of Ag^+ on Polyacrylate Chains in Aqueous Solution. *J. Phys. Chem. B* **1998**, *102*, 10663–10666.

(21) Petty, J. T.; Zheng, J.; Hud, N. V.; Dickson, R. M. DNA-Templated Ag Nanocluster Formation. *J. Am. Chem. Soc.* **2004**, *126*, 5207–5212.

(22) Vosch, T.; Antoku, Y.; Hsiang, J.; Richards, C. I.; Gonzalez, J. I.; Dickson, R. M. Strongly Emissive Individual DNA-Encapsulated Ag Nanoclusters as Single-Molecule Fluorophores. **2007**, *104*, 12616-12621.

(23) Ritchie, C. M.; Johnsen, K. R.; Kiser, J. R.; Antoku, Y.; Dickson, R. M.; Petty, J. T. Ag Nanocluster Formation Using a Cytosine Oligonucleotide Template. **2007**, 175–181.

(24) Peyser, L. a. Photoactivated Fluorescence from Individual Silver Nanoclusters. *Science,* **2001**, *291* (January), 103–106.

(25) Zheng, J.; Dickson, R. M. Individual Water-Soluble Dendrimer-Encapsulated Silver Nanodot Fluorescence. *J. Am. Chem. Soc.* **2002**, *124*, 13982–13983.

(26) Zhang, J.; Xu, S.; Kumacheva, E. Photogeneration of Fluorescent Silver Nanoclusters in Polymer Microgels. *Adv. Mater.* **2005**, *17*, 2336–2340.

(27) Shen, Z.; Duan, H.; Frey, H. Water-Soluble Fluorescent Ag Nanoclusters Obtained from Multiarm Star Poly(acrylic Acid) As "molecular Hydrogel" templates. *Adv. Mater.* **2007**, *19*, 349–352.

(28) Makarava, N.; Parfenov, A.; Baskakov, I. V. Water-Soluble Hybrid Nanoclusters with Extra Bright and Photostable Emissions: A New Tool for Biological Imaging, *Biophys. J.* **2005**, *89,* 572–580.

(29) Clary, D. R.; Nabil, M.; Sedeh, M. M.; El-Hasadi, Y.; Mills, G. Photochemical Generation of Ag, Pd and Pt Particles in Octane. *J. Phys. Chem. C* **2012**, *116*, 9243-9250.

(30) Bönnemann, H.; Botha, S. S.; Bladergroen, B.; Linkov, V. M. Monodispersed copper- and silver-nanocolloids suitable for heat conductive fluids. *Appl. Organometal. Chem.* **2005**, *19*, 768-773.

(31) Heller, H. G.; Langan, J. R. Photochromic Heterocyclic Fulgides. Part 3. The Use of (E)-a-(2.5- Dimethyl-3-furylethylidene) (isopropylidene)succinic Anhydride as a Simple Convenient Chemical Actinometer. *J. Chem. Soc., Perkin Trans. 2* **1981**, 341-343.

(32) Carstens, D. H. W.; Brashear, W.; Eslinger, D. R.; Gruen, D. M. The Correlation between Gaseous Atomic Spectra and the Absorption Spectra of Atoms Isolated in Noble-Gas Matrices. *Appl. Spectrosc.* **1972**, *26*, 184–217.

(33) Rabin, I.; Schulze, W.; Ertl, G. Absorption Spectra of Small Silver Clusters Ag_n ($n \geq 3$), *Chem. Phys. Lett.* **1999**, 312, 394–398.

(34) Maretti, L.; Billone, P. S.; Liu, Y.; Scaiano, J. C. Facile Photochemical Synthesis and Characterization of Highly Fluorescent Silver Nanoparticles; *J. Am. Chem. Soc.* **2009**, 131, 13972–13980.

(35) Xu, H.; Suslick, K. S. Sonochemical Synthesis of Highly Fluorescent Ag Nanoclusters. *ACS Nano* **2010**, *4*, 3209–3214.

(36) Freedhoff, M. I.; Marchetti, A. P.; McLendon, G. L. Optical Properties of Nanocrystalline Silver Halides. *J. Lumin.* **1996**, *70*, 400-413.

(37) Bitterwolf, T. E.; Ling, a. C. Metallocene Basicity. II. Reaction of the Ferrocenonium Cation with O_2 and SO_2. *J. Organomet. Chem.***1972**, *40*, 29–32.

Chapter V

Efficient photochemical route for introducing unsaturation in hydrocarbons.

Oxidation of alkanes to alkenes is an area of significant interest given that olefins are precursors to a wide range of important chemicals. This transformation is a particular case of alkane functionalization reactions (also known as C-H activations), which traditionally have required elevated temperatures and catalysts to proceed.[1]

Illumination of air-free octane, cyclohexane and pentane solutions containing benzophenone (BP) and Cu(II) neo-decanoate with 350 nm photons results in the formation of the corresponding olefins. Reduction of the Cu(II) complex to a Cu(I) product by photogenerated free radicals occurs with quantum yields ≥ 1.5; olefins are formed with efficiencies that are one half of those for the Cu(II) photoreduction. The Cu(II) complex acts as an electron acceptor, oxidizing the BP and solvent radicals and preventing undesirable radical reactions. Oxidation of Cu(I) product by O_2 enables complete recovery of Cu(II) neo-decanoate, allowing this complex to act as a catalyst for the alkane Oxidation. Undesirable side reactions of products and catalyst deactivation can take place under such conditions but utilization of metal complexes as catalysts have led to decreases in the alkene formation temperatures.[2,3] Photochemical oxidation of hydrocarbons catalyzed by metal complexes is another strategy that has lowered the reaction temperature by using electromagnetic radiation as the source of energy.[4] However, these processes generally require high energy photons and exhibit low quantum efficiencies even when operating above room temperature. Reported here is a photochemical process that enables efficient conversion of liquid alkanes to alkenes at ambient temperature using 350 nm photons according to the general equation:

$C_nH_{2n+2} + h\nu \rightarrow C_nH_{2n} + 2e^- + 2H^+$ (1)

In this transformation benzophenone (BP) serves as a sensitizer and Cu (II) neo-decanoate (from Strem, CuL_2, with L = $C_{10}H_{19}O_2^-$) acts as an electron acceptor. Photolysis of solutions containing BP and CuL_2 in octane, cyclohexane or pentane induces reduction of the Cu(II) ions to a Cu(I) neo-decanoate complex (CuL) with high quantum yields and simultaneous oxidation of solvent molecules to form olefins. Subsequent oxidation of CuL by O_2 regenerates CuL_2, which can function as a redox catalyst over numerous reduction-oxidation cycles. These findings are significant as they demonstrate that the photochemical transformation of alkanes toalkenes can occur at ambient temperature via an efficient free-radical process initiated by BP.

The present research was stimulated by a previous study on the photochemical synthesis of nanometer-sized Cu crystallites in alkanes.[5]Photolysis of air-free solutions containing BP and a Cu(II) oleate complex yielded first a Cu(I) product with quantum yields (Q.Y.) > 1, followed by a slow photoreduction of the latter into Cu particles. Interestingly, O_2 induced complete reoxidation of the metallic particles to the initial Cu(II) complex. The first photoreduction step was significantly more efficient when octane served as a solvent instead of toluene. Although such findings suggested that solvent molecules served as reducing agents, the employed photochemical system was not well suited to test such hypothesis. For instance, the presence of olefinic groups in the oleate ligands complicated identification of alkenes as possible reaction products. Other issues were that the Cu(II) complexes inhibited the photoreactions via quenching excited states of BP, and that rigorous exclusion of water was needed to achieve reproducible results.

CuL_2 seemed a viable electron acceptor since the neodecanoate ligands are free of olefin groups. Also, reproducible data were obtained with this complex in the alkane solvents (Alfa, Aldrich)

not purified from water following the experimental procedures described previously.[5] Shown in Figure 1a is the optical spectrum of CuL_2 recorded in octane exhibiting a signal with a wavelength of maximum absorbance of 686 nm (ε = 245 M^{-1} cm^{-1}), which is located in the range typical for Cu(II) transitions of carboxylate complexes.[6] Similar spectra resulted in pentane and cyclohexane; the monomeric nature of CuL_2 in the solutions was confirmed by the absence of the 350 nm band characteristic of dimeric Cu(II) carboxylates.[5,6] Illumination of air-free alkane solutions containing BP (Aldrich) and CuL_2 induced a color change from green to colorless. As depicted in Figure 4.1 (a) for a C_8H_{18} solution, this color change originated from the decay of the CuL_2 signal centered at 686 nm without formation of any signal in the visible range.

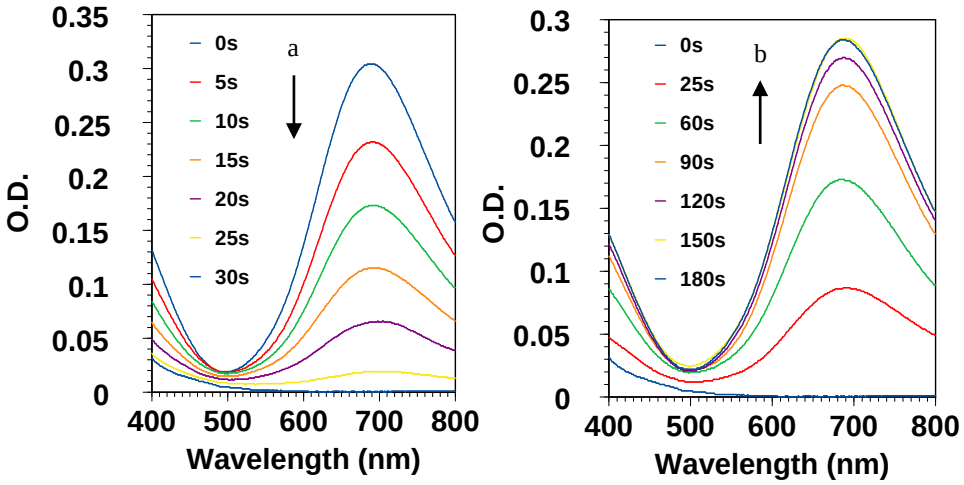

Figure 5.1: (a) Spectral changes during photolysis of an air-free octane solution with 2 mM BP, 1.2 mM CuL_2, and I_0 = **6 x 10^{-5}M(hν)/s**, cycle 6. (b) Spectral evolution during the regeneration of **CuL_2** in the presence of O_2.

The photoreaction product was diamagnetic (induced no interferences during NMR experiments) and was also indefinitely stable in the absence of O_2. Complete regeneration of CuL_2 occurred in the presence of air; a faster reformation process took place upon exposure of the solutions to pure

O_2. Figure 4.1 (b) shows the spectral evolution resulting from introduction of oxygen into a CuL_2 solution in C_8H_{18} previously photolyzed for 30 s. Complete reformation of CuL_2 occurred in about 450 s. Water is the main product of the CuL oxidation since only 3.8% of the consumed O_2 was detected as H_2O_2 via iodometry.[7] Results very similar to those shown in Figure 4.1 were obtained previously with the Cu(II) oleate complex.[5]Reduction of Cu(II) ions in solution usually proceeds via two consecutive steps involving Cu(I) species as intermediates.[8] In water the cuprous ions exist as hydroxide/oxide colloids with an absorption band at around 460 nm; disproportionation or further reduction of the Cu(I) species yields Cu crystallites exhibiting a plasmon signal between 560-580 nm.[9] On the other hand, complexation of Cu(I) with ligands unable to induce charge-transfer transitions yields colorless complexes.[8] Furthermore, cuprous compounds are generally sensitive to air and disproportionation of Cu(I) is not a viable process in non-aqueous solvents.[10] Based on this knowledge, a logical conclusion is that the species formed during the BP-initiated photoreaction of CuL_2 corresponds to the Cu(I) compound CuL. Plotted in figure 4.2 is the optical density at 686 nm as a function of irradiation time, showing that the reduction of CuL_2 follows an apparent zero-order rate law. Evaluation the quantum yield of CuL_2 reduction used the reaction rate, r, obtained from the slope of the straight line shown in Figure 4.2 according to the equation Q.Y. = $r/(fI_0)$ where f = fraction of photons absorbed by BP and I_0 = light intensity. The photoreaction is highly efficient since a yield of 1.8 is obtained from $r = 4 \times 10^{-5}$ M/s and f = 0.37.

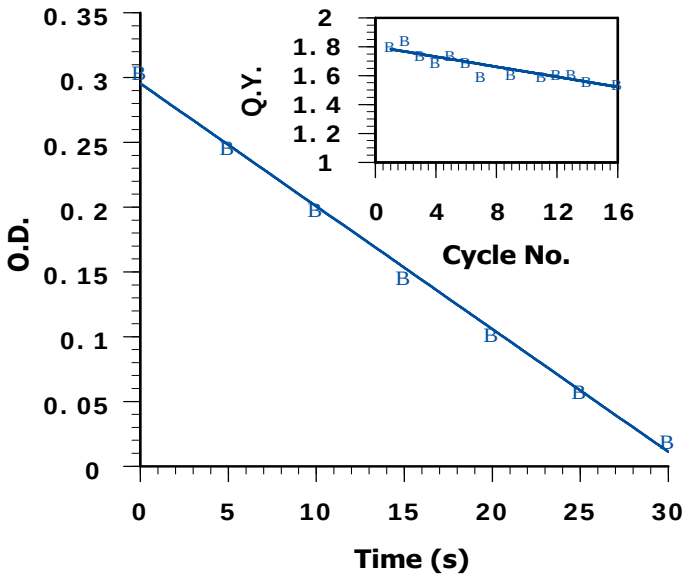

Figure 5.2: Time-evolution of the optical density of CuL_2 at 686 nm during photolysis of an air-free C_8H_{18} solution with 2 mM BP, 1.2 mM CuL_2, and $I_0 = 6 \times 10^{-5}$ M(hν)/s, first cycle. Inset: dependence of the quantum yield of CuL_2photoreduction on the number of reduction-oxidation cycles.

The ability of reforming CuL_2 via exposure of CuL solutions to O_2 enabled to test the reversibility of the Cu(II) photoreduction. Presented in the inset of Figure 2 is the dependence of Q.Y. for the photoreduction on the number of reduction-oxidation cycles performed on a C_8H_{18} solution of CuL_2. Only a slight decrease in Q.Y. from 1.8 to 1.6 occurred, indicating that CuL_2 could act as a catalyst for the photooxidation of alkanes. In fact, the data displayed in Figure 4.1 was obtained during the sixth reduction-oxidation cycle and the kinetics of both steps was practically identical to that of the first cycle. The CuL_2photoreduction efficiency remained unchanged when pentane or cyclohexane served as solvents instead of octane. No change in Q.Y. was noticed in experiments conducted with C_8H_{18} solutions containing twice as much BP and CuL_2. This finding verified that CuL_2 is not a quencher of the photogenerated excited states of BP. The quantum yields of photoreduction were not corrected for the fraction of photons

absorbed by CuL_2 and by CuL given that their concentrations changed during the course of the reaction. However, an experiment with 2 x 10^{-3} M BP and 6 x 10^{-4} M CuL_2 resulted in a Q.Y. = 2. This means that the results presented in the inset of Figure 4.2 represent lower limits of the quantum yields of photoreduction.

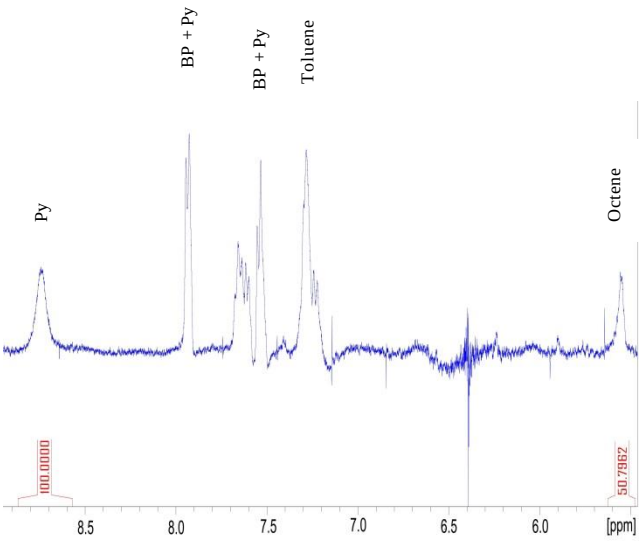

Figure 5.3: ^{1}H NMR spectrum of an octane solution containing 4mM BP and 2 mM CuL_2, after 4 reduction-oxidation cycles. Resonance shifts are relative to the pyridine signal at 8.74 ppm.

The highly efficient photoreduction of CuL_2 required an effective reducing agent and solvent molecules seemed logical candidates given their high concentrations in the solutions. Participation of solvent molecules in the photoreaction was confirmed by means of ^{1}H and ^{13}C NMR analyses (Bruker Avance 400). Characteristic signals of alkenes were detected in photolyzed samples of all the three solvents. A thorough product analysis was carried out on an octane solution containing 4 x 10^{-3} M BP and 2 x 10^{-3} M CuL_2. The solution was subjected to four reduction-oxidation cycles (to accumulate reaction products), followed by extraction of

CuL_2 with water. ^{13}C NMR measurements indicated that all possible octene isomers were present in the reaction mixture. Quantification of the olefin yield employed ^{1}H NMR determinations after addition of pyridine (py) at a concentration two times higher than the expected [alkene] of 4 mM. Figure 4.3 shows the resulting spectrum where chemical shifts are reported relative to the pyridine signal at 8.74 ppm. (Toluene signals are present because this is the solvent of the commercial CuL_2 samples). Integration of the pyridine and octane signals resulted in a ratio of $[py]/[C_6H_{16}] = 2/1$. Hence, the quantum yield of olefin formation amounted to ½ of the Q.Y. of CuL_2 reduction, implying that each reduction-oxidation cycle resulted in the same ratio of Cu(II) reduced vs. olefin formed. Furthermore, these results demonstrate that C_8H_{18} can be oxidized to C_8H_{16} with high quantum yields and that CuL_2 is a very efficient catalyst for this process.

The photochemical oxidation of the alkane solvents can be rationalized in terms of the well-known photochemical processes of BP that result in formation of a triplet (n, π^*) excited state ($^3BP^*$) with Q.Y. = 1.[11]This excited state can abstract a H-atom from numerous compounds, including alkanes. Such reaction generates a α-hydroxy radical of BP (BPH•) together with a radical of the H-atom donor. In view of the high quantum yields of CuL_2 reduction, formation both alkane radicals ($\bullet C_nH_{2n+1}$) and BPH• must occur with efficiencies close to 100% during photolysis of BP in the hydrocarbons. The following mechanism is consistent with the available data,

$$BP + h\nu \rightarrow {}^3BP^* \qquad (2)$$

$$^3BP^* + C_nH_{2n+2} \rightarrow BPH\bullet + \bullet C_nH_{2n+1} \qquad (3)$$

$$CuL_2 + \bullet C_nH_{2n+1} \rightarrow CuL + LH + C_nH_{2n} \qquad (4)$$

$CuL_2 + BPH\bullet \rightarrow CuL + LH + BP$ (5)

Low reaction efficiencies were reported for the photolysis of BP in alkanes which were attributed to combination of BPH• and $\bullet C_nH_{2n+1}$ with reformation of the starting materials.[12] Scavenging of both radicals by CuL_2 is the reason for the efficient formation of olefins. In water $E^o[Cu^{2+}/Cu^+] = 0.168$ V whereas the estimated oxidation potential of BPH• amounts to 1.31 V.[13,14] Step 5 is exergonic in H_2O and probably as well in the linear alkanes if the potentials are not drastically different in the hydrocarbons. While the oxidation potentials of the relevant $\bullet C_nH_{2n+1}$ radicals are (to the best of our knowledge) unavailable, rate constants for the reduction of Cu(II) complexes by n-butyl radicals are in the range of 3-17 × 10^6 M^{-1} s^{-1} in acetonitrile/acetic acid mixtures.[15] Hence, a rate constant of similar magnitude can be anticipated for step 4.

The distribution of olefins formed during the photoreaction in octane was determined using GC/MS analysis (Waters GCT Premier, EI detector and ZB-5MS column) of their brominated derivatives.[16]Octene isomers were formed in a ratio of 1:2.1:1.9:1.4 for 1-octene:2-octene:3-octene:4-octene. Both cis and trans isomers of 2-octene were detected but their relative abundance was not determined. Oxidation of octane by O_2 using supported vanadium oxide catalysts at $T \geq 450$ °C produced a similar distribution of octene isomers but dehydrogenation is in competition with formation of aromatic compounds.[17]The rather low selectivity toward olefin formation in the CuL_2 system is a consequence of the indiscriminate attack by $^3BP^*$ on all the C-H bonds present, which resembles the reactivity pattern of H-atom abstraction exhibited by F• atoms.[18]

Conclusions:

In summary, the BP-sensitized oxidation of hydrocarbons catalyzed by Cu(II) neo-decanoate is a simple free-radical procedure for introducing unsaturations in alkanes. This process takes place with high efficiencies at room temperature. The Cu(II) complex plays a key role as an electron acceptor able to scavenge the photogenerated solvent radicals, thus preventing undesirable radical-radical and radical-olefin reactions. The ability to achieve complete reoxidation by O_2 of the photogeneratedCu(I) product enables CuL_2 to function as a catalyst over numerous catalytic cycles without appreciable loss of activity.

References:

(1) (a) Coperet, C. *Chem. Rev.***2010**, *110*, 656-680. (b) Olah, G. A.; Molnár, A. *Hydrocarbon Chemistry*, 2nd edition; Wiley-Interscience: New Jersey, 2003; pp. 44-66.

(2) (a) Findlater, M.; Choi, J.; Goldman, A. S.; Brookhart, M. In *Alkane C-H Activation by Single-Site Metal Catalysis*; Pérez, P. J., Ed.; Springer: Dordrecht, 2012; pp. 113-141. (b) Choi, J.; MacArthur, A. H.; Brookhart, M.; Goldman, A. S. *Chem. Rev.***2011**, *111*, 1761-1779. (c) Dobereiner, G. E.; Crabtree, R. H. *Chem. Rev.***2010**, *110*, 681-703. (d) Gunay, A.; Theopold, K. H. *Chem. Rev.***2010**, *110*, 1060-1081.

(3) (a) Conde, A.; Vilella, L.; Balcells, D.; Díaz-Requejo, M. M.; Lledós, A.; Pérez, P. J. *J. Am. Chem. Soc.***2013**, *135*, 3887-3896. (b) Khaskin, E.; Lew, D. L.; Pal, S.; Vedernikov, A. N. *J. Chem. Soc., Chem. Comm.***2009**, 6270-6272.

(4) Maguire, J. A.; Boese, W. T.; Goldman, A. S. *J. Am. Chem. Soc.***1989**, *111*, 7088-7093. (b) Burk, M. J.; Crabtree, R. H. *J. Am. Chem. Soc.***1987**, *109*, 8025-8032. (c) Nomura, K.; Saito, Y. *J. Chem. Soc., Chem. Comm.***1988**, 161-162. (d) Sakakura, T.; Sodeyama, T.; Tokunaga, Y.; Tanaka, M. *Chem. Lett.***1988**, 263-264. (e) Burk, M. J.; Crabtree, R. H.; McGrath, D. V. *J. Chem. Soc., Chem. Comm.***1985**, 1829-1830.

(5) Clary, D. L.; Mills, G. *J. Phys. Chem. C***2011**, *115*, 14656-14663.

(6) (a) Tonnet, M. L.; Yamada, S.; Ross, I. G. *Trans. Faraday Soc.***1964**, *60*, 840-849. (b) Braddon, D. P. *J. Inorg. Nucl. Chem.***1961**, *17*, 222-231.

(7) Kormann, C.; Bahnemann, D. W.; Hoffmann, M. R. *Environ. Sci. Technol.***1988**, *22*, 798-806.

(8) Cotton, F. A.; Wikinson, G. *Advanced Inorganic Chemistry*, 4th edition; Wiley-Interscience: New York, 1980; pp. 800-810.

(9) (a) Korchev, A. S.; Shulyak, T. S.; Slaten, B. L.; Gale, W. F.; Mills, G. *J. Phys. Chem. B***2005**, 109, 7733-7745. (b) Khatouri, J.; Mostafavi, M.; Amblard, J.; Belloni, J. *Chem. Phys. Lett.***1992**, *191*, 351-356.

(10) Tsarevsky, N. V.; Braunecker, W. A.; Matyjaszewski, K. *J. Organomet. Chem.***2007**, *692*, 3212-3222.

(11) Gilbert, A.; Baggott, J. *Essentials of Molecular Photochemistry*; CRC Press: Boca Raton, FL, 1991; pp. 287-353.

(12) Beckett, B.; Porter, G. *Trans. Faraday Soc*. **1963**, *59*, 2038-2050.

(13) Ciavatta, L.; Ferry, D.; Palombari, R. *J. Inorg. Nucl. Chem*. **1980**, 42, 593-598.

(14) Canonica, S.; Hellrung, B.; Wirz, J. *J. Phys. Chem. A***2000**, *104*, 1226-1232.

(15) Kochi, J. K.; Bemis, A.; Jenkins, C. L.; *J. Am. Chem. Soc.* **1968**, *90*, 4616-4625.

(16) Burk, M. J.; Crabtree, R. H.; McGrath, D. V. *Anal. Chem.***1986**, *58*, 977-978.

(17) (a) Dasireddy, V. D. B. C.; Singh, S.; Friedrich, H. B. *Appl. Catal. A***2012**, *421-422*, 58-69. (b) Elkhalifa, E. A.; Friedrich, H. B. *Catal. Lett.***2011**, *141*, 554-564. (c) Elkhalifa, E. A.; Friedrich, H. B. *Appl. Catal. A,* **2010**, *373*, 122-131.

(18) Nonhebel, D. C.; Walton, J. C. *Free-Radical Chemistry*; Cambridge University Press: Cambridge,1974; pp. 172-176.

Chapter VI

Synthesis of concentrated Ag particles in eicosane for NePCM application.

Introduction:

Efficient cooling of machineries such as electronic devices, car engines, power plants, industrial equipment and batteries is extremely important for ensuring that they operate efficiently. In general, cooling processes involve a medium that can extract thermal energy from the system and transfer the heat to the surroundings. Air or liquids such as water and ethylene glycol are commonly used to dissipate thermal energy from a hot medium. However, their low thermal conductivities (as compared to that of metals or ceramics) restricts their efficiencies as coolants and new systems are needed to boost heat transfer.[1,2]

Long chain hydrocarbons such as eicosane and tetracosane possess impressive thermophysical properties such as high enthalpy of fusion and chemical stability over a wide range of temperatures for both solid and liquid phases. Thermal energy storage (by the so-called latent heat method) relies on absorption of heat at a constant temperature during phase change. Due to the high heat of fusion, low melting temperature and good stability long chain hydrocarbons are very desirable for many applications as PCM. The low thermal conductivity of hydrocarbons limits their use as heat sinks and therefore attempts to enhance the heat transfer coefficient has been a major focus for many researchers over the last decade.

Thermal conductivity enhancement of PCM can be achieved by incorporation of solid and conductive particles to those media. Suspensions of particles were claimed to possess excellent thermal properties.[3,4] However, the published results turned out to be irreproducible since they were based on experiments with unstable time-dependent suspensions which have no practical

value in terms of applications. Colloidal solutions are stable dispersions of particles and should enable determination of time-independent thermal properties.

In this study, the objectives were the preparation of the NePCM of ultra-stable colloidal solution of metallic silver nanoparticles (1-10 wt %) in eicosane ($C_{20}H_{42}$). In addition, determination of the thermal properties from the resulting fluid-particle systems such as thermal conductivity, latent heat and melting point using the transient plane source technique and differential scanning calorimetry was of interest. Finally, the dependence of thermal conductivity of the NePCM on the loading of Ag nanoparticles, the samples temperature and the specific method of freezing were all investigated.

Preparation of the Silver-Based NePCM Samples:

The procedure in the present study was a one-step straightforward synthesis that takes about 1 hour. Eicosane ($C_{20}H_{42}$) with a melting point of 36.4 °C was selected as the base PCM and samples with a purity of 99% were purchased from Sigma Aldrich; silver neodecanoate ($C_{10}H_{19}O_2$) was purchased from Strem Chemicals and served as precursor of the silver particles. Oleoyl Sarcosine (OS) was obtained from TCI America and used as a particle stabilizer. Different concentrations of Ag particles (1-10 wt %) were stabilized via keeping a constant mass ratio of Ag to OS of Ag:OS = 1:1.25. The procedure involves addition of silver neo-decanoate to a solution containing OS in eicosane preheated to 160 °C in an oil bath under vigorous stirring. The solvent eicosane can act as a reducing agent forming metallic Ag at high temperatures. Indeed, simple addition of Ag neodecanoate to hot eicosane without OS produced unstable particles that aggregated to form large greyish Ag clumps. In this case, the concentration ratio of

Ag to OS was 1.25 for all samples. The constant concentration ratio helped to maintain similar particles size distributions for all Ag samples. In order to check the long-term stability of the prepared liquid samples, specimen of different mass fractions (1, 5 and 10 wt%) were placed inside a vacuum oven at 50 ºC for 1 week. No precipitation was visually observed for all the three Ag/eicosane samples. The long term stability of Ag particles in liquid state was also confirmed by preparing particles in liquid hydrocarbons using a similar procedure and noticing that the resulting colloids remained stable after one year.[5]

Results and Discussion:

Colloidal silver particles were characterized by transmission electron microscopy. A 0.1 M of liquid Ag eicosane colloid was diluted using hexane to 5×10^{-5} M. Shown in Figure 6.1 is a typical TEM image obtained from such a sample. The particles were found to be nearly spherical in shape and an average particle diameter of 5.5 nm was obtained from a size histogram that resulted after analyzing about 300 particles. Presented in Figure 6.2 are room temperature images of solid PCM samples that resulted from preparation of Ag colloids in eicosane as described previously. A solid eicosane PCM containing 1 wt % of Ag exhibits a black color whereas a sample with 10 wt % Ag appears dark blue. An analogous procedure was used previously to obtain 1 wt % Ag in dodecane and the particles were found to be stable in the hydrocarbon even after one year. Ag colloids prepared in eicosane were kept at 40 ºC (liquid eicosane) in an

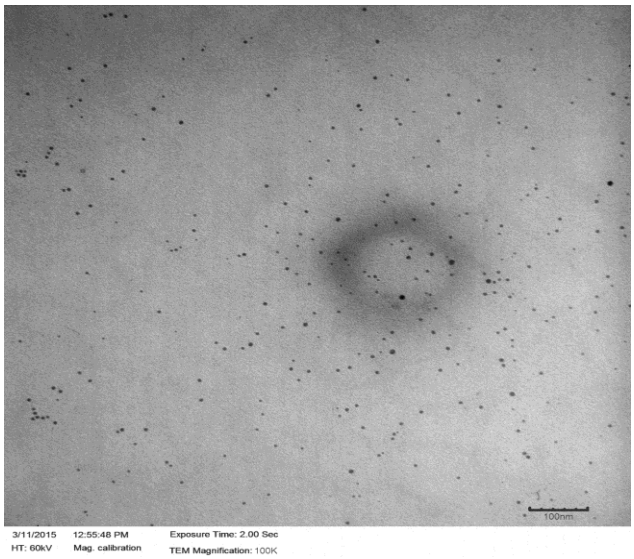

Figure 6.1: TEM image of a sample made via diluting a 0.1 M Ag colloid in eicosane to a metal concentration of 5×10^{-5} M using hexane followed by drying under air. The size bar corresponds to 100 nm.

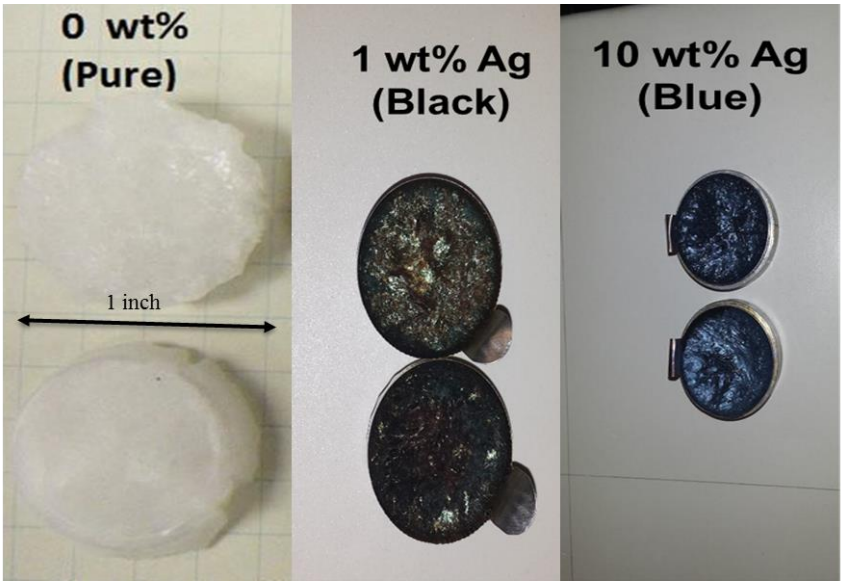

Figure 6.2: Image of solid eicosane (left) and of solid eicosane PCM containing Ag nanoparticles at room temperature (center and right).

oven for 2 weeks and no precipitation was observed. This observations implied that the colloids were similarly stable in eicosane as those prepared in dodecane.

The melting point and heat of fusion of the colloids were the same as those of pure eicosane and were not affected by the different amounts of Ag present in the hydrocarbon. However, since the ratio of Ag and OS were kept constant for all different samples, the melting point and heat of fusion values were affected by the amount of OS present in the systems. Variations of the melting points for all compositions were important parameters that were needed during thermal conductivity measurements to define temperature ranges away from the melting point of a particular sample. The reported heats of fusion and melting points of Ag/eicosane PCM corresponded to the average value calculated from data of three runs. Illustrated in Figure 6.3 and 5.4 are results obtained during the third heating cycle with a heating rate of 5 ^{o}C/min.

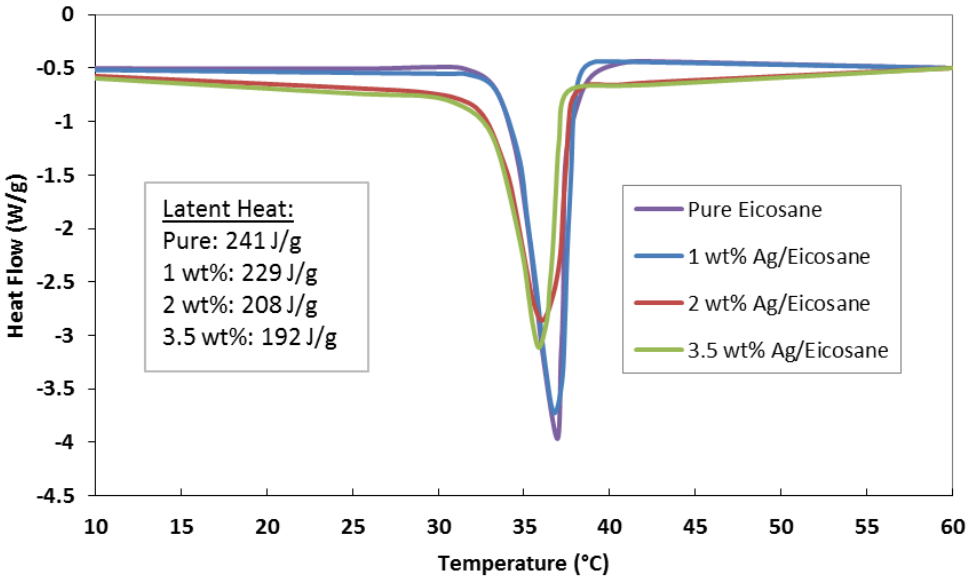

Figure 6.3: DSC curves showing melting of pure eicosane and Ag/eicosane samples of 1, 2 and 3.5 wt% prepared following the room temperature solidification approach along with their respective heat of fusion values; DSC ramping rate = 5 ^{o}C/min.

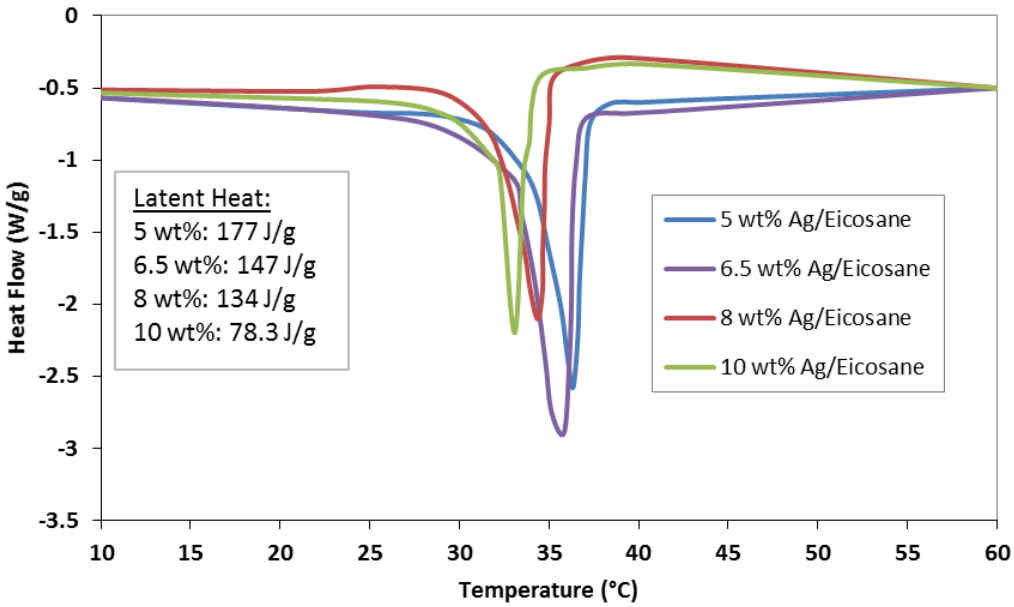

Figure 6.4: DSC curves showing melting of 5, 6.5, 8 and 10 wt% Ag/eicosane samples prepared following the room temperature solidification method along with their respective heat of fusion values; ramping rate = 5 ^{o}C/min.

Increasing the % Ag also increased the concentration of OS since the Ag : OS remained constant for all samples. Since OS is a solute dissolved in the PCM the presence of increasing amounts of sarcosine decreased both the melting temperatures and the heats of fusion since both quantities are colligative properties that are affected by the solute concentrations. An unexpected result was that increasing the particle loading slightly decreased the melting point of the NePCM, although the particles are not considered to behave as classical solutes.

References:

(1) Das, S. K.; Choi, S. U. S.; Patel, H. E. Heat Transfer in Nanofluids—A Review. *Heat Transf. Eng.* **2006**, *27*, 3–19.

(2) Daungthongsuk, W.; Wongwises, S. A Critical Review of Convective Heat Transfer of Nanofluids. *Renew. Sustain. Energy Rev.* **2007**, *11*, 797–817.

(3) Xiang, J.; Drzal, L. T. Investigation of Exfoliated Graphite Nanoplatelets (xGnP) in Improving Thermal Conductivity of Paraffin Wax-Based Phase Change Material. *Sol. Energy Mater. Sol. Cells* **2011**, *95*, 1811–1818.

(4) Turanov, A. N.; Tolmachev, Y. V. Heat and Mass Transport in Aqueous Silica Nanofluids. *Heat Mass Transfer;* **2009**, *45*, 1583–1588.

(5) Darvin J.; Nabil M.; Uertz J.; Mills G.; Concentrated Ag Colloids in Dodecane Relevant to Nanostructure Enhanced PCM; Submitted to *Physical Chemistry Chemical Physics*; 2016.